

**COMPARISON OF THE SOUTHERN CASCADIA SUBDUCTION ZONE
WITH THE TECTONIC SETTING OF THE
1964 ALASKA EARTHQUAKE**

by

**George Plafker, Ph.D.
Plafker Geohazard Consultants**

Prepared for Pacific Gas and Electric Company

George Plafker August, 23, 2002



Humboldt Bay ISFSI Project
Technical Report
TR-HBIP-2002-01

2A-1

Appendix 2A
Rev. 0, August 23, 2002

CONTENTS

<u>Arc Setting</u>	3
<u>Relative Plate and Block Motion</u>	4
<u>Historic Seismicity in the Arc-Transform Transition Region</u>	5
<u>Forearc Fold and Thrust Belt</u>	5
<u>Coseismic Tectonic Displacements</u>	6
<u>Earthquake Recurrence Intervals</u>	7
<u>Coseismic Deformation and Tsunami Generation</u>	7
<u>References Cited</u>	9

FIGURES

- Figure 2A-1. Land-level changes associated with the 1964 Alaska earthquake.
- Figure 2A-2. Simplified tectonic model for present crustal deformation along Pacific-North American plate boundary in southern and southeastern Alaska.
- Figure 2A-3. Major structural features along the Gulf of Alaska margin.
- Figure 2A-4. Inferred rupture zones of major plate-boundary earthquakes and the “Yakataga seismic gap” along the Gulf of Alaska margin.
- Figure 2A-5. Tectonic uplift and subsidence, and surface faults at Montague Island associated with the 1964 Alaska earthquake.
- Figure 2A-6. Submarine extension of the zone of maximum uplift and faulting on Montague Island.
- Figure 2A-7. Schematic cross sections showing the suggested mechanisms for the 1964 Alaskan earthquake and the 1960 Chilean earthquake.
- Figure 2A-8. Profiles and sections of coseismic deformation associated with the 1964 Alaska earthquake and a hypothetical large megathrust earthquake across the southern Cascadia margin.



COMPARISON OF THE SOUTHERN CASCADIA SUBDUCTION ZONE WITH THE TECTONIC SETTING OF THE 1964 ALASKA EARTHQUAKE

The purpose of this report, is to consider the ways in which the southern end of the Cascadia subduction compare with, and differ from, the eastern end of the Aleutian subduction zone, which was ruptured most recently in the great 9.2 (M) 1964 Alaska earthquake. This comparison is made because of the striking overall similarities between the southern and eastern ends, respectively, of these two arcs. References for data sources on the 1964 earthquake are given in the text and figure captions. Discussion and description of the Cascadia subduction zone, seismotectonics, paleoseismology, and geology of Cascadia are presented in Section 2 of PG&E (2002) and are not repeated here.

Both the eastern Aleutian and Cascadia arcs are continental margin arcs with shallow-dipping megathrusts. Both have wide forearc accretionary sequences of Mesozoic and Cenozoic rocks that strike obliquely into the continental margin at one end so that a wide cross-section of the deformation zone is exposed on land. They both have complex transition zones where they intersect the continental margin in which the structural styles change within a broad, complex zone from dominantly near-orthogonal compression to dextral strike-slip. Until the great 1964 Alaska earthquake, historic seismicity in both regions was low and it continues to be low in the megathrust region of the Cascadia arc since the last great earthquake there about 300 years ago. They both have long late Holocene paleoseismic records of major earthquakes that document sudden regional vertical displacement of shorelines and accompanying tsunamis. Because of these striking similarities, I infer that regional warping, faulting, and tsunami generation associated with the 1964 Alaska earthquake is the best analog available for forecasting tectonic displacements and associated tsunamis that are likely to accompany future large Cascadia subduction zone earthquakes.

Arc Setting

The 1964 Alaska earthquake occurred at the eastern end of the Aleutian arc, which is defined by the Aleutian trench, the arc of active volcanoes of the Aleutian Islands, Alaska Peninsula, and Wrangell Mountains, and an associated zone of high seismicity that is mainly related to the Aleutian megathrust (Figure 2A-1). The Aleutian subduction zone is within oceanic crust in its western part. To the east, it extends along the continental margin of North America from the western end of the Alaska Peninsula to the rupture region of the 1964 earthquake at the eastern end of the Aleutian arc in the Gulf of Alaska where it trends obliquely onto the continental margin. The earthquake occurred as a complex rupture along ~800 km of the Aleutian megathrust between the Pacific and North American plates and by large-scale subsidiary thrust faulting within the upper plate.

Interpretation of the 1964 earthquake as a result of convergence and thrusting along this plate boundary provided strong support for the theories of plate tectonics and seafloor spreading that were emerging as the dominant theme in earth science during the late 1960's.



Similarly, the Cascadia arc is defined by subduction of the oceanic Juan de Fuca and Gorda plates beneath the continental North American plate and by the Cascades volcanic arc. From northern Vancouver Island to southern Oregon the arc trends roughly parallel to the continental margin. In northern California the seaward part of the arc intersects the continental margin and connects with the San Andreas dextral-slip fault system via a complex structural zone of fault-bounded tectonic blocks (Carver, 1987; Clarke, 1992).

Relative Plate and Block Motion

In Alaska, relative motion between the Pacific and North American plates, when averaged over the last 3 million years (Ma) increases from 49 mm/yr in southeastern Alaska to 77 mm/yr at the west end of the Aleutian arc. In the 1964 earthquake area it is 58 mm/yr (Figure 2A-2).

The primary boundary between the Pacific and North American plates is the Queen Charlotte-Fairweather right-slip transform zone in southeastern Alaska and the Aleutian megathrust system of thrust, right-oblique, and right-slip faults that extend from the western Gulf of Alaska to the western end of the Aleutian Islands. Significant northwest-southeast relative motion is concentrated mainly along the boundaries of the Yakutat, Saint Elias, and Wrangell structural blocks in the complex region between the northern Gulf of Alaska, the Denali fault system, and the western Alaska Range (Figure 2A-2). Most of the Pacific-North American relative motion in the northern Gulf of Alaska region is taken up by dominantly strike-slip faulting of about 52 mm/yr on the northwest-trending Fairweather transform fault between the Yakutat and Saint Elias blocks, by shortening and deformation along the northeast-trending fold and thrust zone that represents an extension of the Aleutian megathrust zone between the Yakutat and Wrangell blocks, and by shortening and deformation (58 mm/yr) between the Pacific and North American plates (Figs. 2A-2 and 2A-3).

Rates of right oblique thrusting (<10 mm/yr) are inferred to be relatively low along nearly east-west trending structures such as the Transition and Chugach-Saint Elias fault zones that bound the southern and northern margins of the Yakutat block, respectively. Slip rates of 10 to 20 mm/yr occur on the eastern Denali and Totschunda right-slip faults between the Wrangell block and North American plate. North of the Denali fault deformation within the North American plate is widespread but relatively minor. Indicators of principal horizontal stress directions in Alaska are broadly compatible with the relative Pacific-North American plate motions; however, the style of faulting within plates and blocks is generally more variable than along boundaries (Figure 2A-3).

The general transition from convergence along the Aleutian megathrust to right-slip in southeastern Alaska is comparable to the change in structural style in the transition from the southern Cascadia subduction zone to the region south of the Mendocino triple junction. There are two noteworthy differences, however. In Alaska the change is due to the concave-southward oroclinal bend around the Gulf of Alaska that formed in the Paleogene whereas in

Cascadia it is due to differences in motion of the oceanic plates north and south of the Mendocino triple junction.

In addition, deformation in the transition zone between strike-slip and thrust faulting in Alaska is complicated by the presence of the Yakutat block (Figure 2A-2), a large allochthonous block that has moved with the Pacific plate from a source area at least 600 km to the southeast along the continental margin (Plafker and others, 1994). Continued northwestward movement of the block results in complex folding and thrust faulting along its margins, and subduction beneath the continental margin to the north and northwest with consequent rapid uplift, great topographic relief, and exceptionally active seismicity.

Historic Seismicity in the Arc-Transform Transition Region

During the 20th century, most of the plate boundary in the complex transition region between the east end of the 1964 rupture of the Aleutian megathrust and the transform fault system of southeastern Alaska has ruptured in a series of plate-boundary and intraplate earthquakes (Figure 2A-4). The entire transform boundary of the composite Pacific plate and northern Yakutat block boundary experienced major earthquakes in 1958 (7.3 M) and 1972 (7.4 M) and the segment to the southwest ruptured in the 1949 (8.1 M) Queen Charlotte earthquake. Rupture of a down-dip segment of the Aleutian megathrust and associated intraplate splay faults occurred during the Mount St. Elias earthquake in 1979 (7.5 M). A segment of the plate boundary about 100 km long between the 1979 and 1964 earthquakes, termed the "Yakataga seismic gap" is not known to have been filled by an historic earthquake (Tobin and Sykes, 1968). However, at least part of this area may have been within the focal region of a great series of earthquakes (8.1-8.5 M in 1899 that resulted in about 1 m of coastal uplift near the center of the gap at Cape Yakataga and 14 m of emergence near the head of Yakutat Bay (Thatcher and Plafker, 1977). The southern boundary of the Yakutat block is strongly coupled to the Pacific plate as indicated by a general absence of seismicity and late Cenozoic deformation within the block. Minor relative Pacific-Yakutat movement is suggested by the occurrence of an earthquake (6.3 M_s) with a thrust mechanism along the Transition fault.

In the Cascadia forearc, virtually all the historic seismicity is in the structurally complex Mendocino triple junction region where relative plate motion changes from about 30 mm/yr convergence north of the Mendocino fracture zone to dominantly right-slip south of the zone. The southern Cascadia transition region is similar to the eastern Aleutian arc-transform transition in that they are both characterized by complex faulting and seismicity along both plate and block boundaries that reflect the change from dominant compressional shortening in the arc to dominant dextral-slip in the transform margin.

Forearc Fold and Thrust Belt

In general, the overwhelming majority of the active faults and folds are related to the Aleutian megathrust and its northeastward extension onto the continental margin to the junction with the Fairweather transform (Plafker and others, 1994). Pacific oceanic crust is being subducted along the Aleutian megathrust and the composite Pacific plate and oceanic lower crust of the Yakutat block is being subducted in the region east of the Kayak Island zone (Brocher and others, 1994). Mesozoic and Cenozoic subduction has resulted in



accretion of a complex of flysch and ocean crust rocks along the continental margin that ranges in width from ~300 km at the east end of the 1964 rupture zone to ~200 km at the southwest end. In the northern part of the rupture zone, dip of the megathrust is northwest at 9° beneath the zone of active faulting and it is 16–17 km deep at the inner margin of the zone near Montague Island.

The zone of active faulting associated with the megathrust near the northeastern end of the 1964 earthquake rupture zone is at least 150 km wide as evidenced by major thrust displacement on the Patton Bay fault zone in 1994 (Figure 2A-2). Within the Yakutat block to the northeast the deformed belt widens an additional 125 km between the Kayak Island zone and the Pamplona zone where it crosses the continental slope and extends onshore between the Bering and Malaspina Glaciers (Figure 2A-3). The Pamplona zone is presently the eastern leading edge of the deformation front as evidenced by growing folds, young faults, and active seismicity.

In summary, the data from the 1964 Alaska earthquake clearly show that intraplate deformation can take up much of the plate convergence, and that this deformation can extend as far as 150 km landward from the plate boundary at the trench to areas where the megathrust is ~17 km deep. In southern Cascadia, comparable intraplate deformation is manifested by the active Little Salmon and Mad River fold and thrust zones which occur in a segment of the forearc region where the megathrust is 12–18 km deep (Figure 2A-8a).

Coseismic Tectonic Displacements

The 1964 Alaskan earthquake resulted from rupture of a segment of the eastern Aleutian megathrust 650–800 km long and 150–250 km wide (Figure 2A-5). This major tectonic event was characterized by: (1) shallow seismicity (<30 km), with most of the earthquakes located between the Aleutian trench and the zero isobase between the zones of major uplift and subsidence; (2) regional vertical displacements in a broad asymmetric downwarp of up to 2 m centered over the Kodiak, Kenai, and Chugach Mountains with flanking zones of marked uplift of up to 11.3 m on the seaward side and minor uplift to about 0.3 m on the landward side that extends north of the Alaska Range; and (3) horizontal displacements that involved measured systematic shifts of the land in a generally seaward direction of up to 18 m in the region between the Anchorage and Montague Island areas. Data on coseismic displacements in the 160-km-wide segment of the rupture zone seaward of Montague island are available only at Middleton Island near the edge of the continental shelf where there was 3.5 m of uplift.

Subordinate northwest-dipping intraplate reverse faults, the Patton Bay and Hanning Bay faults, displaced the surface on Montague Island. The Patton Bay fault, with at least 7.9 m dip-slip displacement, is part of a zone of imbricate thrust faults that extends to the southwest on the continental shelf ~500 km. Evidence of young submarine faults, and folds, and possible coseismic uplift of the sea floor was found along the zone off Kodiak Island by marine geophysical surveys (von Huene and others, 1972). Two of the largest aftershocks lie within this uplift zone (Figure 2A-6). In addition, slip on a northwest dipping thrust fault that



is seaward of Middleton Island is suggested by the 3.5 m uplift and northeastward tilting of the island during the 1964 earthquake.

Dislocation modeling of the horizontal and vertical displacement data for the 1964 earthquake (Figure 2A-7 (A)) require that coseismic slip be partitioned between the megathrust and known and inferred intraplate faults. Similarly, the vertical displacement data (Figure 2A-7 (B)) for the great (9.5 M) 1960 Chile earthquake (Figure 2A-7 (B)) can not be modeled using slip solely on the megathrust; the best-fit dislocation model requires an intraplate fault with dip of about 35° that intersects the surface offshore on the upper continental slope (Plafker and Savage, 1970; Barrientos and Ward, 1989).

As in the 1964 Alaska, and probably 1960 Chile, earthquakes, faulting and neotectonic deformation in the southern Cascadia margin is likely to be partitioned between the megathrust and the active intraplate faults that splay off the megathrust in the forearc region. Coseismic slip on intraplate faults within the active Little Salmon and Mad River fold and thrust zones in southern Cascadia could result in nearshore or onshore surface ruptures, vertical displacements, and tilts comparable to those that accompanied the Alaska earthquake.

Earthquake Recurrence Intervals

Paleoseismic data at the Copper River delta in the eastern Aleutian arc indicate that 8 large pre-1964 megathrust earthquakes occurred in the same region in the last 5,600 years (Plafker and others, 2000). Because each of these paleoearthquakes involved sudden regional uplift (0.5–2.5 m) comparable to the 2 m coseismic uplift at the same localities in 1964, they are interpreted as probable subduction zone events. Recurrence intervals range from ~400–900 years and average ~700 years. For the orthogonal plate convergence rate of ~50 mm/yr, maximum dip slip/event ranges from 20–45 m and averages ~35 m. The penultimate event was ~750 years ago and plate convergence during that interval was 37.5 m. Thus, only about 50% of this slip budget appears to have been recovered by coseismic slip in 1964.

In southern Cascadia, paleoseismic data indicate somewhat shorter recurrence intervals for 6 or 7 large paleoearthquakes in the past 2,900 years (summarized in Sections 2 and 9 of the report, Seismic Hazard Assessment for the Humboldt Bay ISFSI Project). Recurrence intervals range from a minimum of ~200–300 yrs to a maximum of ~900 yrs and average 430–520 years. For the orthogonal convergence rate of ~30 mm/yr, maximum dip-slip per event ranges from 6–27 m and averages ~14 m. The most recent event was the earthquake in 1700 AD some 300 years ago and the southern part of the megathrust has been loaded ~9 m during this 300-year interval.

Coseismic Deformation and Tsunami Generation

The 1964 Alaska earthquake tsunami was generated offshore by sudden coseismic uplift of the continental shelf and slope. The tsunami crest, as determined from initial arrival times at the adjacent coast, corresponds with the maximum uplift on the southwestward offshore extension of the Montague Island zone of intraplate faults (Figure 2A-6). Maximum tsunami runup height of 12.7 m (described in Section 9 of PG&E, 2000 and its Annex 9A by Plafker,



2002), closely matches the maximum coseismic onshore uplift (11.3 m) along the Montague island zone, despite marked differences in the local bathymetry and configuration of the coast in the earthquake source region

The intraplate splay faults on Montague Island and off Middleton Island accommodated ~80% of the 18–20 m maximum available slip on the Aleutian megathrust and most of the vertical tectonic displacements (Figure 2A-8-(A)). No more than 3 m of the regional uplift is attributable to slip solely on the seismogenic segment of the megathrust, which has an average dip of 9° (Brocher and others, 1994).

The Alaska data demonstrate that a major fraction of the total fault slip can be partitioned between the gently dipping megathrust and intraplate splay faults that break relatively steeply to the surface. As a consequence, the vertical component of seafloor uplift can be considerably larger than for an equivalent displacement entirely on the megathrust. For tsunami generation, this means that the initial wave at the source is higher and closer to shore than it would be for slip entirely on the megathrust. Similarly, in southern Cascadia an earthquake on the subduction zone alone would result in less than 2 m tectonic uplift for an average dip of 8° on the megathrust and 12 m slip (for 30 mm/yr orthogonal convergence and the average 470-year recurrence). The fact that most large megathrust earthquakes (those that rupture the full extent of the megathrust) in this part of the arc have been accompanied by tsunamis with large runups strongly indicates that they involve slip on one or more offshore intraplate faults such as those in the Little Salmon and Mad River zones (Figure 2A-8 (B)). Thus, partitioning of a significant fraction of the total slip onto steeply dipping intraplate thrusts is entirely consistent with the data on neotectonic deformation and paleotsunamis along the southern Cascadia margin.



References Cited

- Barrientos, S.E., and Ward, S.N., 1990, The 1960 Chile earthquake; inversion for slip distribution from surface deformation: *Geophysical Journal International*, vol.103, no.3, pp.589-598
- Brocher, T.M., Fuis, G.S., Fisher, M.A., Plafker, George, Moses, M.J., Taber, J.J., and Christensen, N.I., 1994, Mapping the megathrust beneath the northern Gulf of Alaska using wide-angle seismic data: *Journal of Geophysical Research*, v. 99, no. B6, p. 11,663-11,685.
- Carver, Gary, 1987, Late Cenozoic tectonics of the Eel River basin region, coastal northern California: *San Joaquin Geological Society Miscellaneous Publication 37*, p. 61-72.
- Carver, G. A., Abramson, H., Garrison-Laney, C. and Leroy, T., 1999, Paleotsunami Evidence from Northern California for Repeated Long Rupture (M 9) of the Cascadia Subduction Zone [abs.]: *Seismological Research Letters*, v. 70, no. 2, p. 245.
- Clarke, S. H. Jr., 1992, Geology of the Eel River Basin and adjacent region: Implications for late Cenozoic tectonics of the southern Cascadia subduction zone and Mendocino triple junction, *American Association of Petroleum Geologists Bulletin* v. 76, p. 199-224.
- Plafker, George, 1965, Tectonic deformation associated with the 1964 Alaska earthquake: *Science*, v. 148, p. 1675-1687.
- Plafker, George, 1969, Tectonics of the March 27, 1964, Alaska Earthquake: U.S. Geological Survey Professional Paper 543-I, 74 p.
- Plafker, George, Kachadoorian, Reuben, Eckel, E.B., and Mayo, L.R., 1969, Effects of the earthquake of March 27, 1964, on various communities: U.S. Geological Survey Professional Paper 542-G, 50 p.
- Plafker, George, and Savage, J.C., 1970, Mechanism of the Chilean earthquakes of May 21-22, 1960: *Geological Society of America Bulletin*, v. 81, p. 1001-1030.
- Plafker, George, 1972, The Alaskan earthquake of 1964 and Chilean earthquake of 1960; Implications for arc tectonics: *Journal of Geophysical Research*, v. 77, no. 5, p. 901-925.
- Lahr, J.C., and Plafker, George, 1980, Holocene Pacific-North American plate interaction in southern Alaska: Implications for the Yakataga seismic gap: *Geology*, v. 8, p. 483-486.
- PG&E, 2002 in preparation, Seismic hazard assessment for the Humboldt Bay ISFSI Project, Report to the USNRC.
- Plafker, George, 1987, Application of marine-terrace data to paleoseismic studies: *in* Crone, A.J. and Omdahl, E.M., eds., *Proceedings of conference XXXIX-Directions in Paleoseismology*: U. S. Geological Survey Open-File Report 87-673, p. 146-156.
- Plafker, George, Gilpin, L.M., and Lahr, J.C., 1994, Neotectonic map of Alaska, *in* Plafker, G., and Berg, H.C., eds., *The geology of Alaska*: Boulder, Colorado, Geological Society of America, *The Geology of North America*, v. G1, Plate 12, 1 sheet with text, scale 1:2,500,000.
- Plafker, George, Carver, G.A., and Clarke, S.H., Jr., 2000, Seismotectonics of the 1964 Alaska earthquake as an analog for future tsunamigenic southern Cascadia subduction earthquakes [abs.]: *Proc. of Penrose Conference 2000, Great Cascadia Earthquake Tricentennial, Program Summary and Abstracts*". Oregon Department of Geology and Mineral Industries, Special Paper 33, p.



- Plafker, George, 2002, A review of empirical data on tsunami runup versus earthquake source parameters: Report to Pacific Gas and Electric Company, 18p. plus figures.
- Thatcher, Wayne, and Plafker, George, 1977, The Yakutat Bay, Alaska, earthquakes [abs.]: Seismograms and crustal deformation: Geological Society of America Abstracts with Programs, v. 9, no. 4, p. 515.
- Tobin, D., and Sykes, L., 1968, Seismicity and tectonics of the northeast Pacific Ocean: Journal of Geophysical Research, v. 73, p. 3821-3845.
- von Huene, R., Shor, G.G., and Malloy, R.J., 1972, Offshore tectonic features in the affected region in The Great Alaskan Earthquake of 1964, Oceanography and Coastal Engineering, Wash., D.C., Nat. Res. Council, National Academy of Science, p. 266-289.



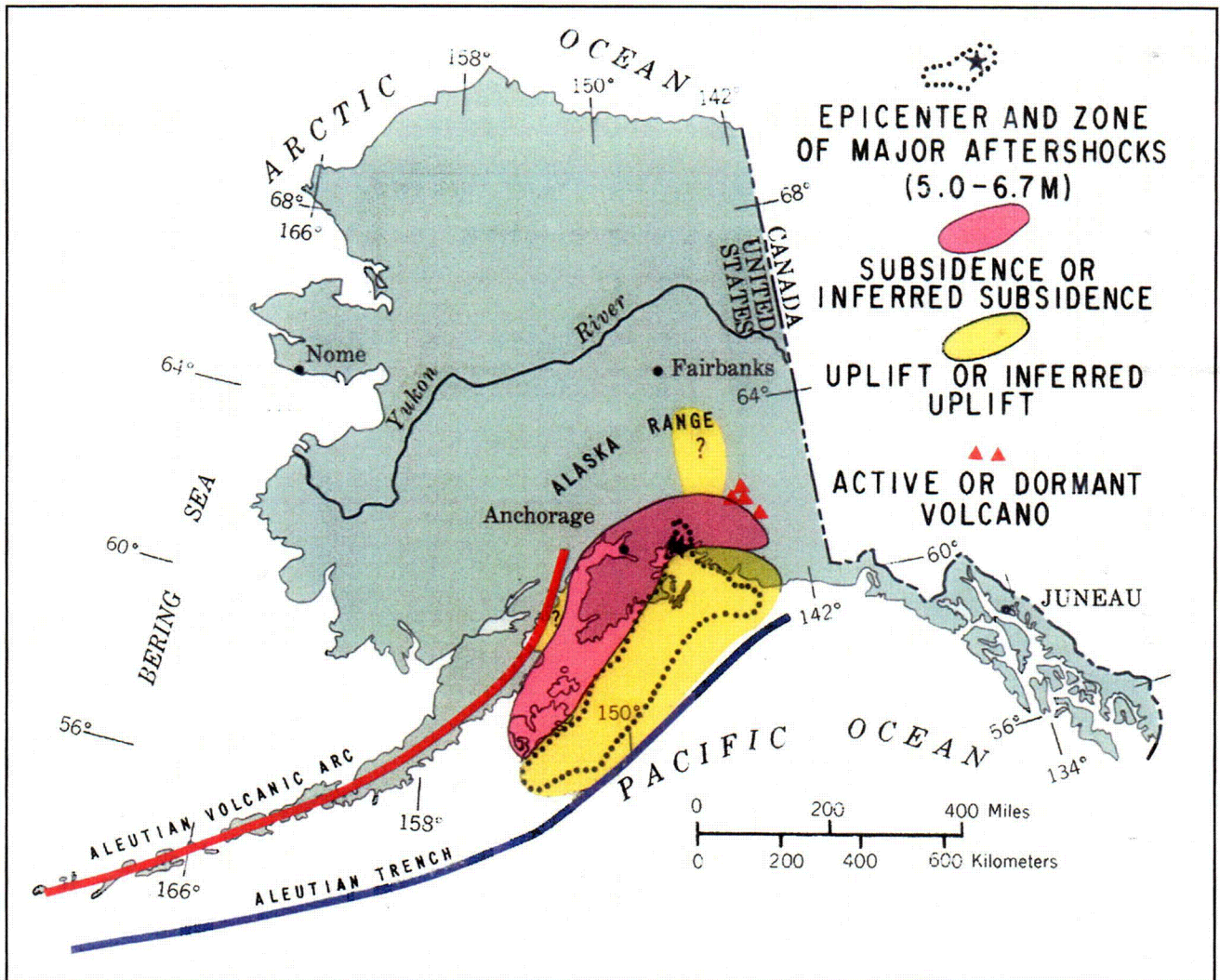


Figure 2A-1 Tectonic setting of the 1964 Alaska earthquake showing the eastern Aleutian volcanic arc and trench, the earthquake epicenter, and the areal distribution of associated zones of vertical land-level change. The Aleutian arc is an ensimatic island arc west of the end of the Alaska Peninsula, and a continental margin arc to the east. (Plafker, 1969).

S:\5100: -117.009\lask_13102_1230_sza_fig_02a-01(01).ai

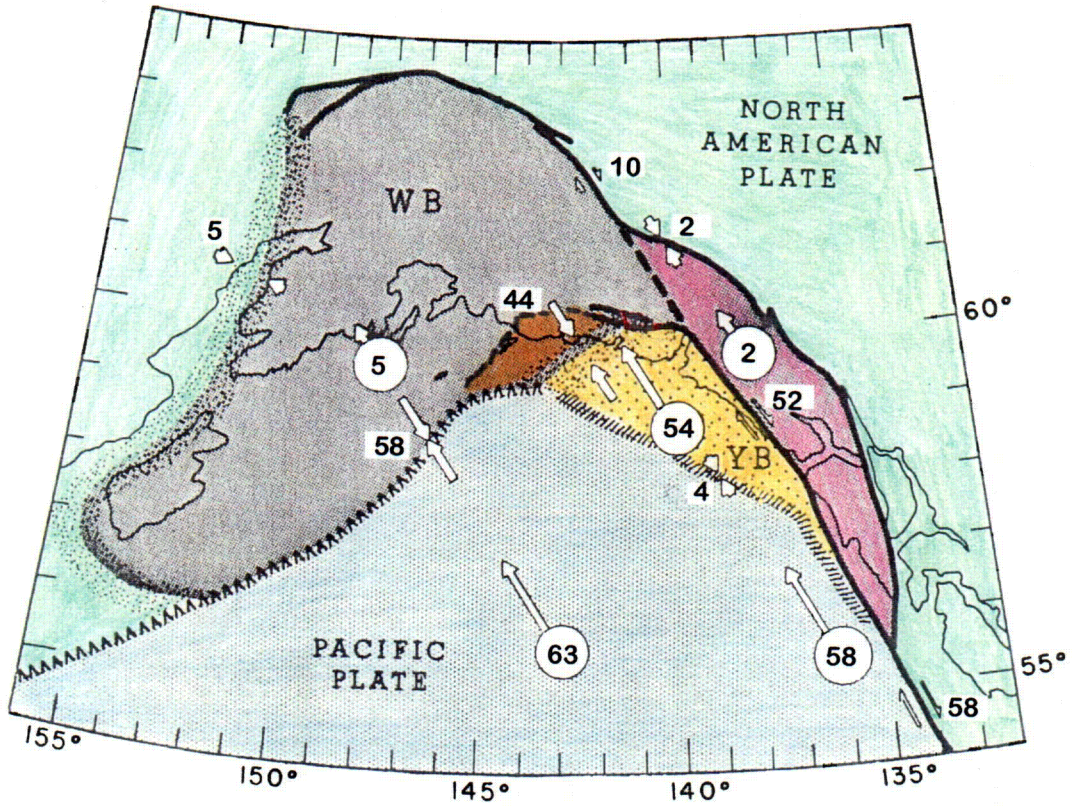


Figure 2A-2 Proposed simplified model for present crustal deformation along Pacific-North American plate boundary in southern and southeastern Alaska. Circled numbers give rate of motion (cm/yr) of Pacific plate, Yakutat block, (YB), St. Elias block (SE), and Wrangell block (WB) relative to North American plate. Numbers next to paired vectors give rate of motion across indicated zone. Dotted bands enclose surface outcrops of major zones of deformation and faulting along the NW and SW margins of the Wrangell block. (Lahr and Plafker, 1980).

S:\5100r\117.009\task_13102_1230_s2a_fig_02a-02(02).ai

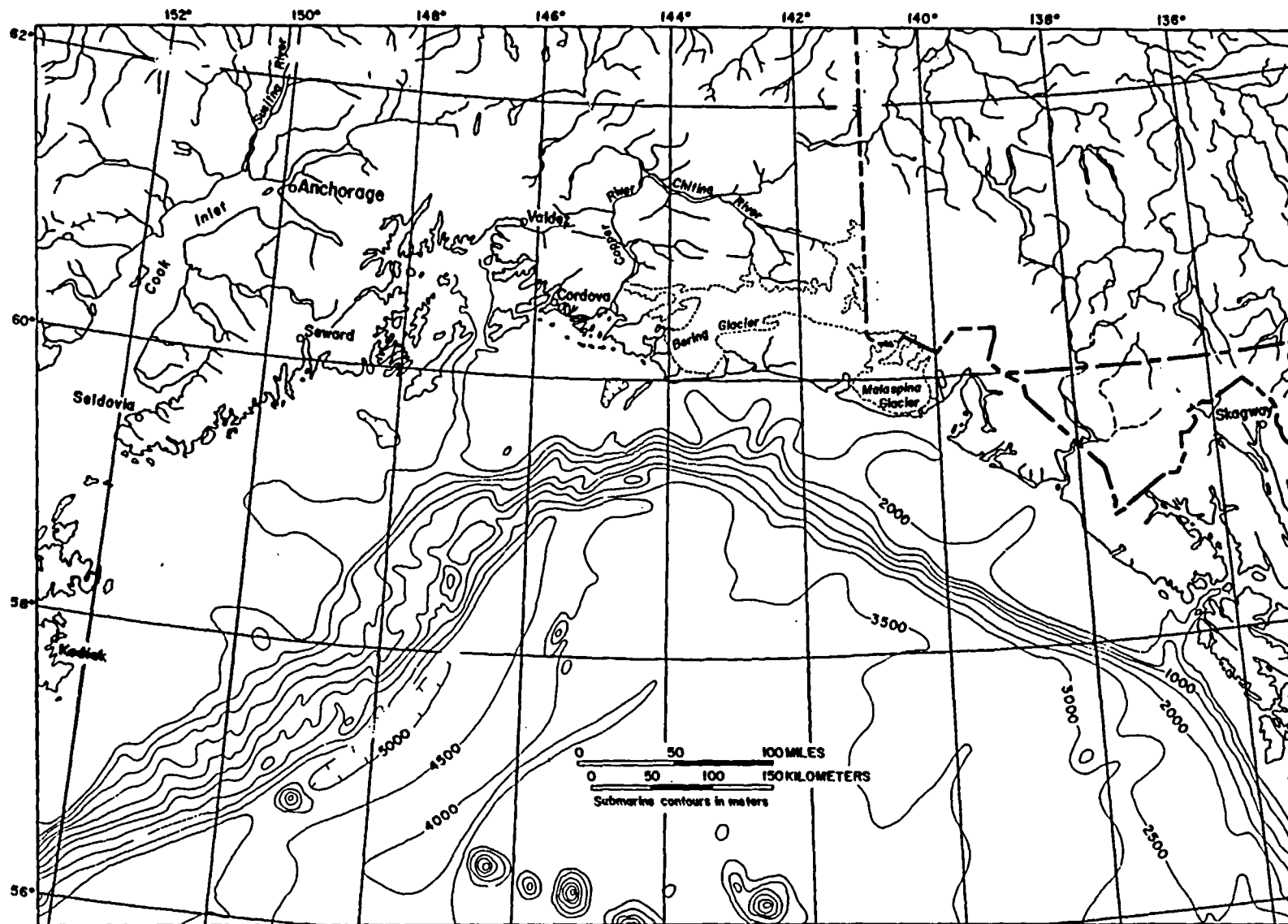


Figure 2A-3 Major structural features along the Gulf of Alaska margin and the northeastern end of the 1964 Alaska earthquake rupture zone (yellow) and known or suspected active faults (red). Fault abbreviations are: AM-Aleutian megathrust; TFS-Transition fault zone; FF-Fairweather fault; KIZ-Kayak Island zone; PZ-Pamplona zone; DRZ-Dangerous River zone; PBF-Patton Bay fault; RMF-Ragged Mountain fault; WF-Wingham fault; RMF-Ragged Mountain fault; CSFS-Chugach-St. Elias fault system; CFS-Contact fault system; CMF-Castle Mountain fault; TF-Totschunda fault; DFS-Denali fault system (Plafker and others, 1994).

2A-14

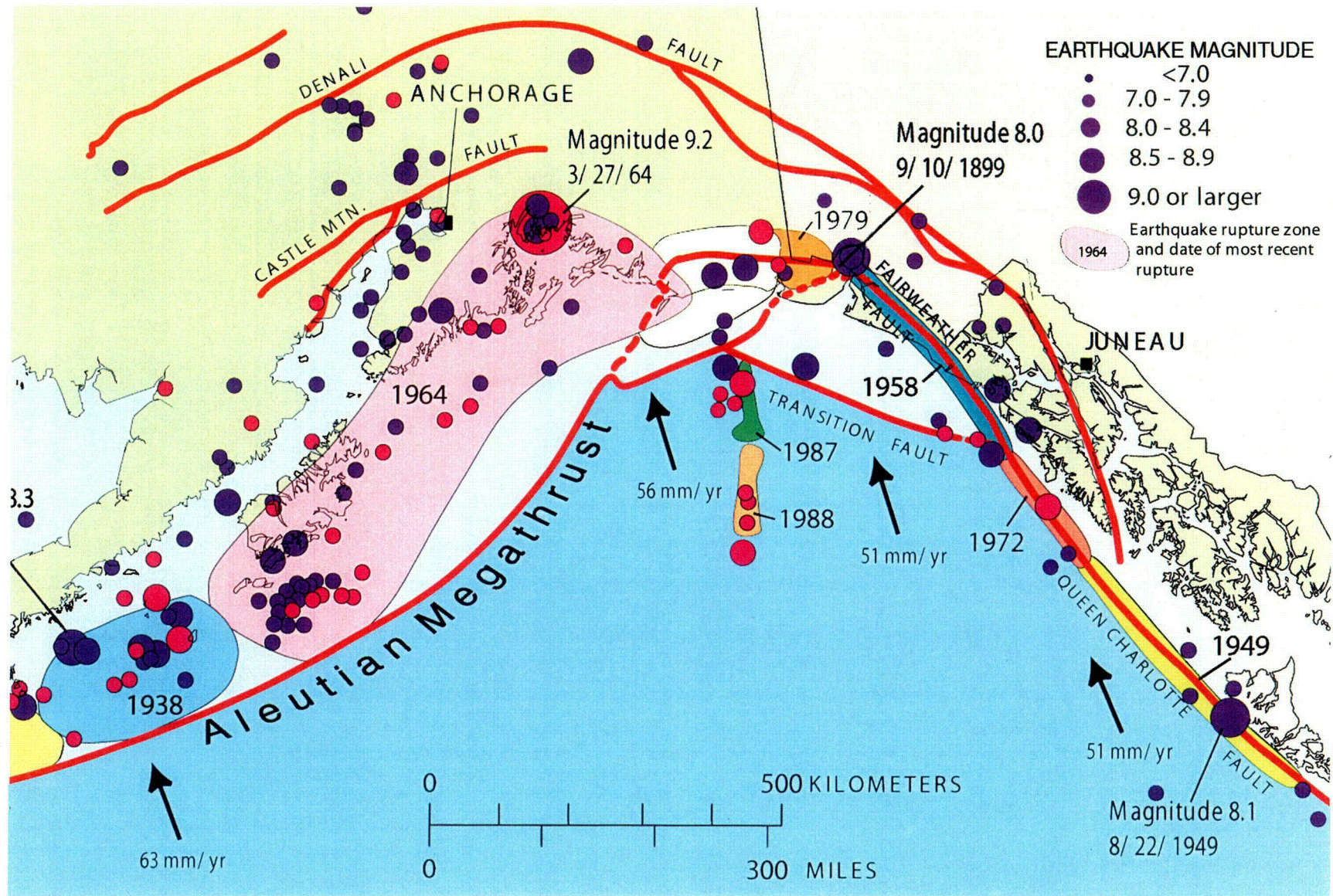


Figure 2A-4 Inferred rupture zones of major plate-boundary earthquakes along the northern Gulf of Alaska margin and location of the "Yakataga seismic gap" (white). Modified from Plafker and others (1994).

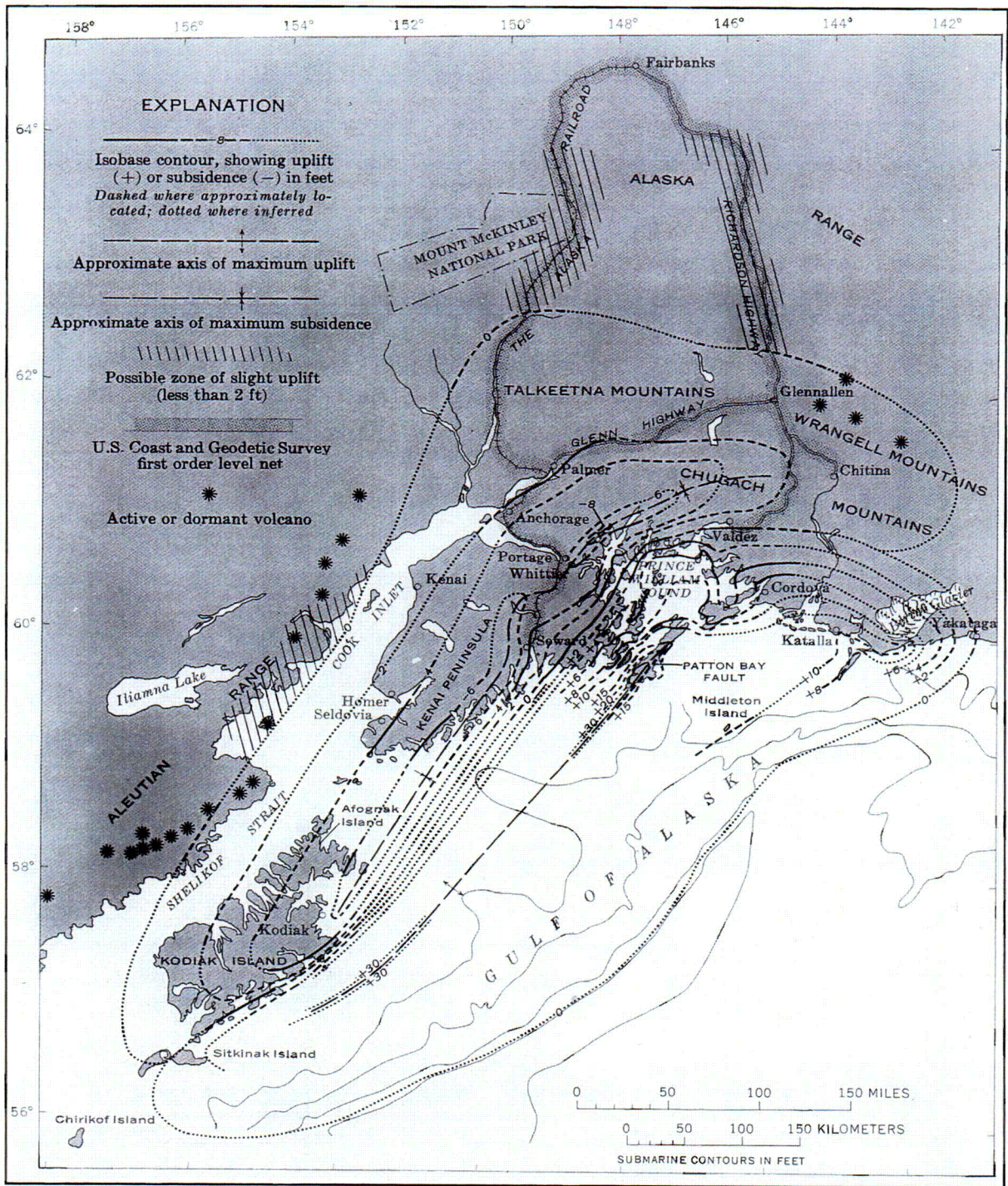
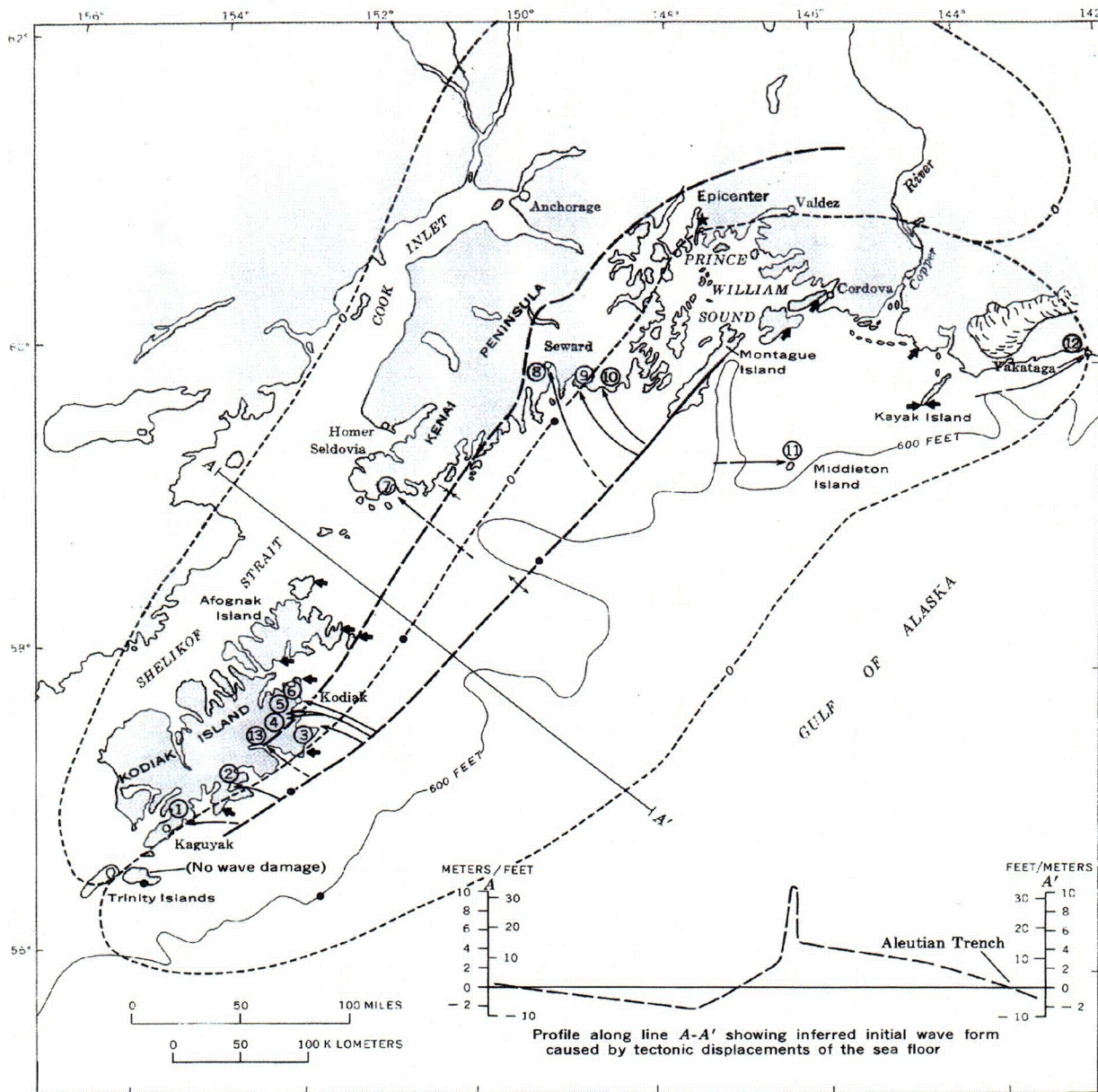


Figure 2A-5 Tectonic uplift and subsidence and surface faults at Montague Island associated with the March 27, 1964 Alaska earthquake. Land level change, in meters, is shown by the contours, which are dashed where approximate or inferred. The outer edge of the continental shelf, at -200 m, is shown by the dotted line. Active or dormant arc volcanoes are shown by stars. The profile shows vertical displacements along line A-A' (dotted where inferred). From Plafker (1965).

S:\5100s\117.009\task_13\02_1230_s2a_fig_02a-05(05).ai



EXPLANATION

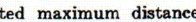
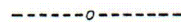
- 
 Wave travel direction inferred from shoreline damage or eyewitness accounts
- 
 Calculated maximum distance travelled by initial wave
Dashed where approximate
- 
 Axis of uplift
Dashed where inferred
- 
 Axis of subsidence
- 
 Zero isobase contour
- 
 Epicenter of major aftershock ($M \geq 6.0$)
- 
 Station listed in table 2

Figure 2A-6 Submarine extension of the zone of maximum uplift and faulting on Montague Island as inferred from movement directions and calculated travel distances of seismic sea waves generated by the tectonic displacements (Plafker, 1969).

S:\5100s\117.009\alask_13102_1230_s2a_fig_02a-06(06).ai

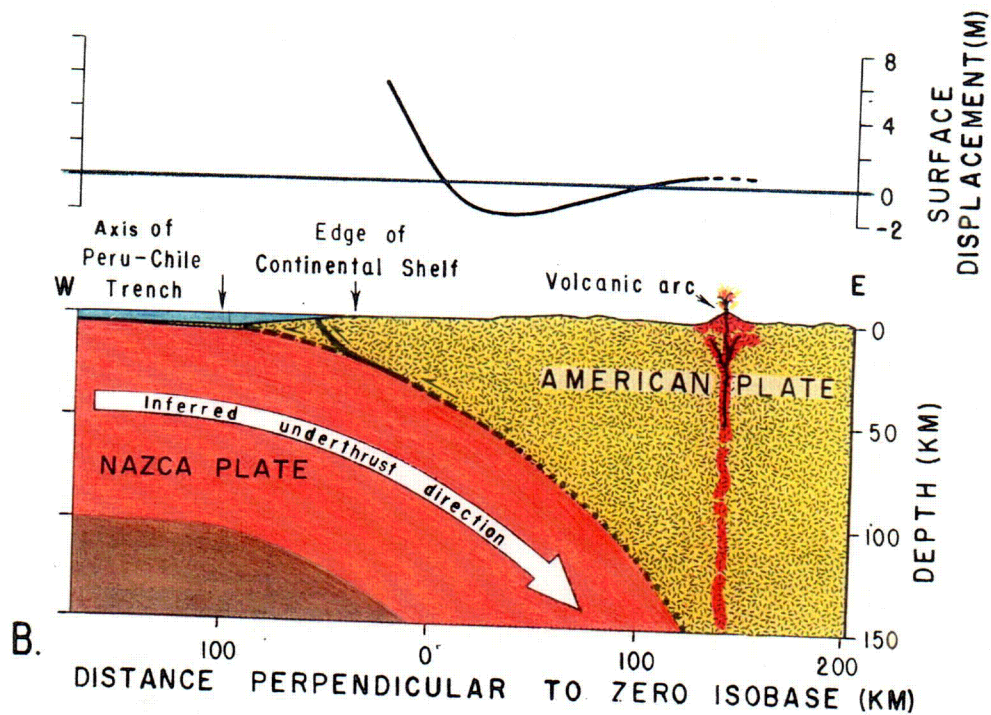
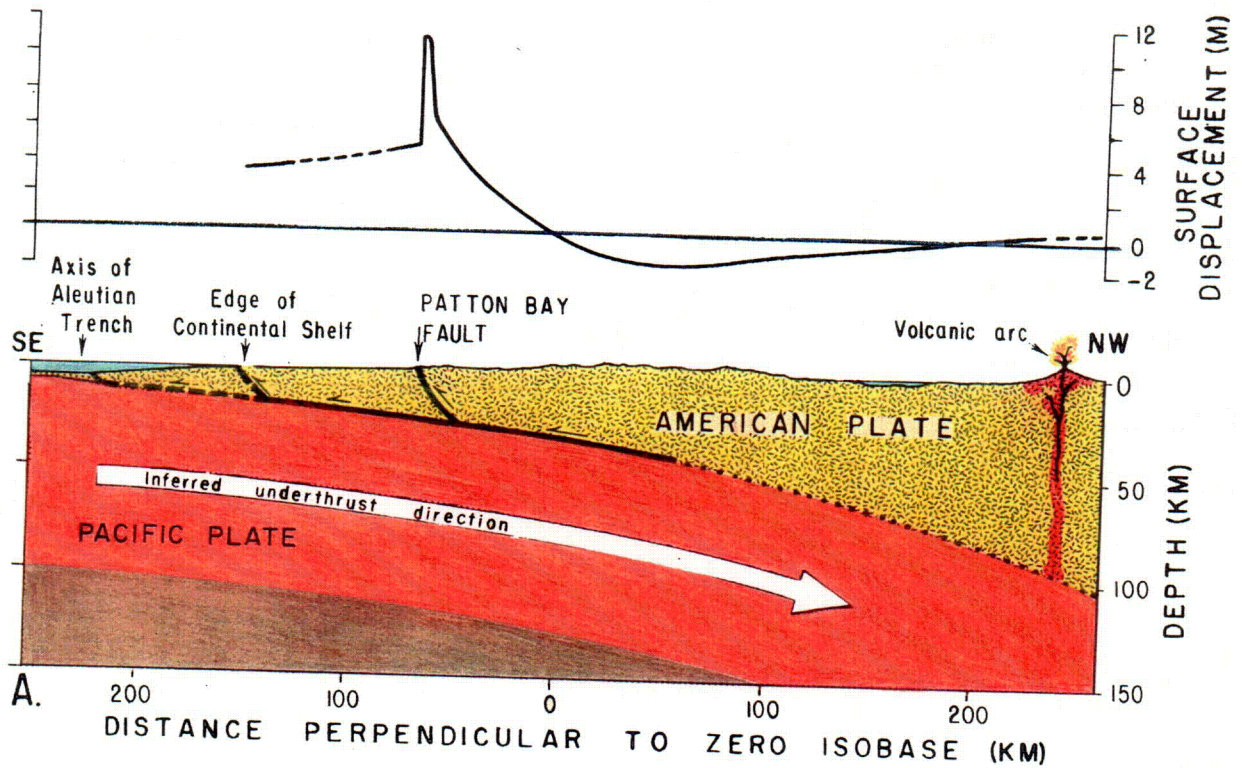


Figure 2A-7 Schematic cross sections showing the suggested mechanisms for (a) the 1964 Alaskan earthquake and (B) the 1960 Chilean earthquake. Inferred earthquake faults are shown by solid lines; possible faults by dashed lines; arrows indicate sense of movement. Dotted lines, possible fault boundaries that did not slip. Profile of vertical displacement above section (A) is the same as in Figure 5 except that it is reversed to have the ocean basin to the left. After Plafker (1972).

S:\5100\117.009\ask_13102_1230_s2a_fig_02a-07(07).ai

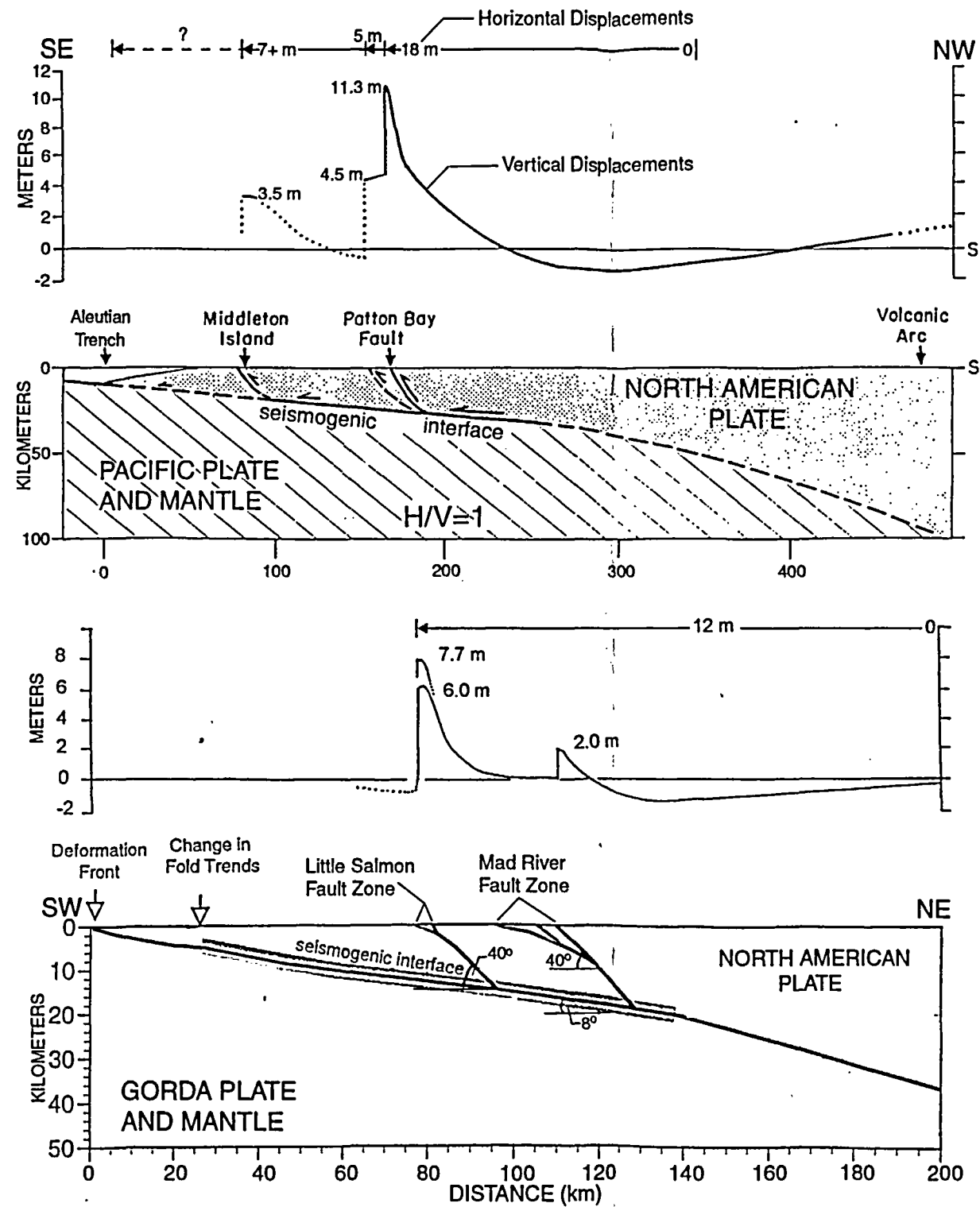


Figure 2A-8 Profile and section of coseismic deformation associated with the 1964 Alaska earthquake (location on Figure 2A-5) and a hypothetical great megathrust earthquake across the southern Cascadia margin (north of Humboldt Bay). (A) Profile of horizontal and vertical components of coseismic slip across the region affected by the 1964 Alaska earthquake (above) and inferred slip partitioning between the megathrust and intraplate faults, assuming average intraplate surface fault dip of 40°-60° (below). (B) Hypothetical profile showing possible vertical component at the Little Salmon fault zone (LSF) and Mad River Fault zone (MRZ) assuming minimum megathrust slip of 12 m and average intraplate surface fault dips of 40°. Two possibilities are shown for vertical displacement assuming either that all 12 m of megathrust slip is transferred to the LSF (7.7 m) or that slip is partitioned between the LSF (6 m) and MRFZ (2 m). Alaska data after Plafker, 1967) and Plafker and others (2000); Cascadia data from Carver and others, (1999).

Appendix 4A

**Logs of Earth Sciences Associates (1977) and
Woodward-Clyde Consultants (1980)
Site Trenches**

Revision 0—September 16, 2002

Appendix 4A

Logs of ESA and WCC Site Trenches

LIST OF FIGURES

Figure 4A-1 Geologic log of Trench BP-1 (*From Earth Sciences Associates, 1977, figures C2 through C34*).

Sheet 1	Explanation of data shown on trench logs
Sheet 2	Trench BP-1, Station 0+00 to 1+10
Sheet 3	Trench BP-1, Station 1+10 to 2+20
Sheet 4	Trench BP-1, Station 2+20 to 3+30
Sheet 5	Trench BP-1, Station 3+30 to 4+40
Sheet 6	Trench BP-1, Station 4+40 to 5+50
Sheet 7	Trench BP-1, Station 5+50 to 6+60
Sheet 8	Trench BP-1, Station 6+60 to 7+70
Sheet 9	Trench BP-1, Station 7+70 to 8+80
Sheet 10	Trench BP-1, Station 8+80 to 9+90
Sheet 11	Trench BP-1, Station 9+90 to 11+00
Sheet 12	Trench BP-1, Station 11+00 to 12+10
Sheet 13	Trench BP-1, Station 12+10 to 13+20
Sheet 14	Trench BP-1, Station 13+20 to 13+75
Sheet 15	Trench BP-1, Station 13+75 to 14+41
Sheet 16	Trench BP-1, Station 14+41 to 15+25
Sheet 17	Trench BP-1, Station 15+25 to 16+10
Sheet 18	Trench BP-1, Station 16+10 to 16+45

Figure 4A-2 Geologic log of northeastern part of trench BP-2 (*Modified from Earth Sciences Associates, 1977, Figure C37*)

Figure 4A-3 Geologic log of trench BP-3 (*Modified from Earth Sciences Associates, 1977, Figure C38*)

Figure 4A-4 Geologic log of trench BP-4 (*From Earth Sciences Associates, 1977, Figure C35*)

Figure 4A-5 Geologic log of trench BP-5 (*From Earth Sciences Associates, 1977, Figure C40*)

Figure 4A-6 Geologic log of trench BP-6A (*From Earth Sciences Associates, 1977, Figure C41*)



APPENDIX 4A
LIST OF FIGURES (Continued)

Figure 4A-7 Geologic log of trench BP-6B (*From Earth Sciences Associates, 1977, Figure C42*)

Figure 4A-8 Geologic log of trench BP-7 (*From Earth Sciences Associates, 1977, Figure C43*)

Figure 4A-9 Geologic log of trench BP-8 (*From Earth Sciences Associates, 1977, Figure C44*)

Figure 4A-10 Geologic log of trench BP-9 (*From Earth Sciences Associates, 1977, Figure C45*)

Note: A geologic log of trench BP-10 is not included in Annex B because "Field inspections of this trench revealed no offsets, but caving and partial flooding by rain water prevented making a detailed geologic log." (Earth Sciences Associates, 1977, Appendix C).

Figure 4A-11 Composite stratigraphic section and lithologic descriptions of trenches 11-T6a, 11-T6b and 11-T6c (*Modified from Woodward-Clyde Consultants, 1980, Appendix C*).

Figure 4A-12 Log of Trench 11-T6a (*From Woodward-Clyde Consultants, 1980, Figure C-29*).

Sheet 1	Trench 11-T6a, Station 0 to 50
Sheet 2	Trench 11-T6a, Station 50 to 103
Sheet 3	Trench 11-T6a, Station 103 to 178
Sheet 4	Trench 11-T6a, Station 178 to 228

Figure 4A-13 Detail of stratigraphy in trench 11-T6a at station 75.5 meters (*From Woodward-Clyde Consultants, 1980, Figure C-30a*).

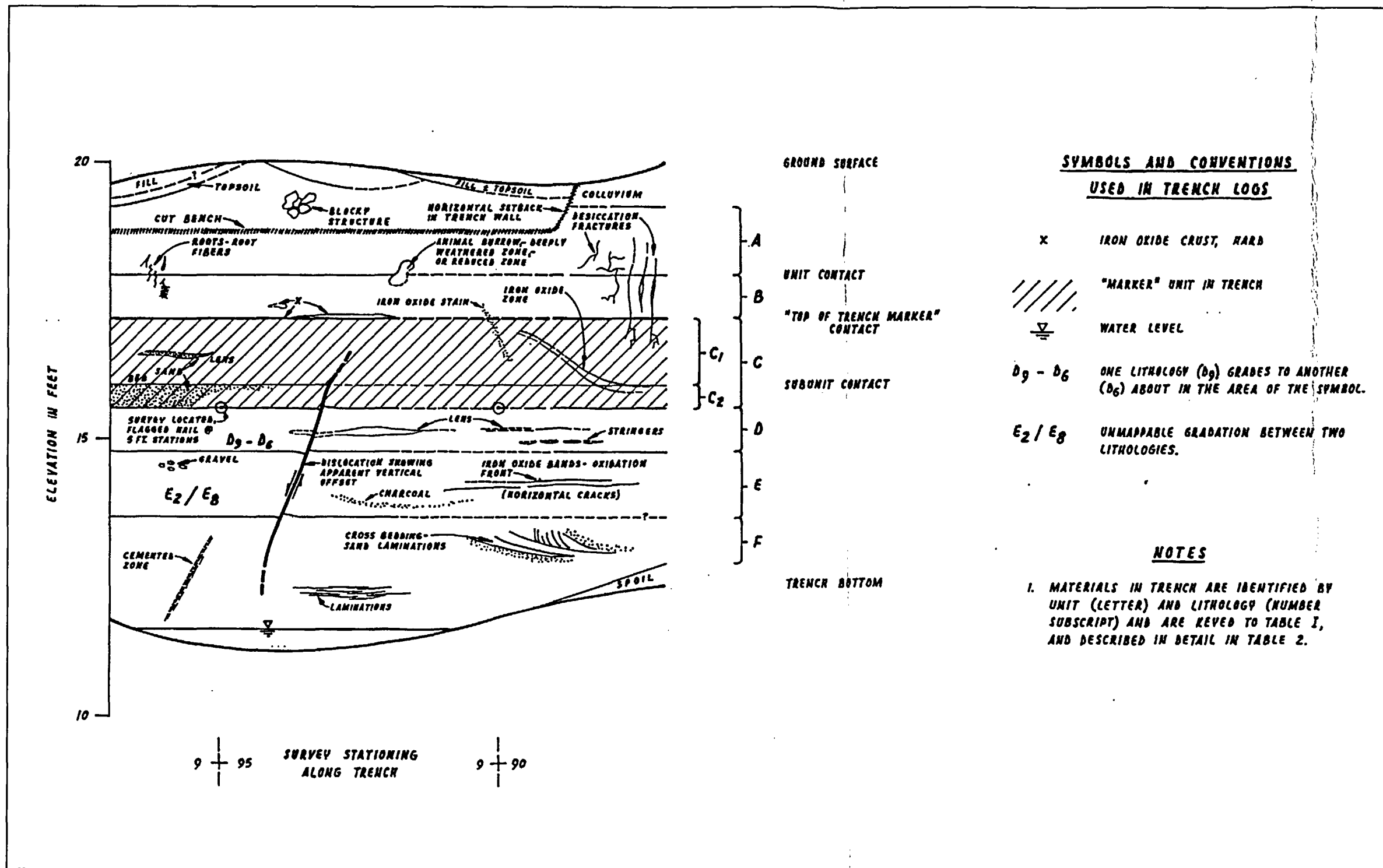
Figure 4A-14 Detail of stratigraphy in trench 11-T6a at station 128 meters (*From Woodward-Clyde Consultants, 1980, Figure C-30b*).

Figure 4A-15 Detail of stratigraphy in trench 11-T6a at station 200 meters (*From Woodward-Clyde Consultants, 1980, Figure C-30c*).

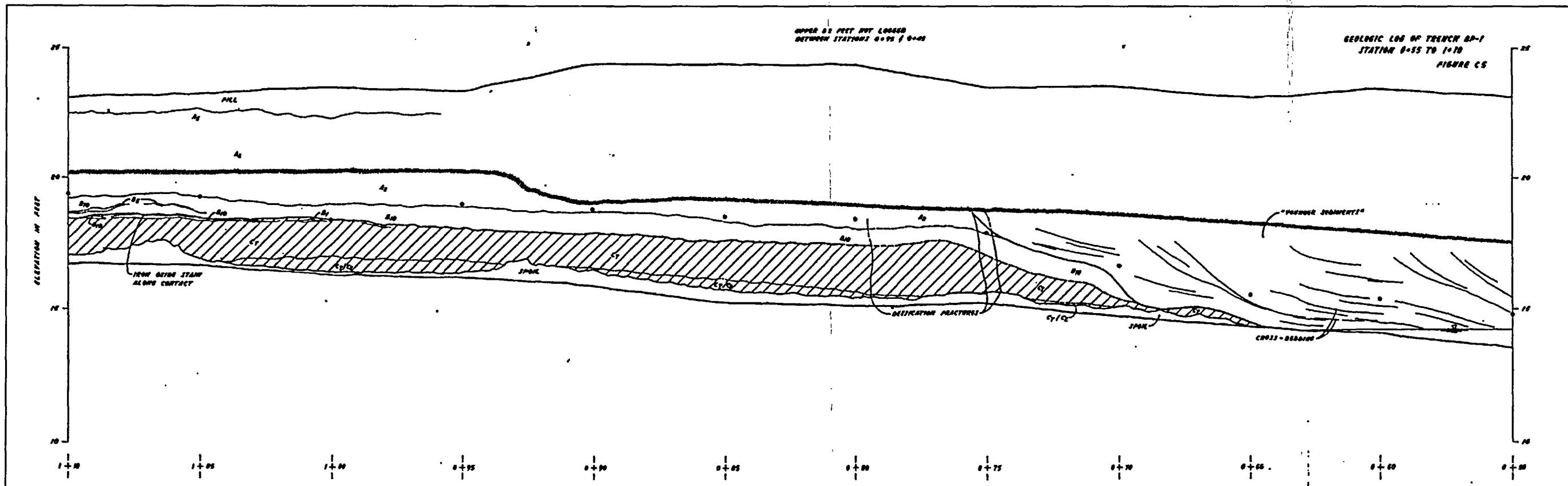
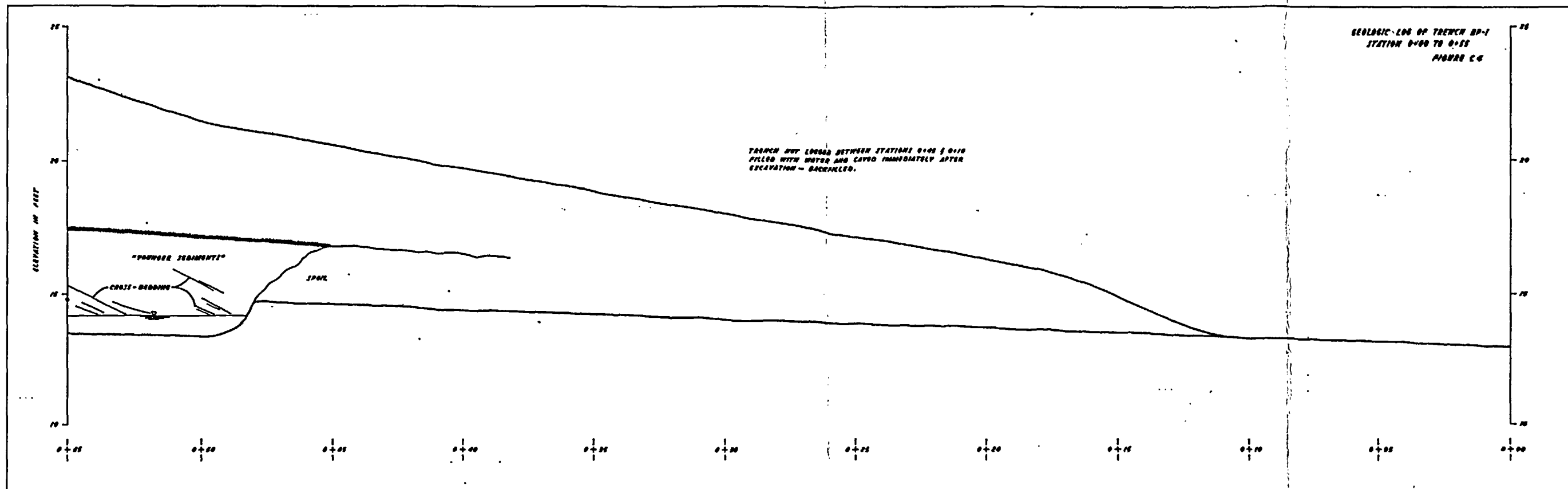
Figure 4A-16 Log of trench 11-T6b (*Modified from Woodward-Clyde Consultants, 1980, Figure C-33*).

Figure 4A-17 Log of trench 11-T6c (*Modified from Woodward-Clyde Consultants, 1980, Figure C-35*).



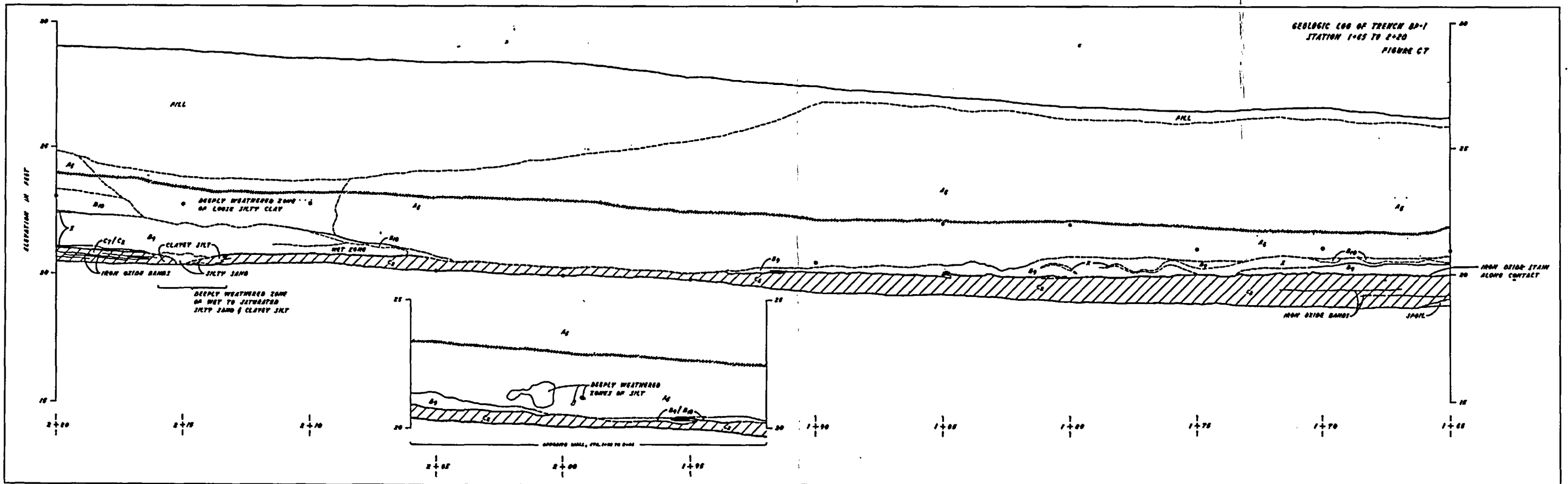
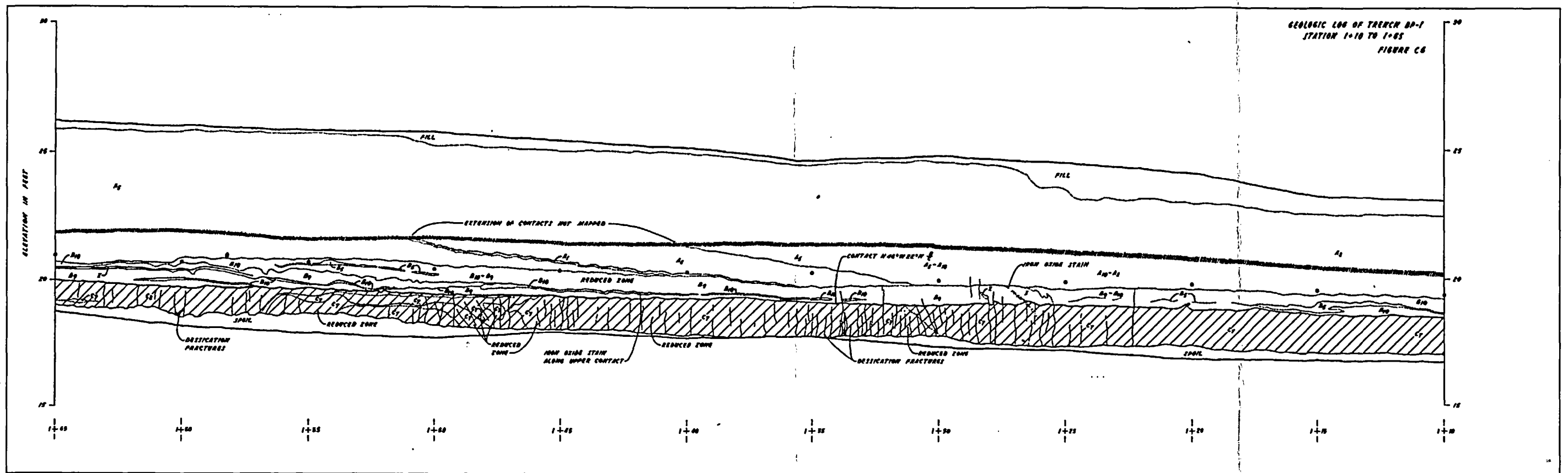


Explanation of data shown on Earth Sciences Associates (1977) trench logs (From Earth Sciences Associates, 1977, Figures C2).



Log of trench BP-1, Station 0+00 to 1+10 (From Earth Sciences Associates, 1977, figures C4 and C5). See Figure 4-2 for location of trench. Station numbers are in feet measured from the eastern end of trench.

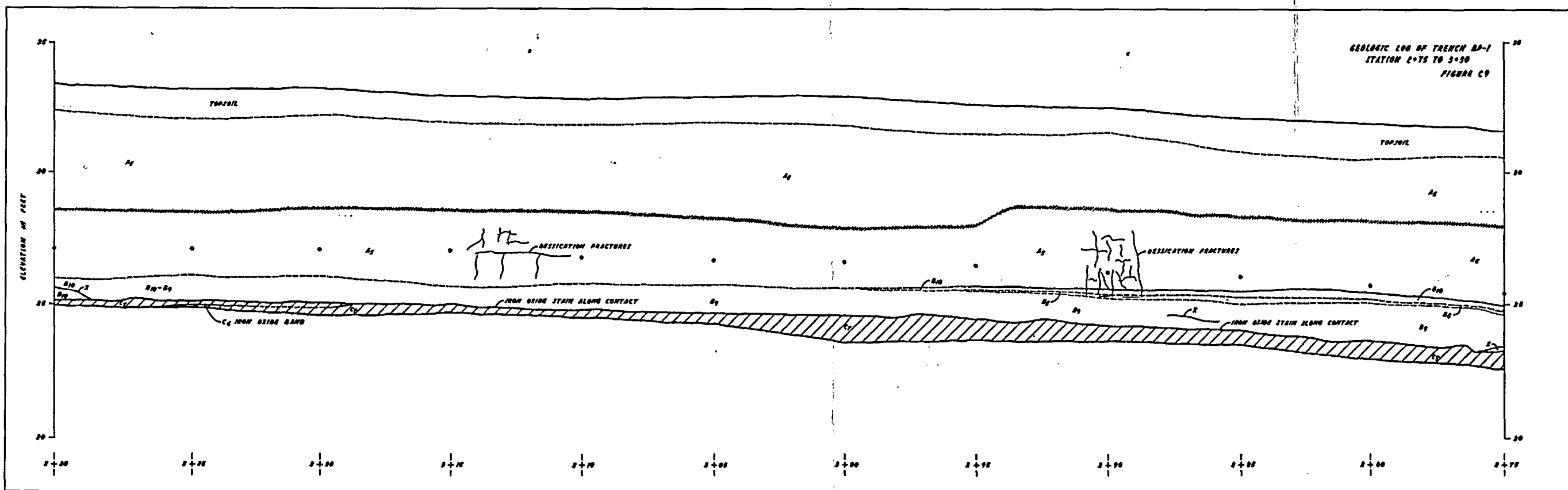
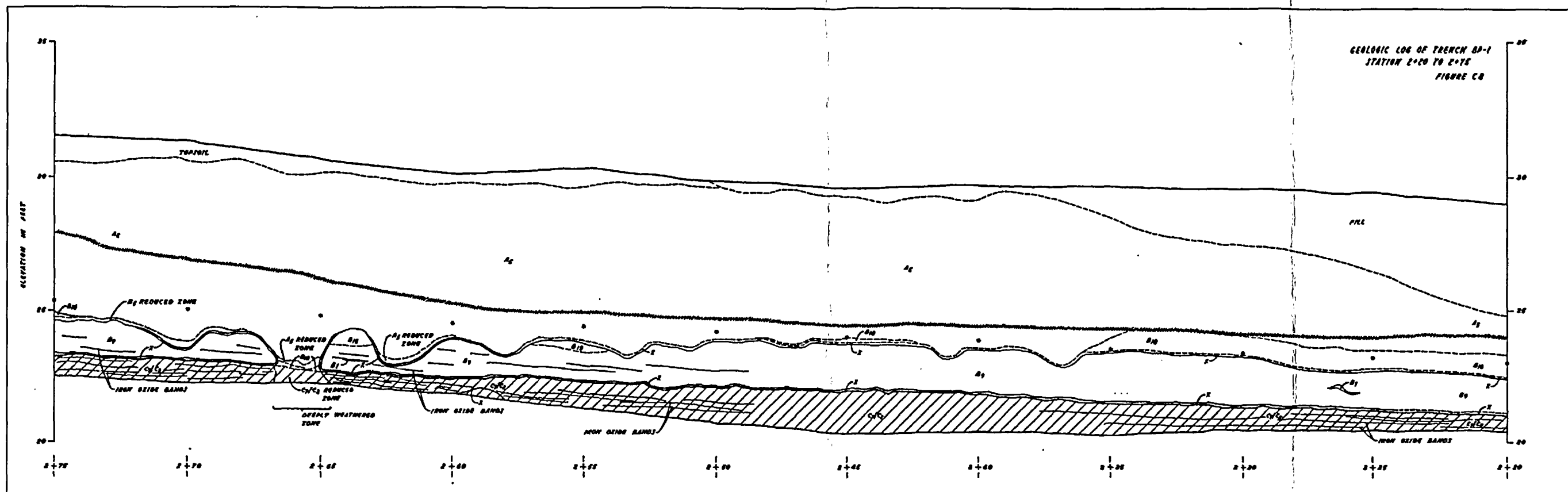
Figure 4A-1 - Sheet 2 of 18



Log of trench BP-1, Station 1+10 to 2+20 (From Earth Sciences Associates, 1977, figures C6 and C7). See Figure 4-2 for location of trench. Station numbers are in feet measured from the eastern end of trench.

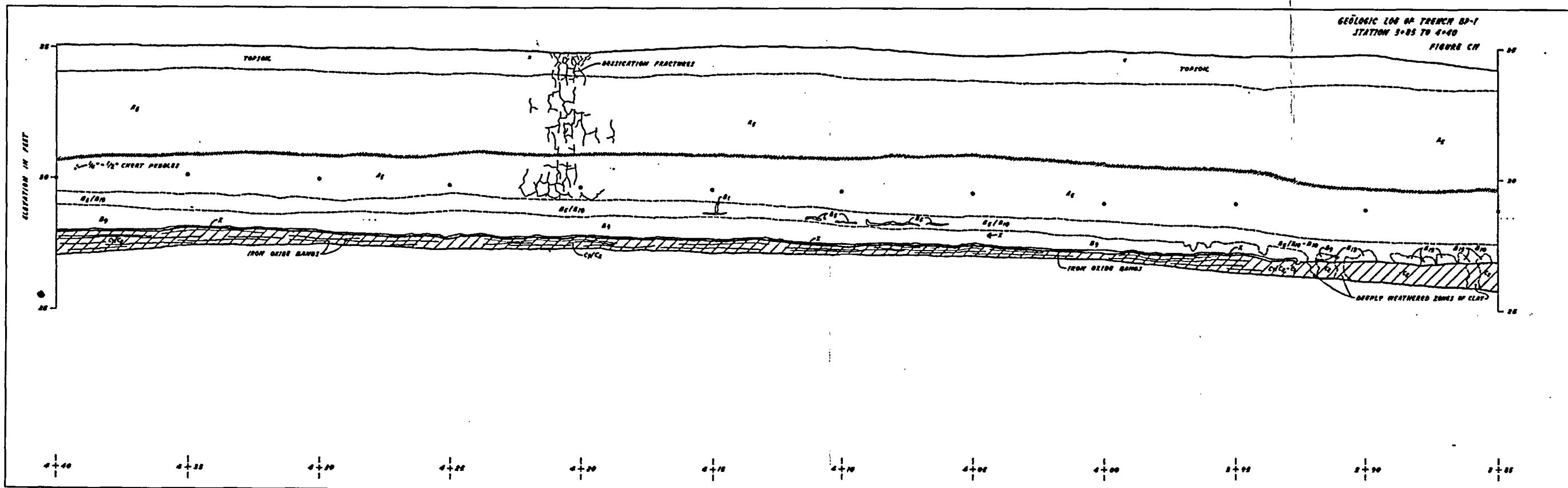
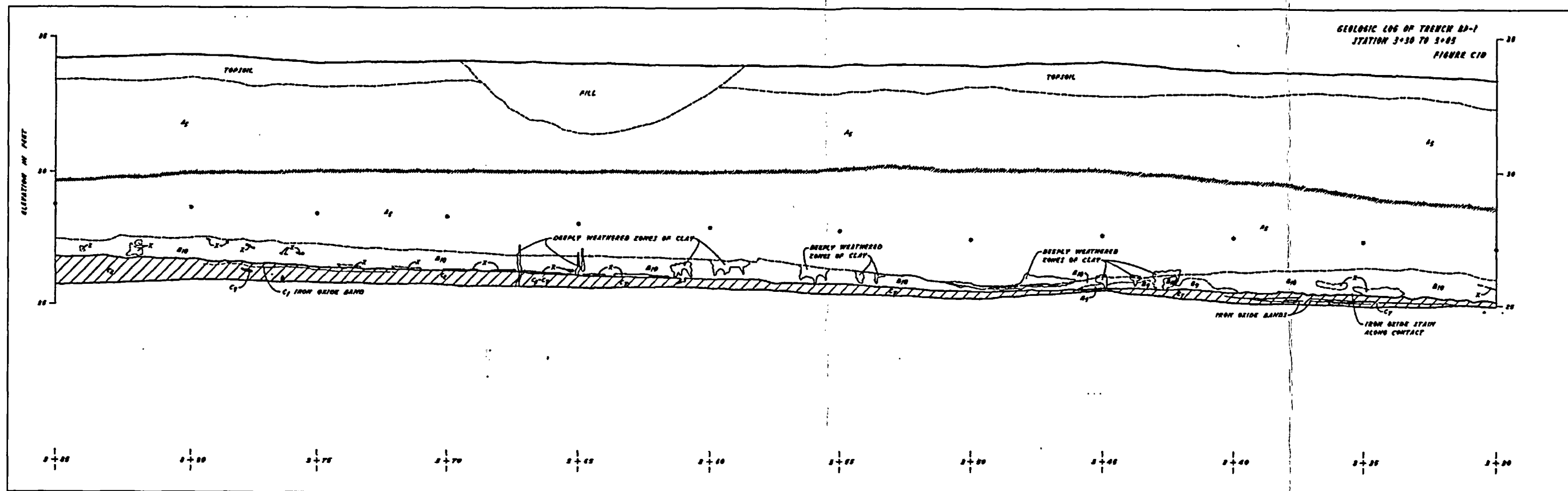
Figure 4A-1 - Sheet 3 of 18

S:\15100s151\17.009task_13102_0916_s4a\fig_4A-01-03(24).ai



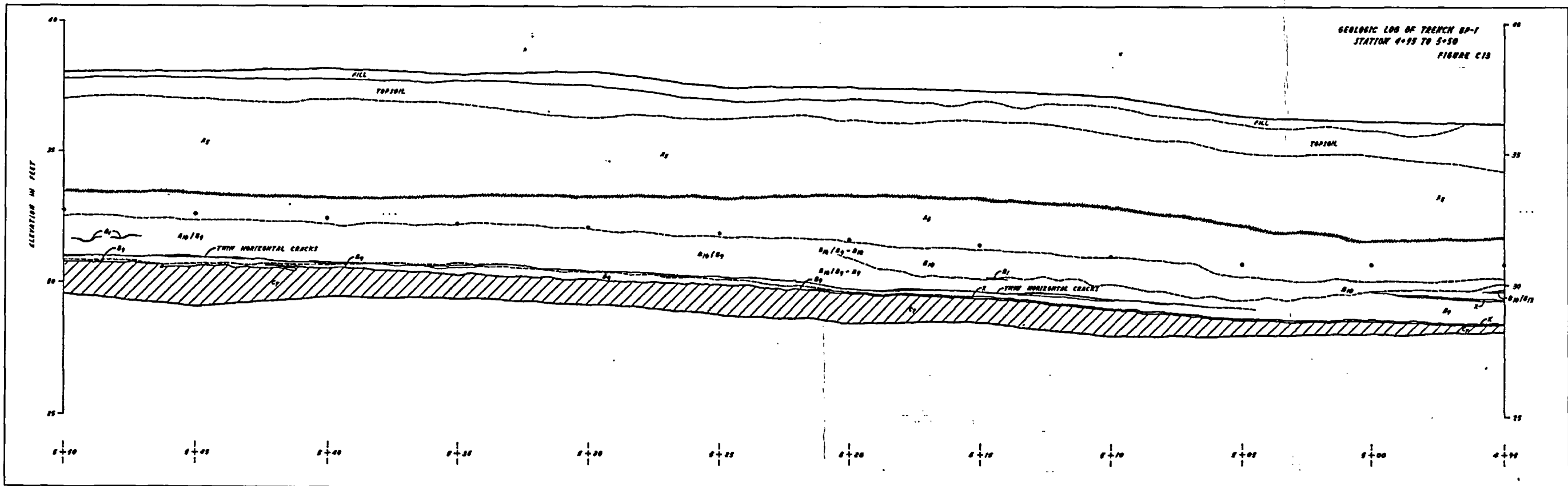
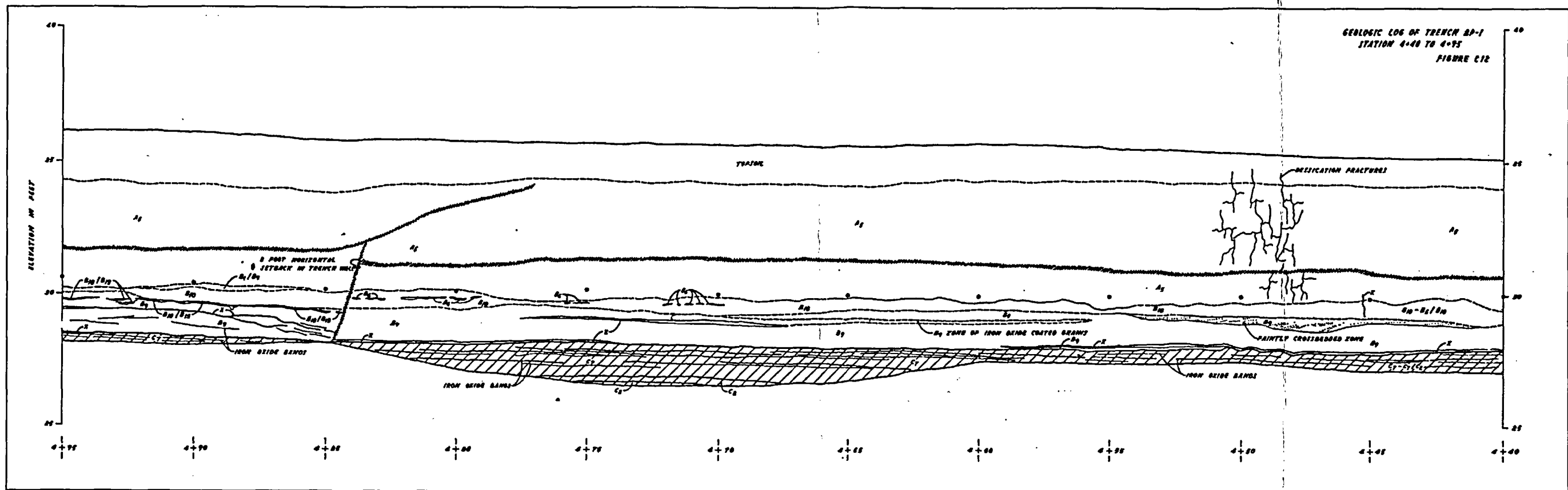
Log of trench BP-1, Station 2+20 to 3+30 (From Earth Sciences Associates, 1977, figures C8 and C9). See Figure 4-2 for location of trench. Station numbers are in feet measured from the eastern end of trench.

Figure 4A-1 - Sheet 4 of 18



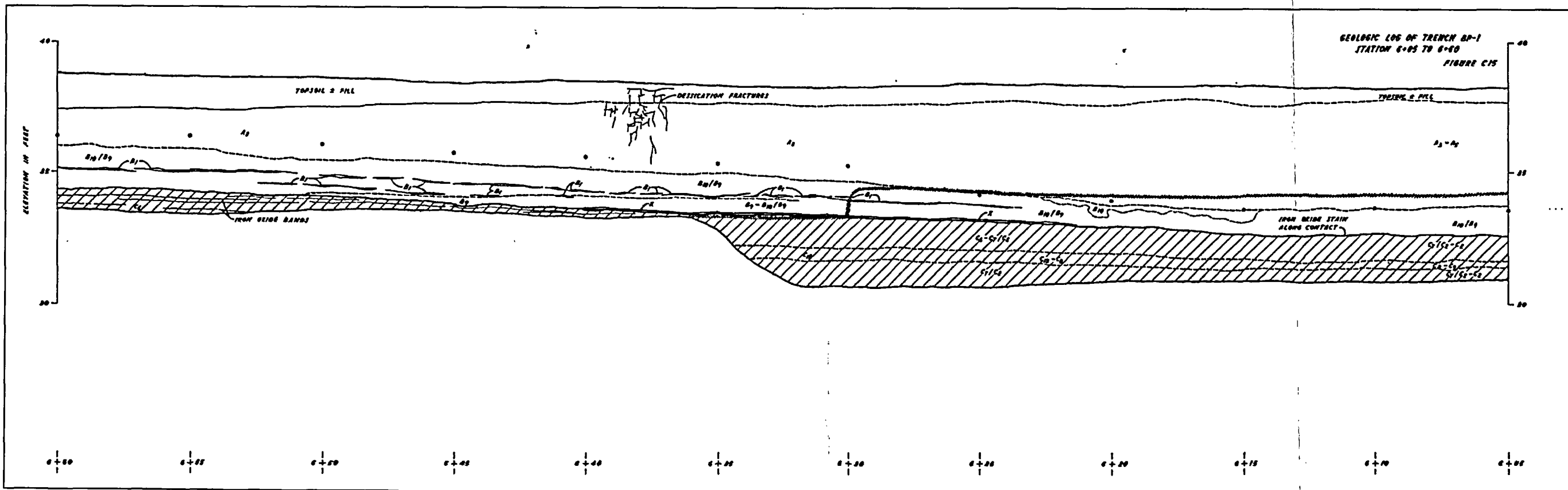
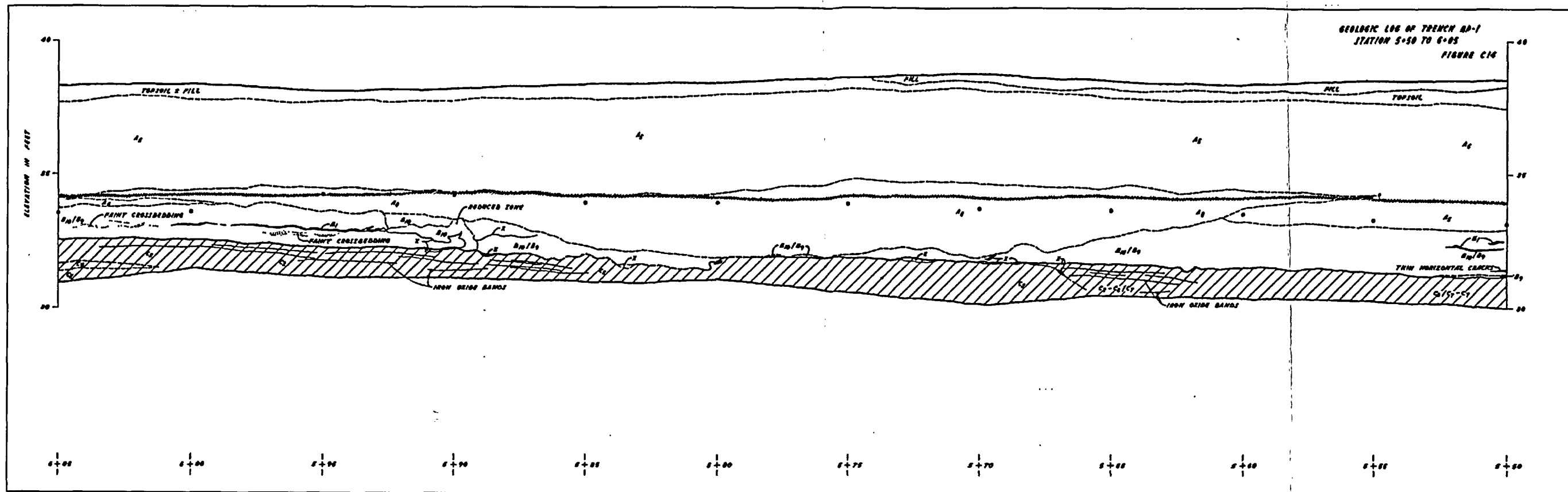
Log of trench BP-1, Station 3+30 to 4+40 (From Earth Sciences Associates, 1977, figures C10 and C11). See Table 4-2 for location of trench. Station numbers are in feet measured from the eastern end of trench.

Figure 4A-1 - Sheet 5 of 18



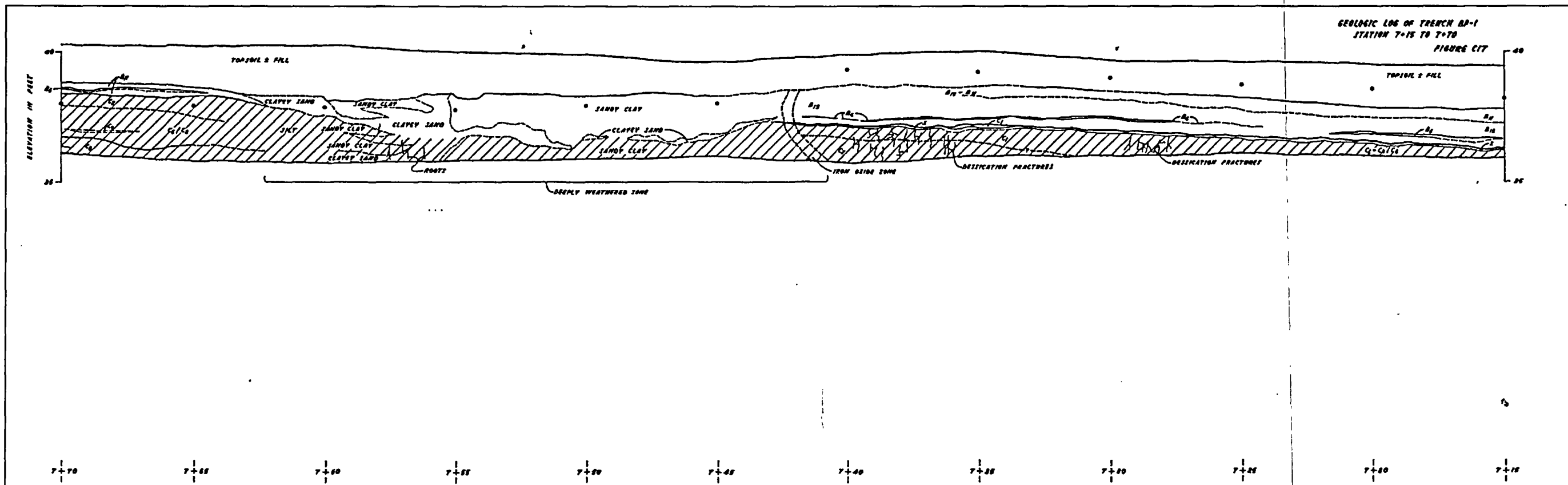
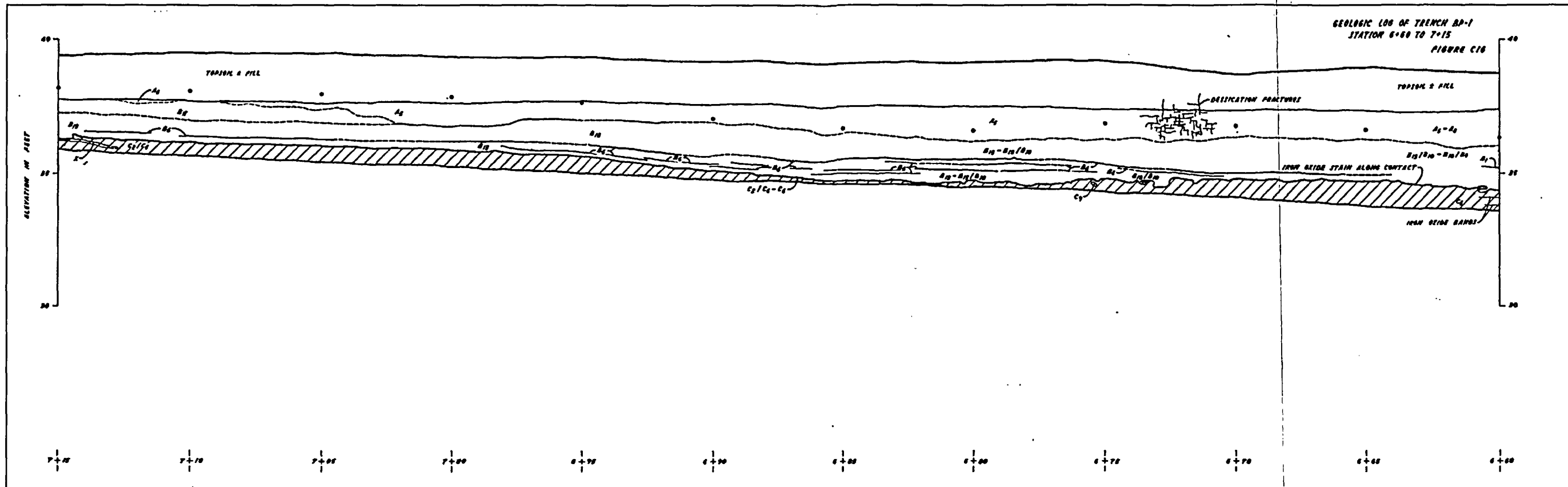
Log of trench BP-1, Station 4+40 to 5+50 (From Earth Sciences Associates, 1977, figures C12 and C13). See Figure 4-2 for location of trench. Station numbers are in feet measured from the eastern end of trench.

Figure 4A-1 - Sheet 6 of 18



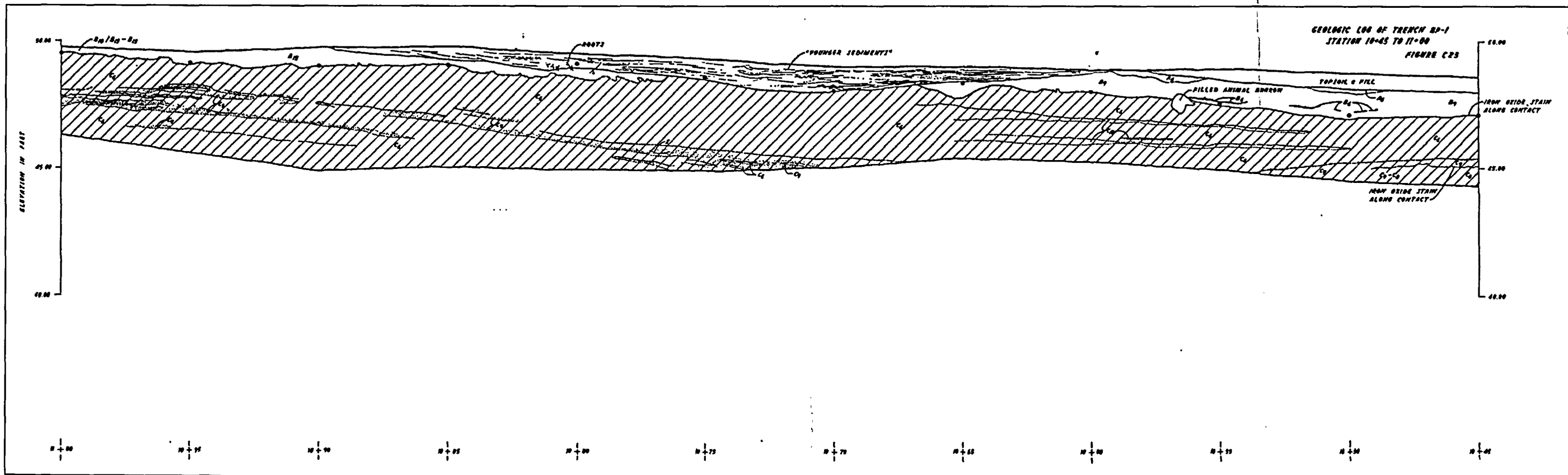
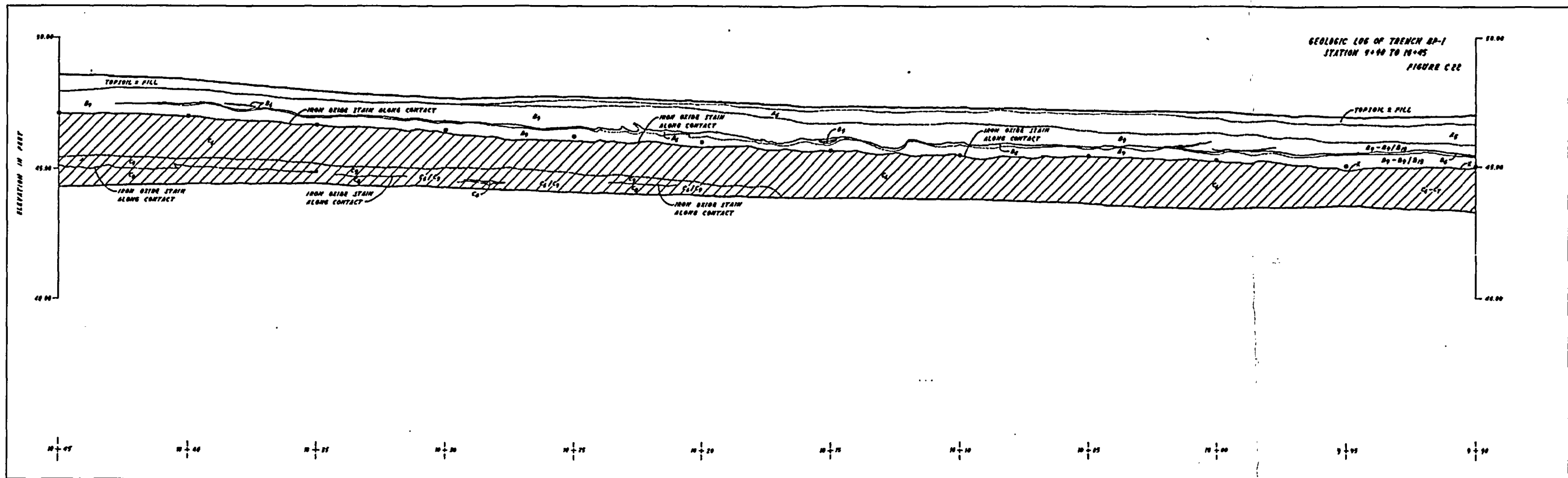
Log of trench BP-1, Station 5+50 to 6+60 (From Earth Sciences Associates, 1977, figures C14 and C15). See Figure 4-2 for location of trench. Station numbers are in feet measured from the eastern end of trench.

Figure 4A-1 - Sheet 7 of 18



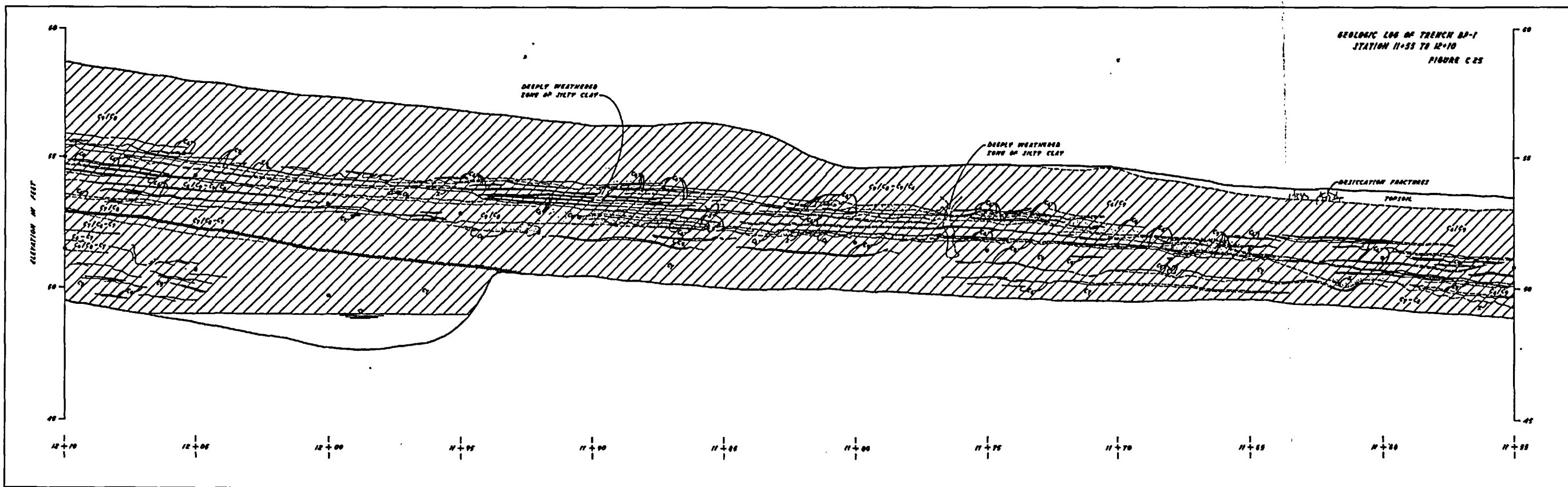
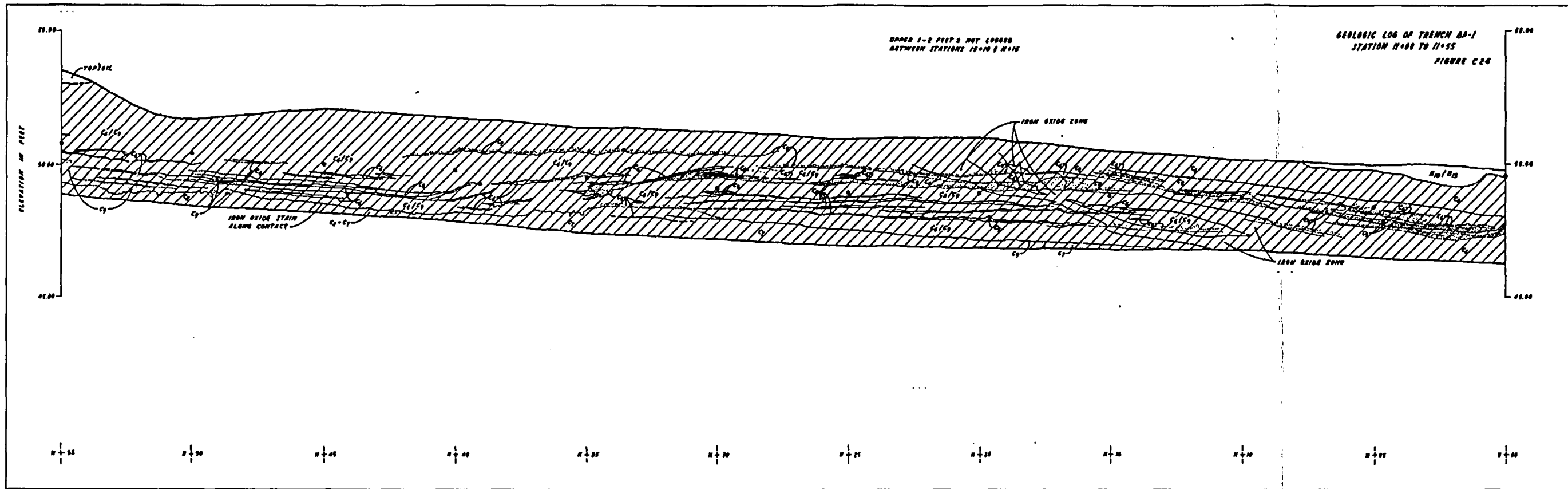
Log of trench BP-1, Station 6+60 to 7+70 (From Earth Sciences Associates, 1977, figures C16 and C17). See Figure 4-2 for location of trench. Station numbers are in feet measured from the eastern end of trench.

Figure 4A-1 - Sheet 8 of 18



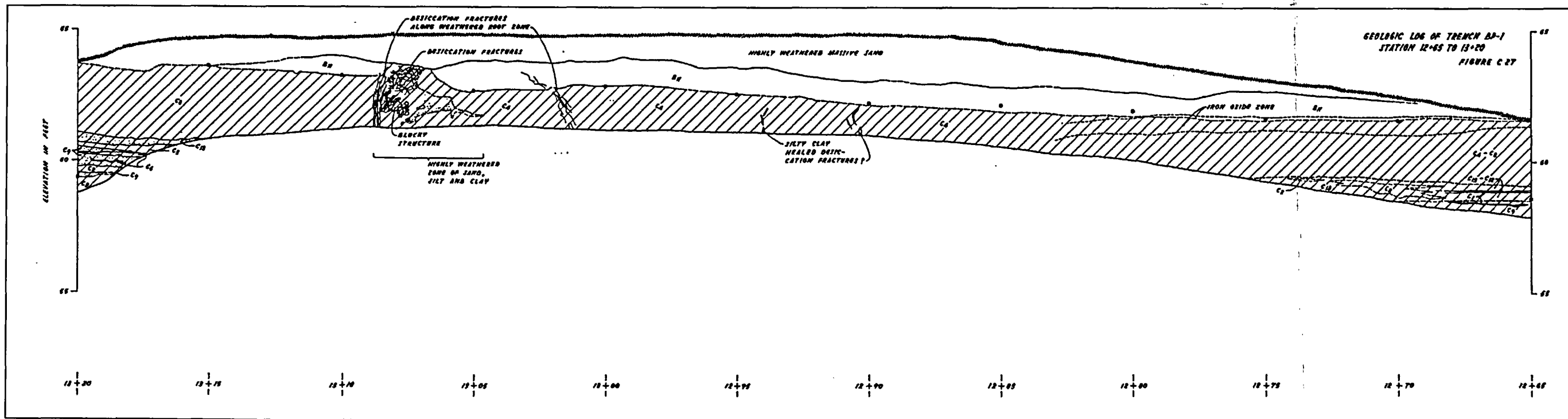
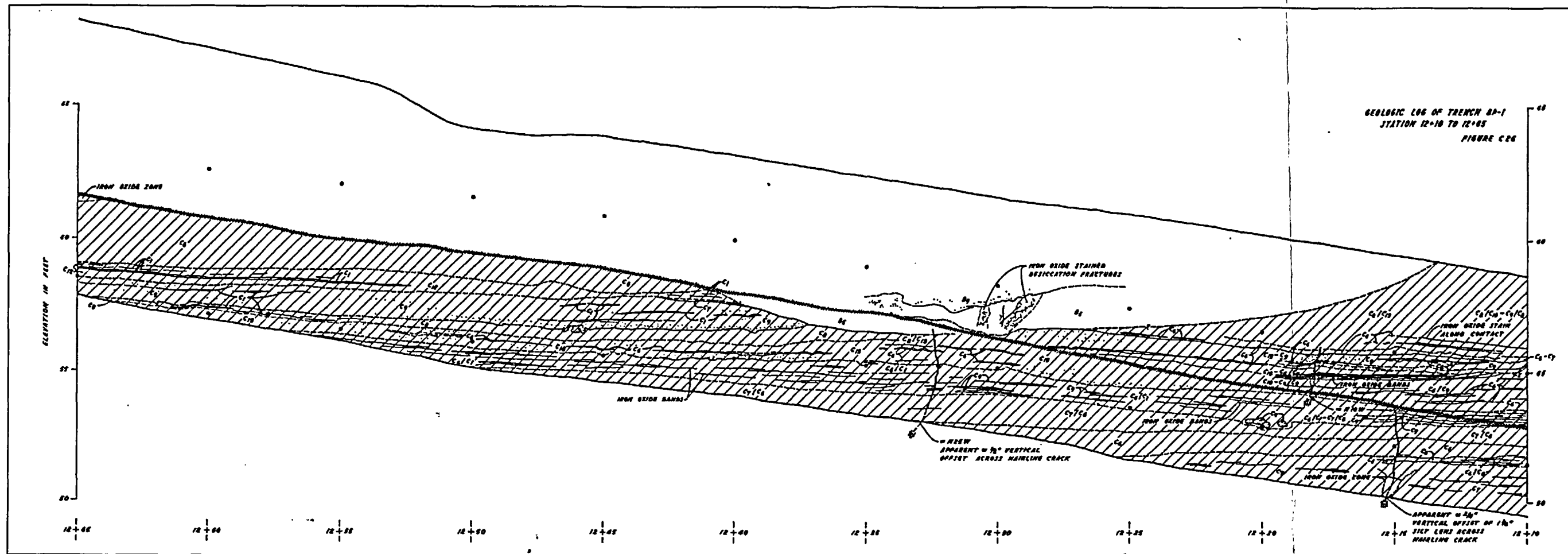
Log of trench BP-1, Station 9+90 to 11+00 (From Earth Sciences Associates, 1977, figures C22 and C23). See Figure 4-2 for location of trench. Station numbers are in feet measured from the eastern end of trench.

Figure 4A-1 - Sheet 11 of 18



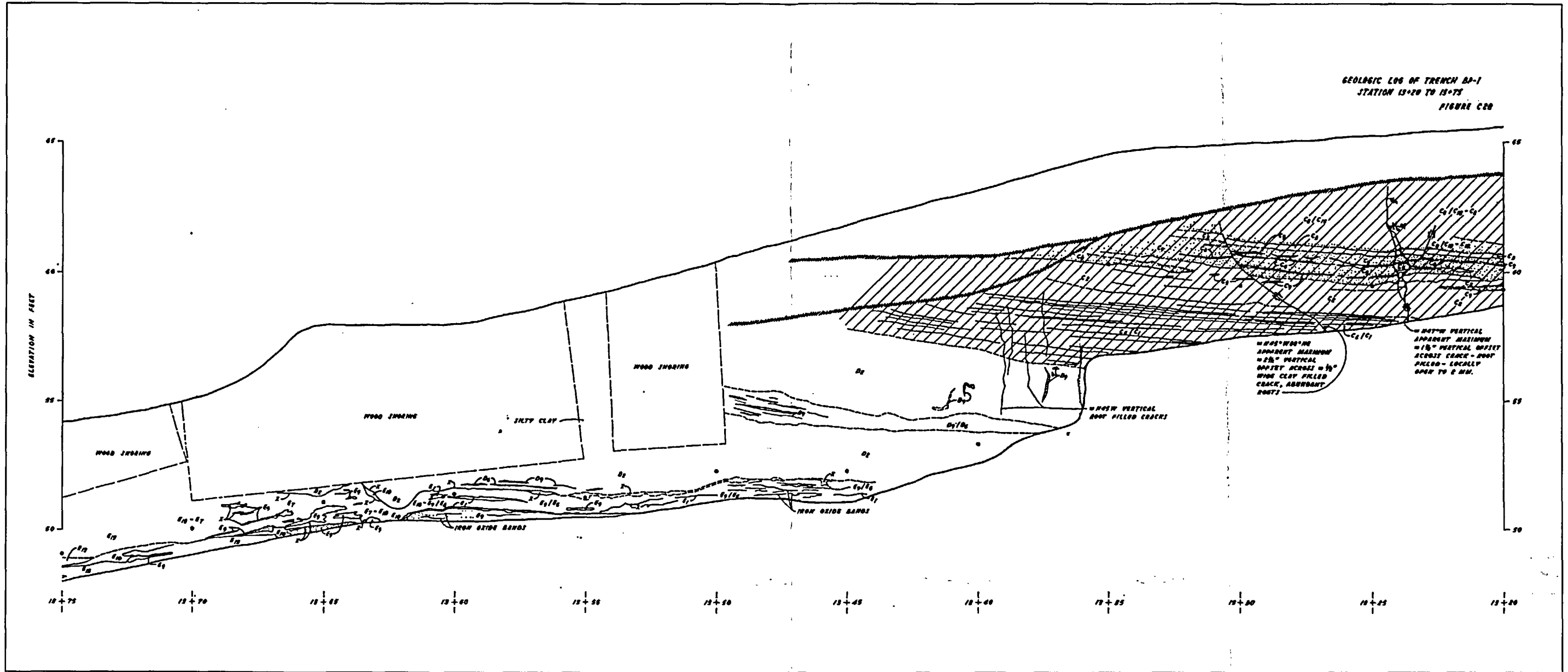
Log of trench BP-1, Station 11+00 to 12+10 (From Earth Sciences Associates, 1977, figures C24 and C25). See Figure 4-2 for location of trench. Station numbers are in feet measured from the eastern end of trench.

Figure 4A-1 - Sheet 12 of 18



Log of trench BP-1, Station 12+10 to 13+20 (From Earth Sciences Associates, 1977, figures C26 and C27). See Figure 4-2 for location of trench. Station numbers are in feet measured from the eastern end of trench.

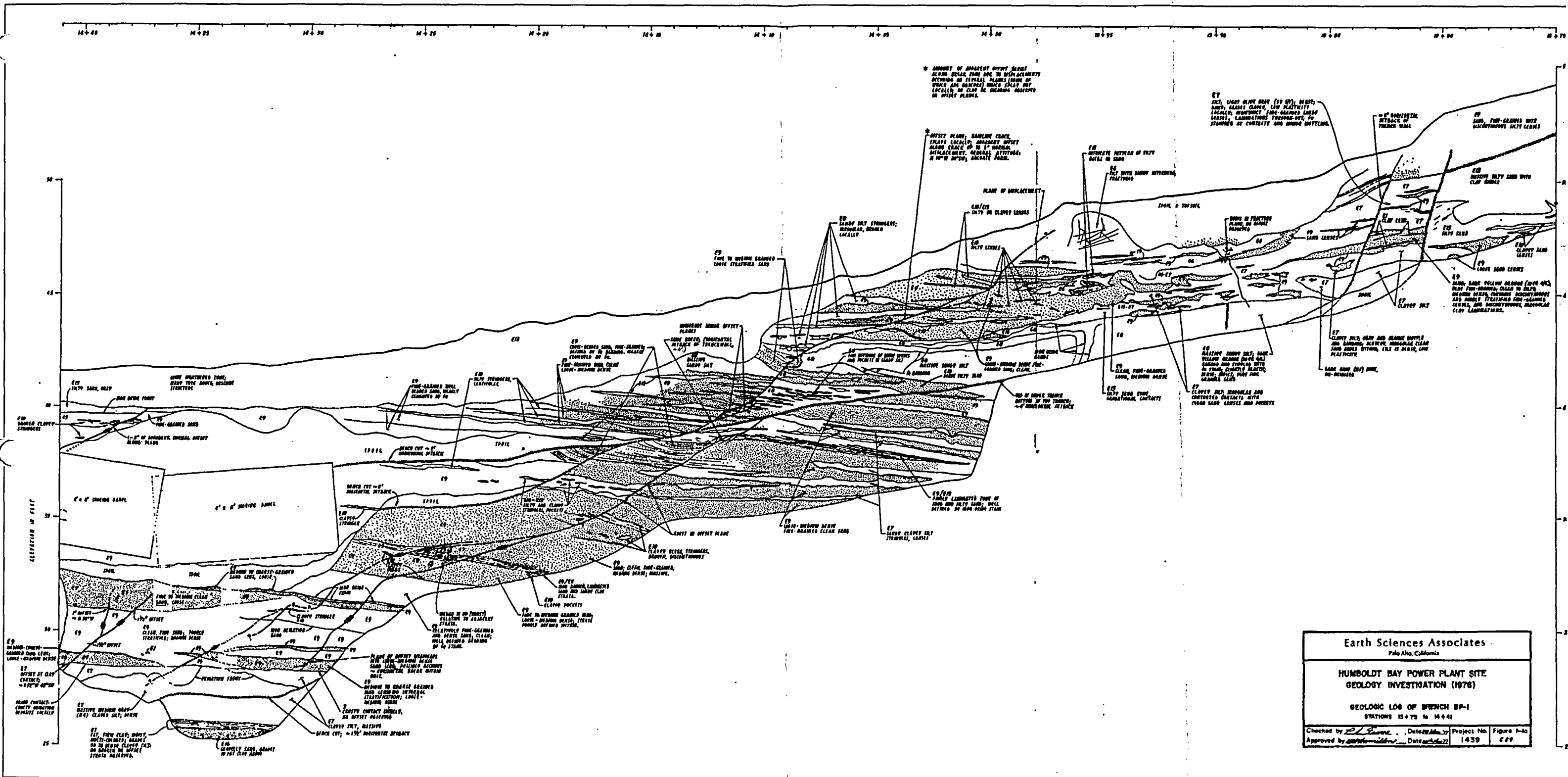
Figure 4A-1 - Sheet 13 of 18



Log of trench BP-1, Station 13+20 to 13+75 (From Earth Sciences Associates, 1977, figure C28). See Figure 4-2 for location of trench. Station numbers are in feet measured from the eastern end of trench.

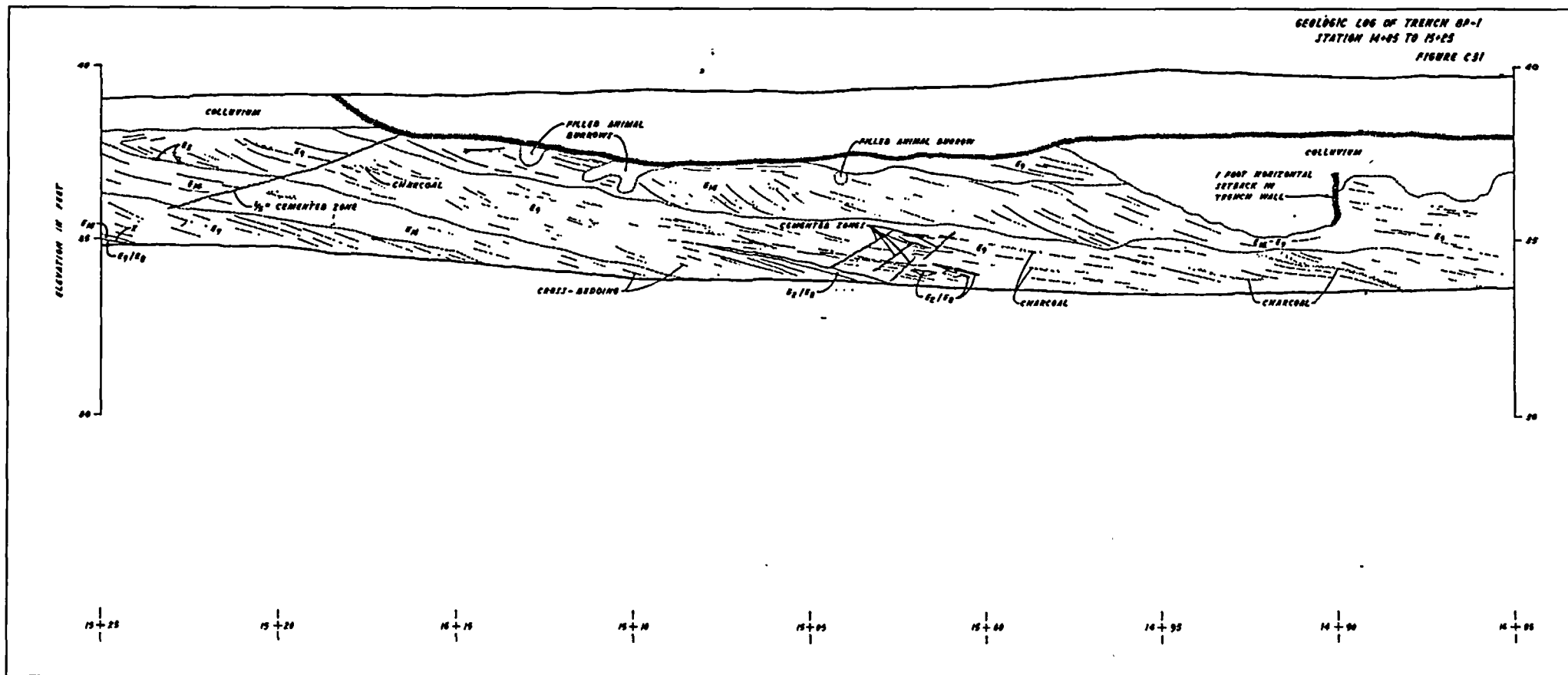
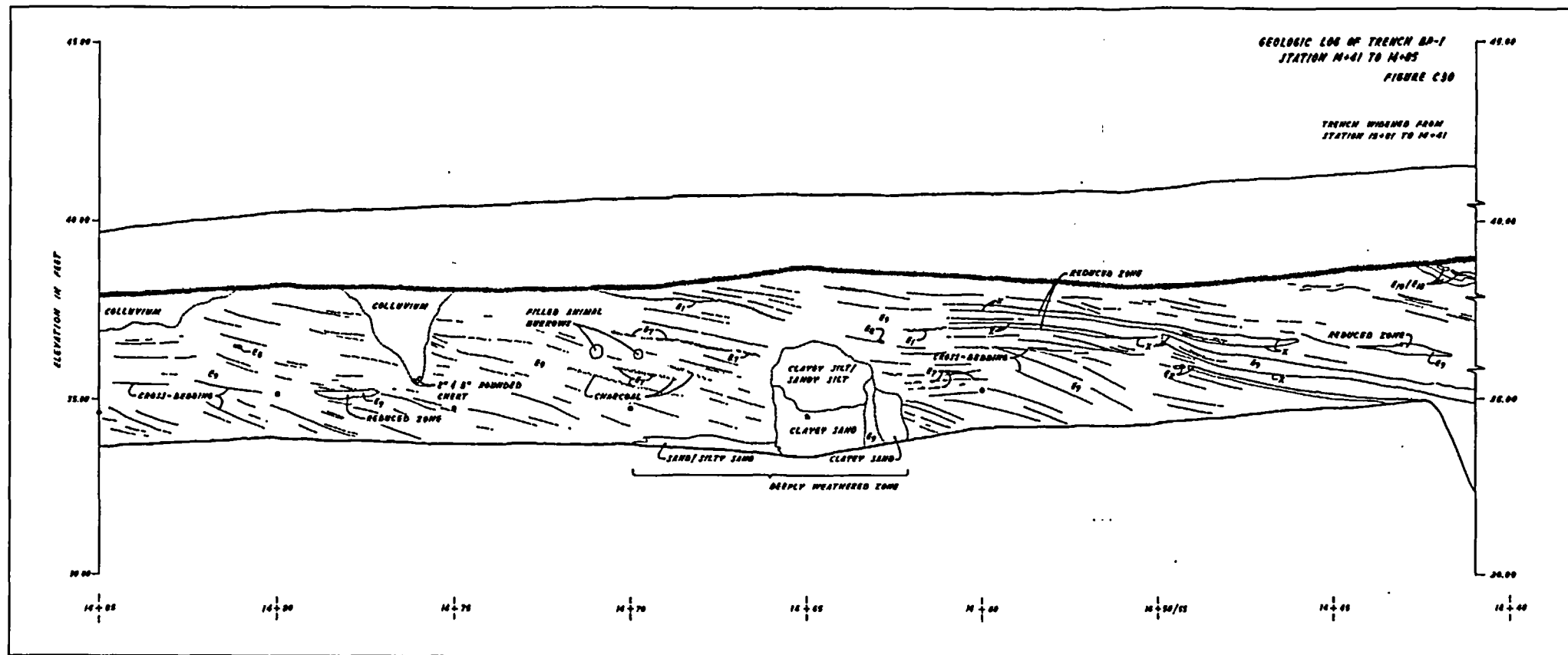
S:\5100s5117\17.009\mask_13102_0916_s4a\fig_4A-01-14(39).ai

Figure 4A-1 - Sheet 14 of 18



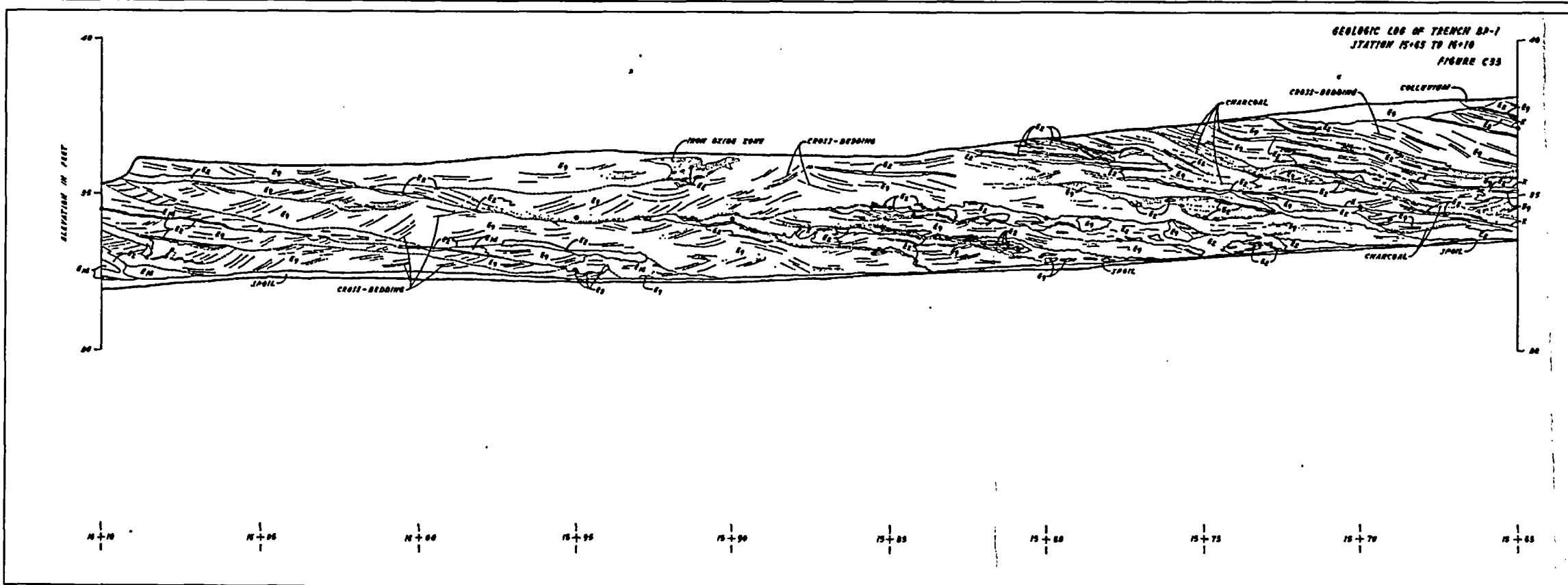
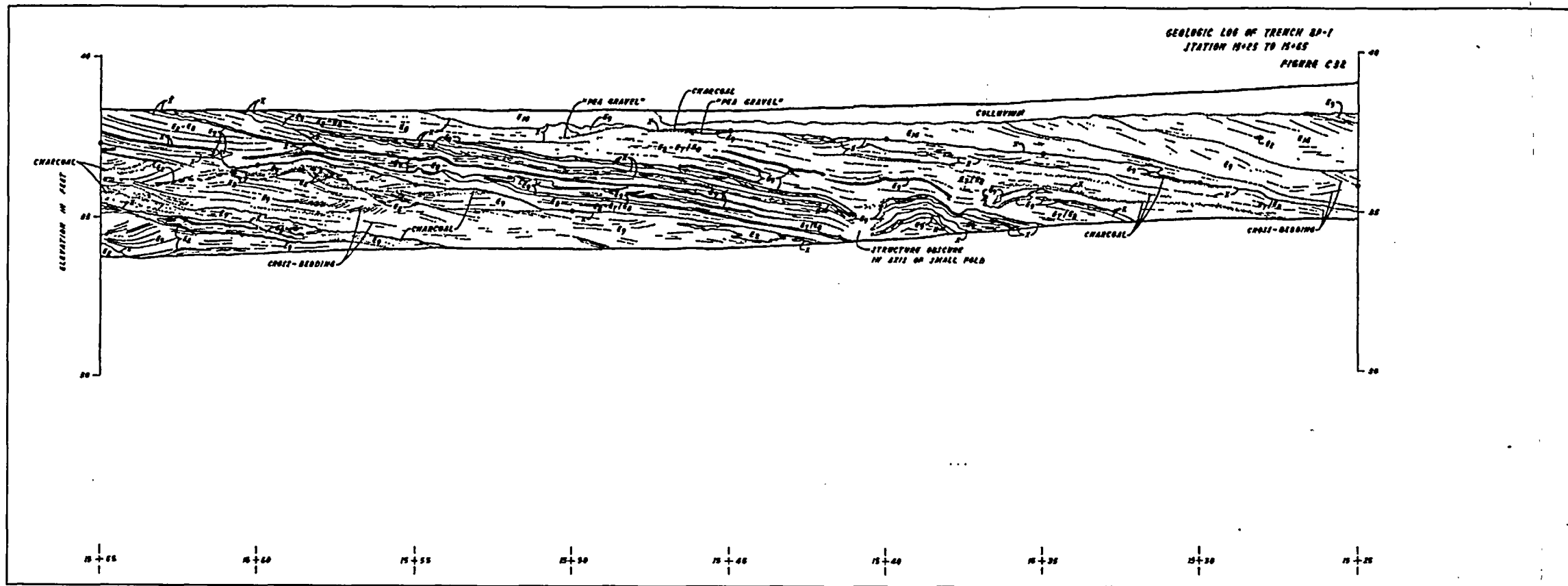
Log of trench BP-1, Station 13+75 to 14+41 (From Earth Sciences Associates, 1977, figure C29). See Figure 4-2 for location of trench. Station numbers are in feet measured from the eastern end of trench.

Figure 4A-1 - Sheet 15 of 18



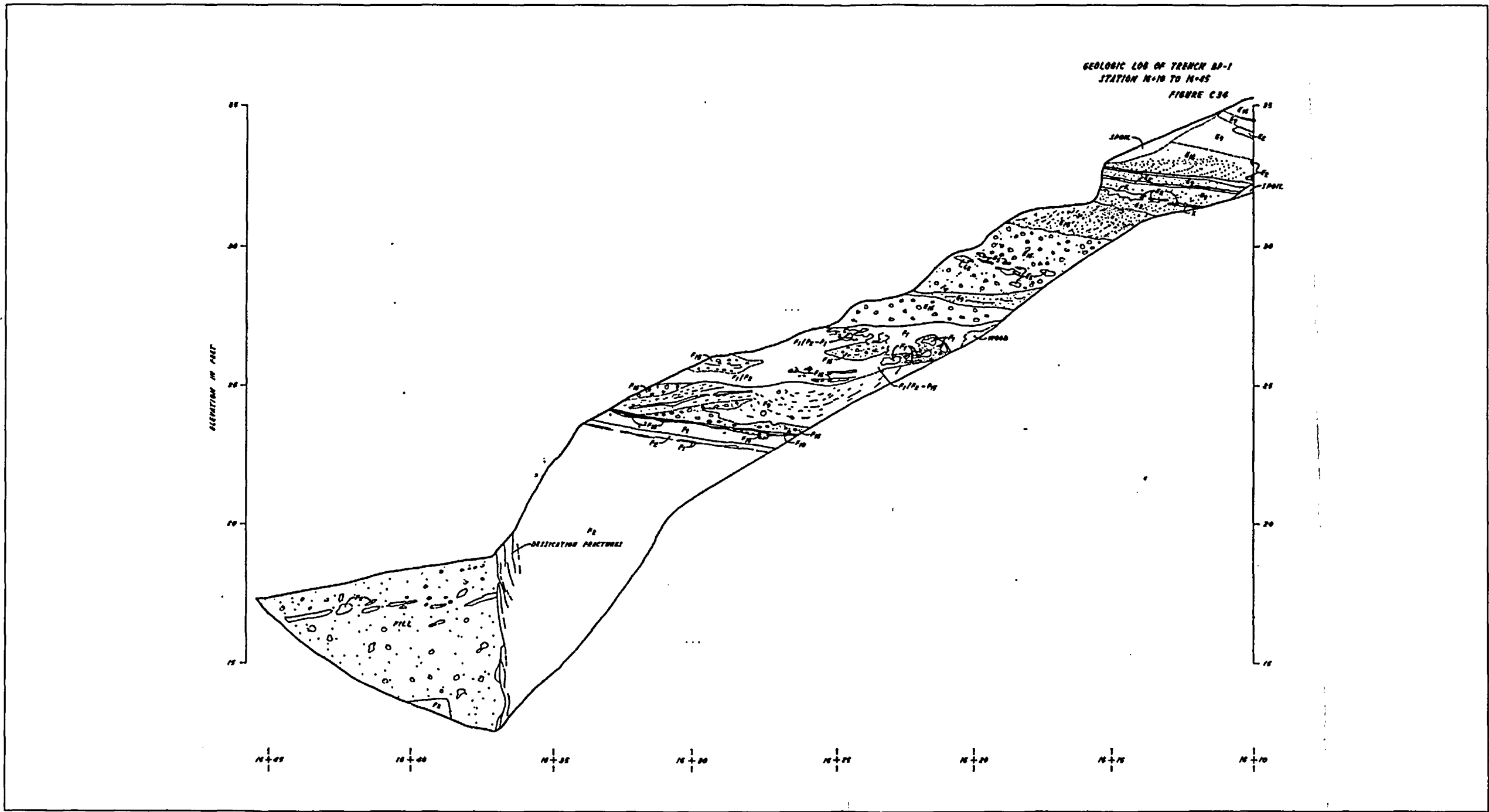
Log of trench BP-1, Station 14+41 to 15+25 (From Earth Sciences Associates, 1977, figures C30 and C31). See Figure 4-2 for location of trench. Station numbers are in feet measured from the eastern end of trench.

Figure 4A-1 - Sheet 16 of 18



Log of trench BP-1, Station 15+25 to 16+10 (From Earth Sciences Associates, 1977, figures C32 and C33). See Figure 4-2 for location of trench. Station numbers are in feet measured from the eastern end of trench.

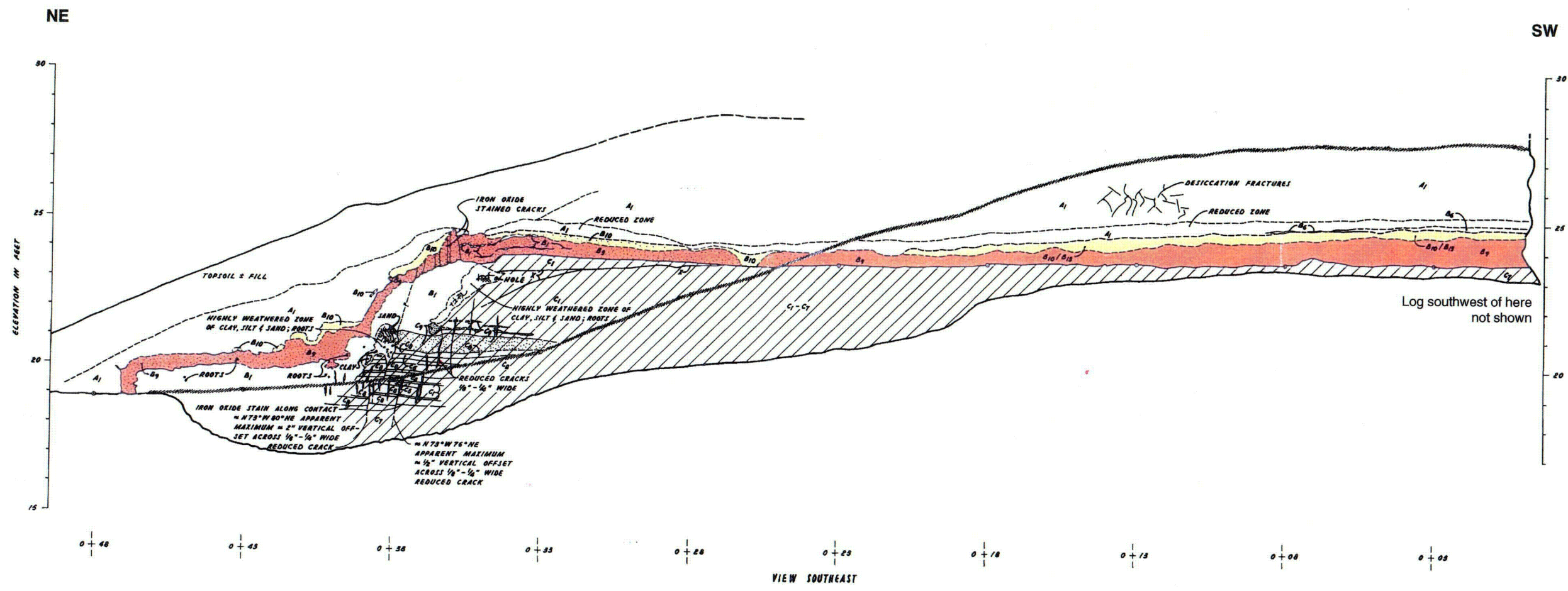
Figure 4A-1 - Sheet 17 of 18



Log of trench BP-1, Station 16+10 to 16+45 (From Earth Sciences Associates, 1977, figure C34). See Figure 4-2 for location of trench. Station numbers are in feet measured from the eastern end of trench.

S:\5100s\5117\...17.009\mask_13\02_0916_s4a\fig_4A-01-18(37).ai

Figure 4A-1 - Sheet 18 of 18

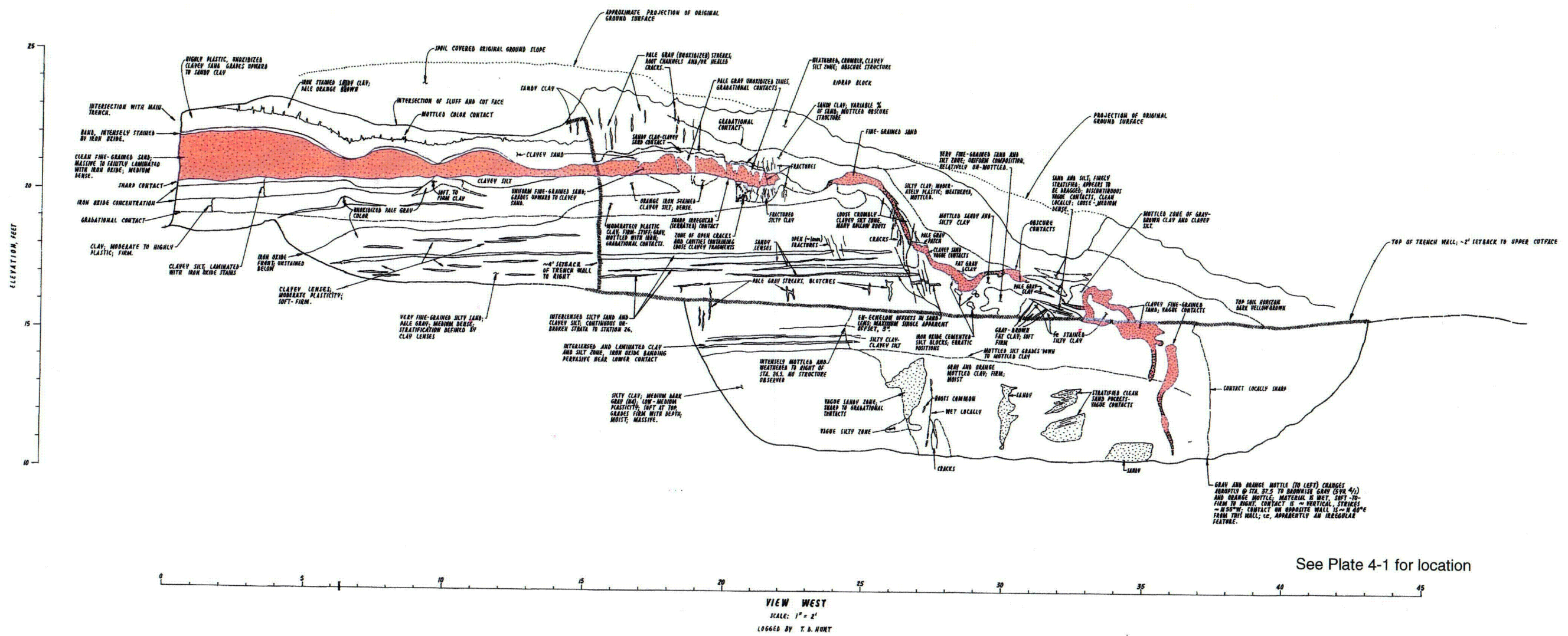


Geologic log of northeastern part of trench BP-2 [Modified from Earth Sciences Associates, 1977, Figure C37 (colors added for emphasis)]. See Figure 4-2 for location of trench. Station numbers are in feet.

S:\5100s\5117\7-009\ask_13102_0916_s4a\fig_4A-02(22).ai

Figure 4A-2

Spoil pile contacts not shown

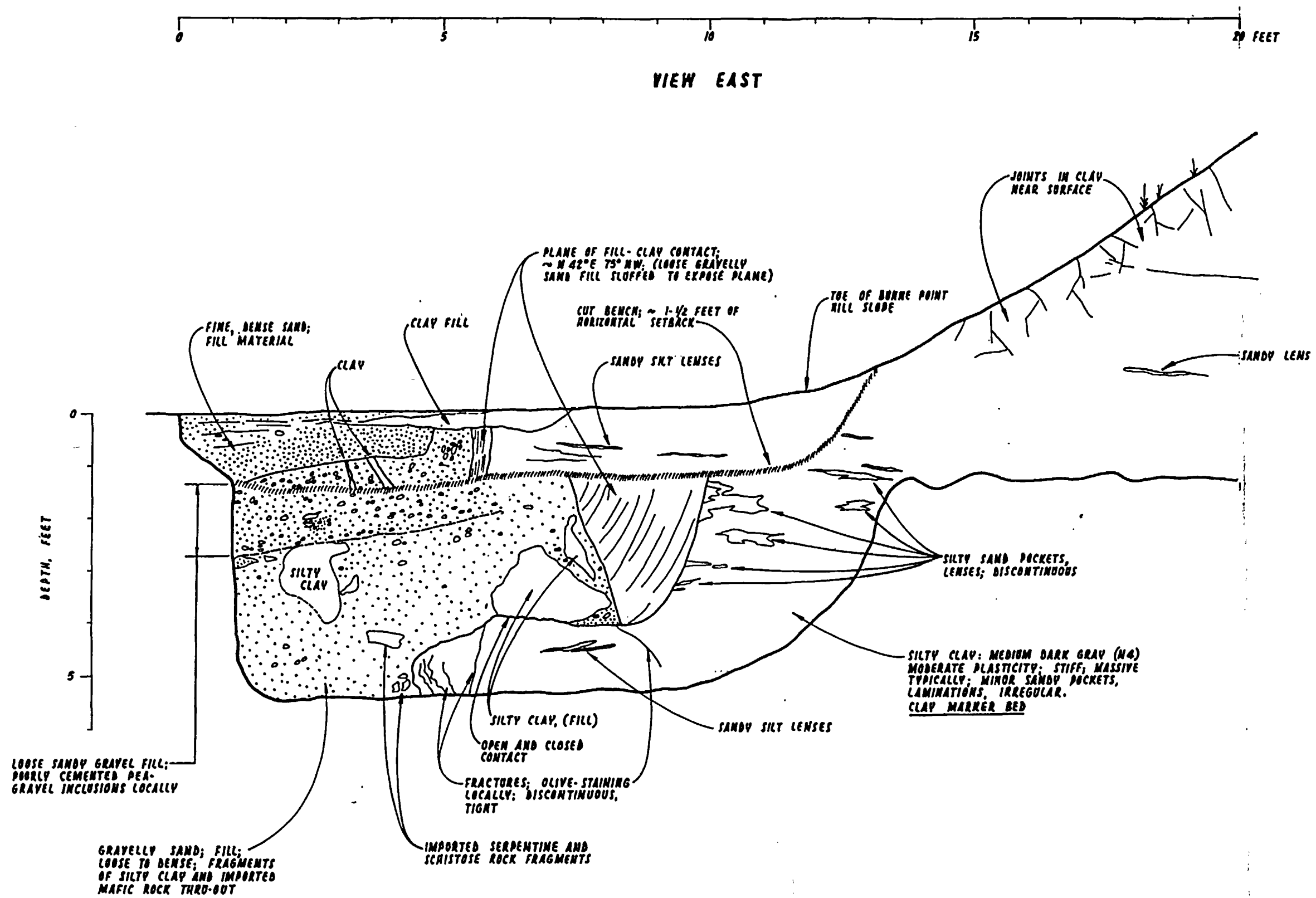


See Plate 4-1 for location

Geologic log of trench BP-3 [Modified from Earth Sciences Associates, 1977, Figure C37 (colors added for emphasis)]. See Figure 4-2 for location of trench. Station numbers are in feet.

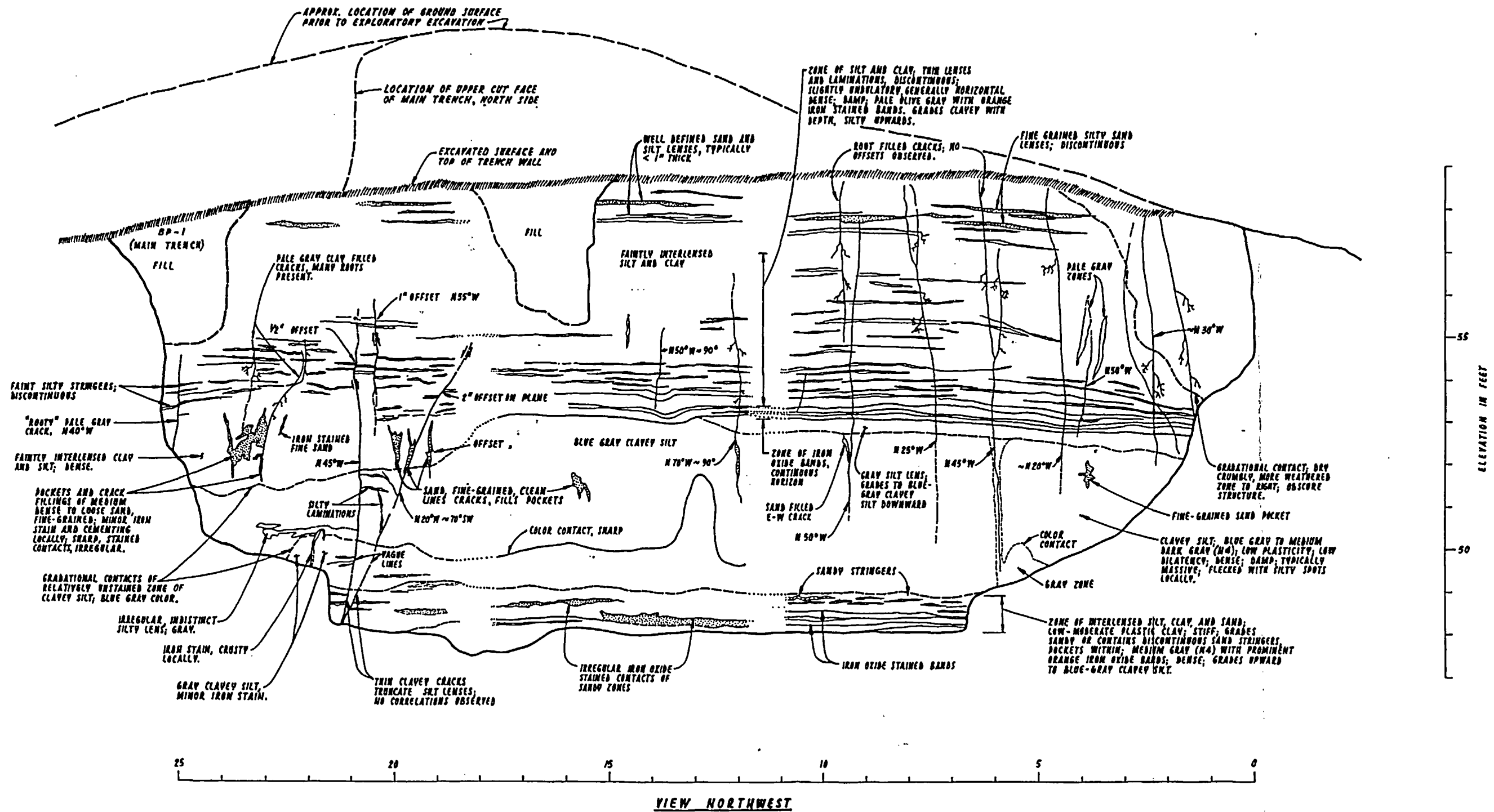
S:\510085117\17.009\task_13102_0916_s4a_fig_4A-03(21).ai

Figure 4A-3



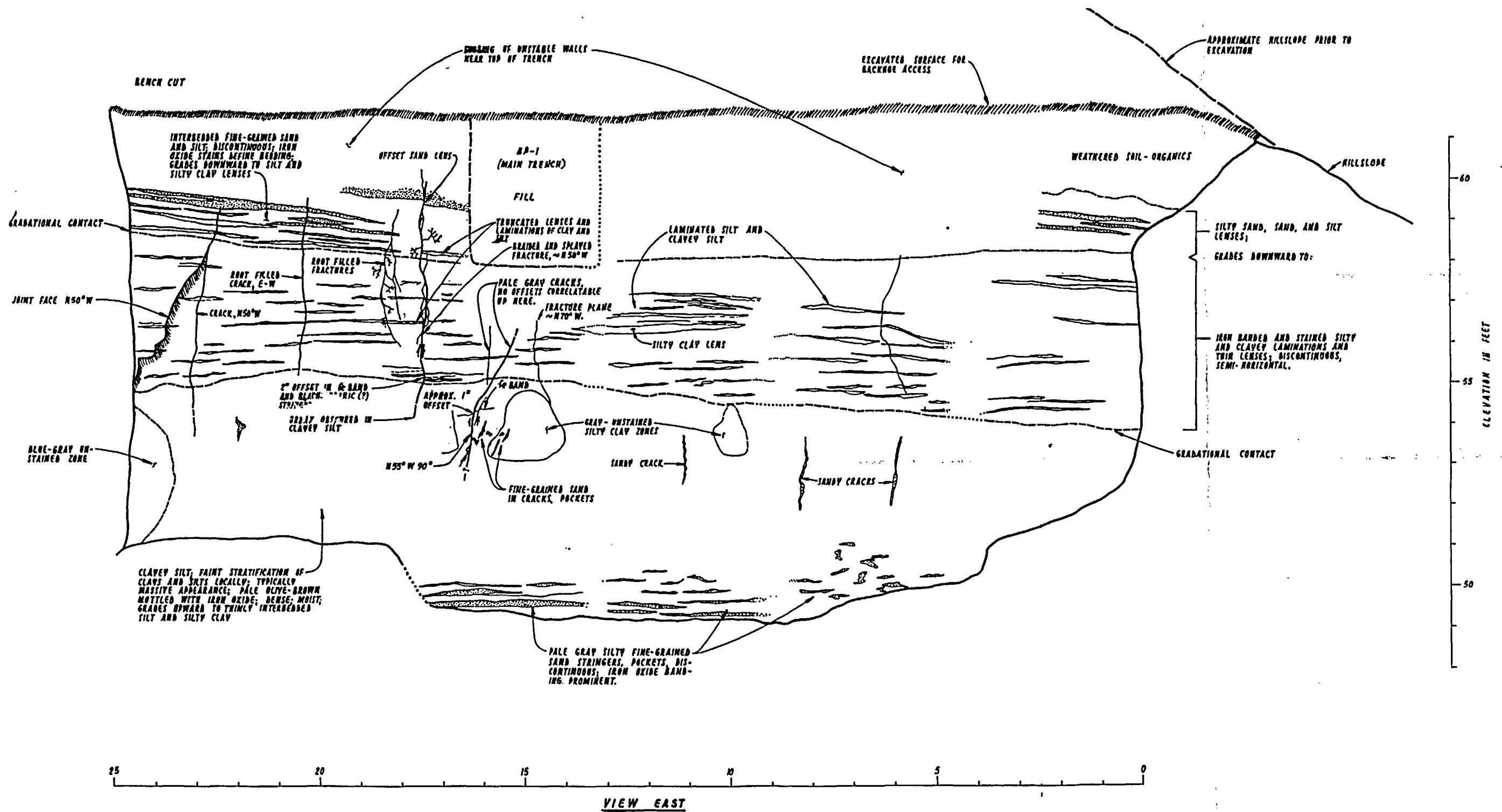
Geologic log of trench BP-4 (From Earth Sciences Associates, 1977; Figure C35).
See Figure 4-2 for location of trench. Station numbers are in feet.

Figure 4A-4



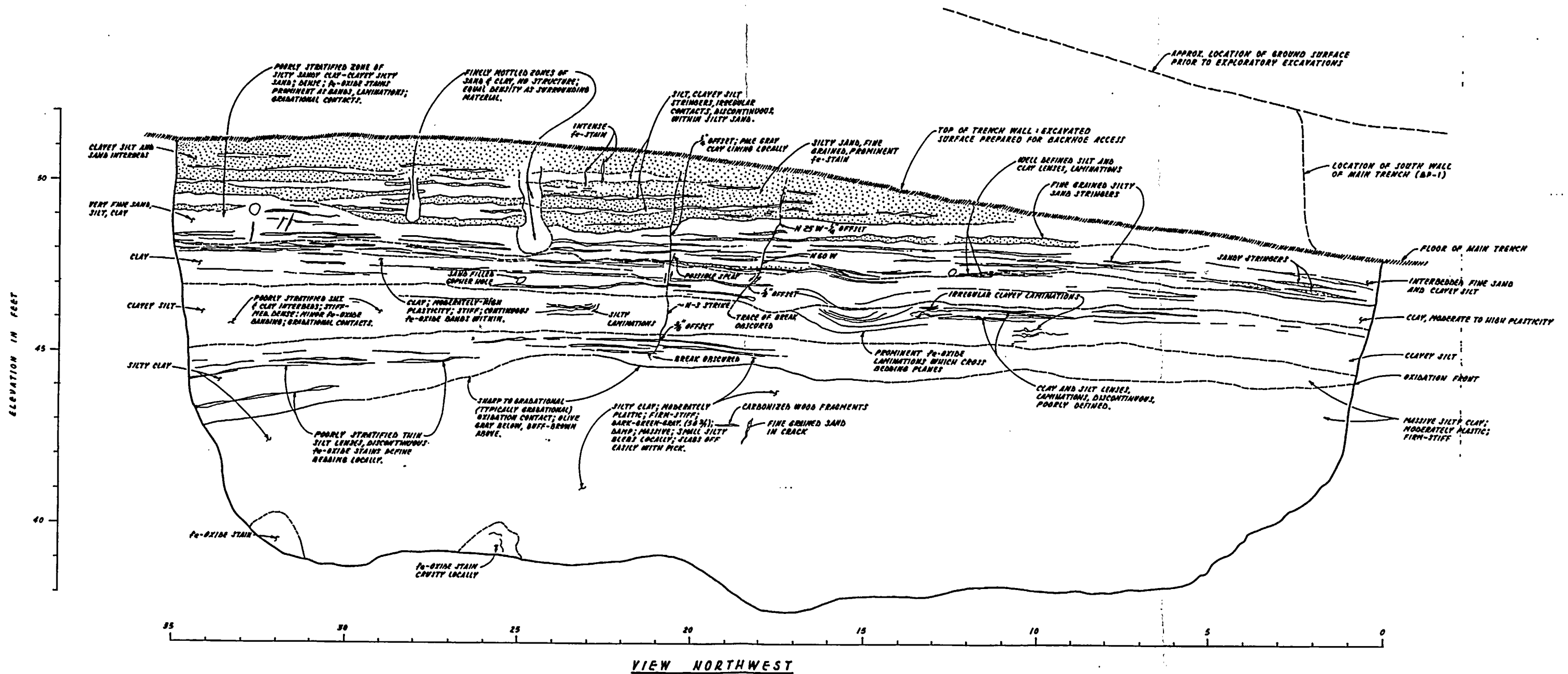
Geologic log of trench BP-6A (From Earth Sciences Associates, 1977; Figure C41). See Figure 4-2 for location of trench. Station numbers are in feet.

Figure 4A-6



Geologic log of trench BP-6B (From Earth Sciences Associates, 1977; Figure C42). See Figure 4-2 for location of trench. Station numbers are in feet.

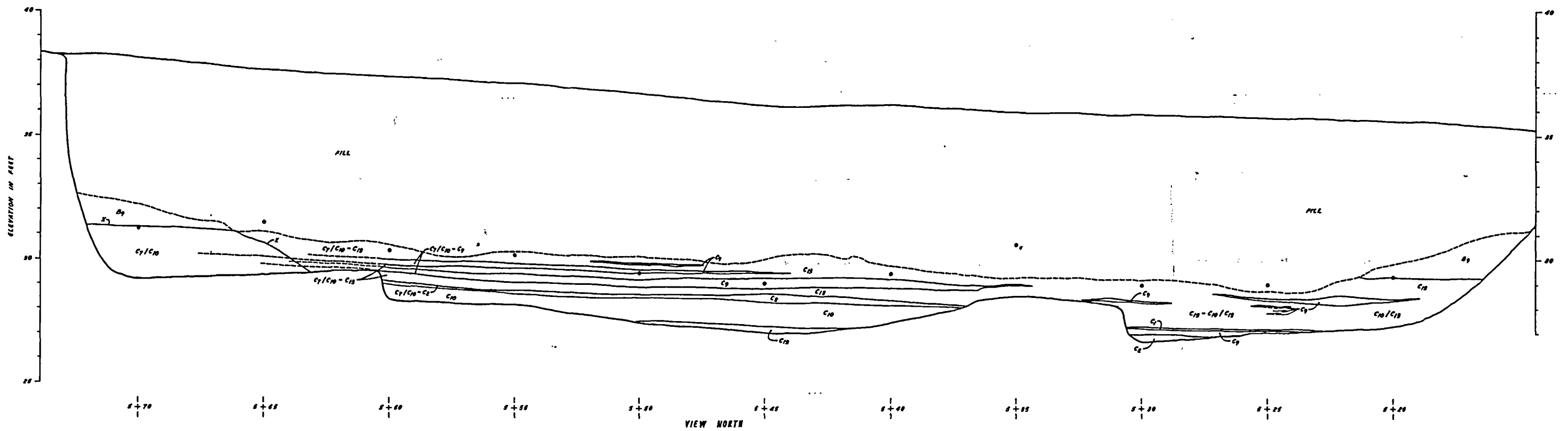
Figure 4A-7



Geologic log of trench BP-8 (From Earth Sciences Associates, 1977; Figure C44). See Figure 4-2 for location of trench. Station numbers are in feet.

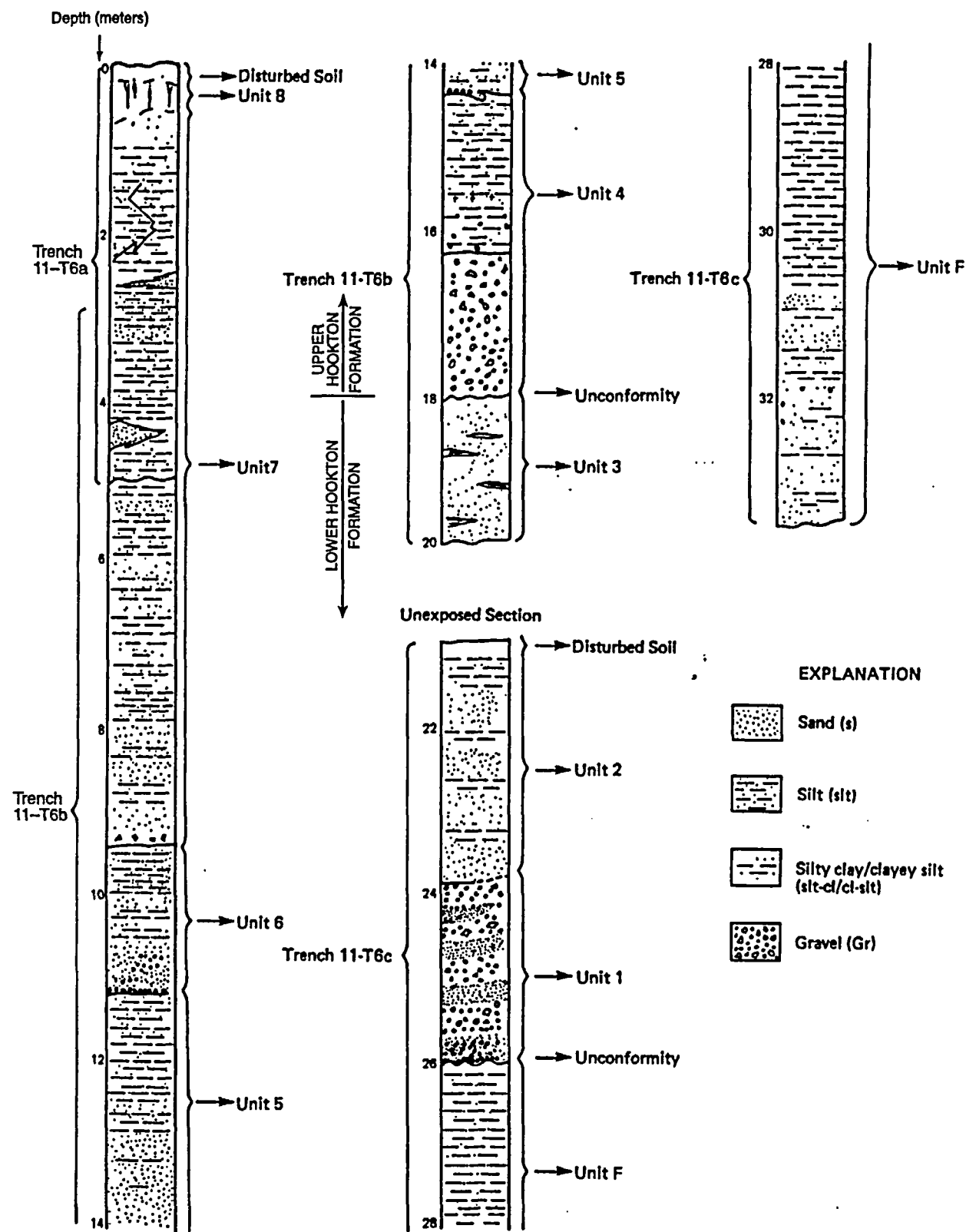
Figure 4A-9

S:\51008\5117\...17.009\mask_13102_0916_s4a_fig_4A-09(61).ai



Geologic log of trench BP-9 (From Earth Sciences Associates, 1977; Figure C45).
See Figure 4-2 for location of trench. Station numbers are in feet.

Figure 4A-10

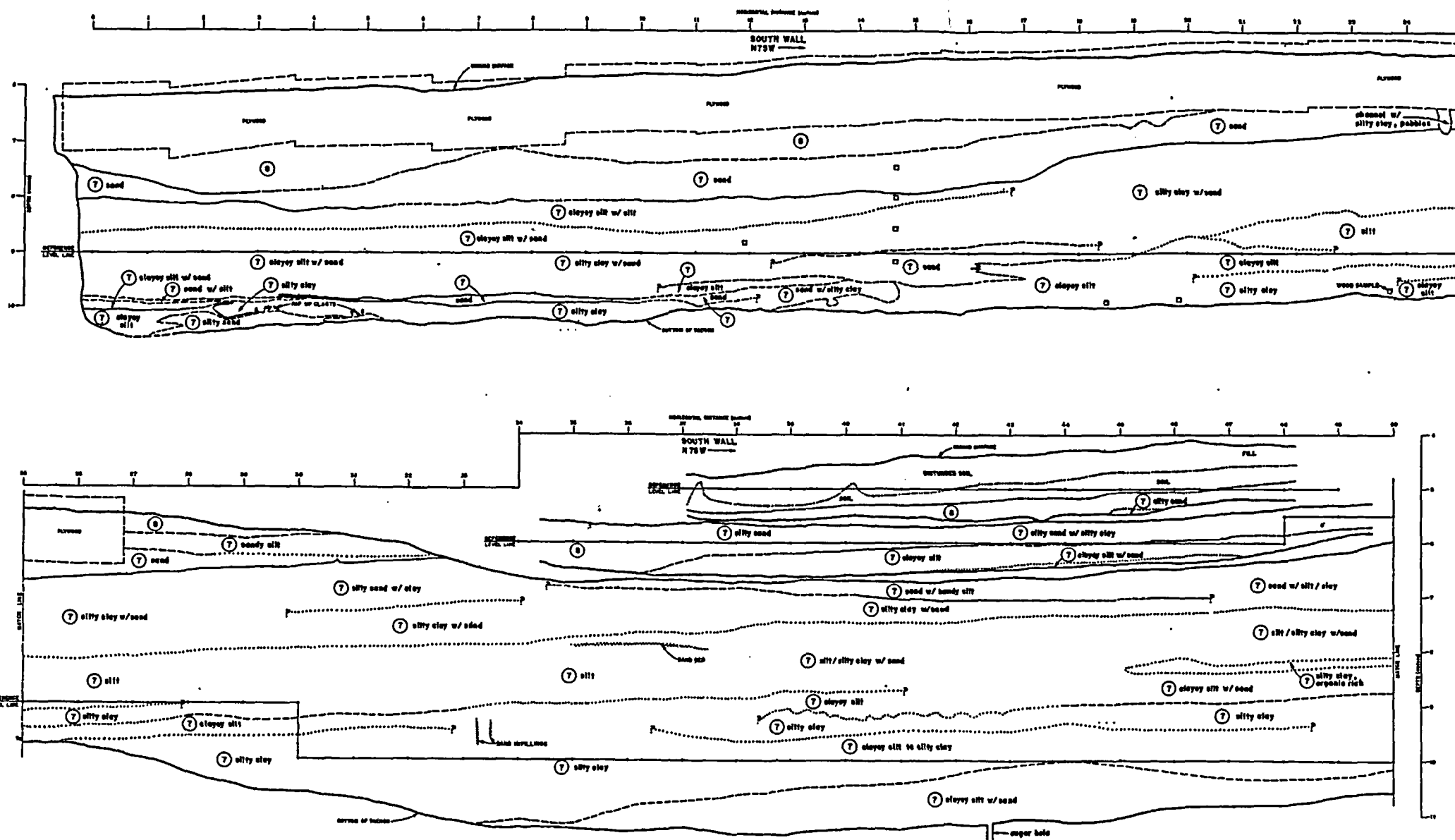


LITHOLOGIC DESCRIPTIONS

- UNIT 8: GLEYED SILTY AND SANDY CLAY**
 Light gray to gray (10 YR 6/1 moist) and strong brown (7.5 YR 5/8 moist); some pebbles; moderately developed ped structures.
- UNIT 7: SAND**
 Brown to dark brown (10 YR 4/3 moist), dark yellowish brown (10 YR 4/6 moist), and yellowish red (5 YR 4/6 moist); fine- to medium-grained; subrounded; contains some discontinuous silty clay laminae and very thin beds (1 to 5 cm).
- INTERBEDDED AND INTERMIXED SILT, SAND, AND SILTY CLAY**
 Pale brown (10 YR 6/3 moist), strong brown (7.5 YR 5/8 moist), and dark gray (2.5 Y N/4 moist).
- SILT**
 Strong brown (7.5 YR 5/8 moist), light olive-brown (2.5 Y 5/4 moist), and dark gray (2.5 Y N/4 moist); discontinuous interbeds and lenses of silty clay and fine-grained quartz sand.
- SILTY CLAY / CLAYEY SILT**
 Dark gray (2.8 Y N/4 moist); slightly sticky and slightly plastic; many organic fragments, some pyritized.
- INTERBEDDED AND INTERMIXED SILT AND SAND**
 Unit fines upwards. Yellowish red (5 YR 5/8 moist) and strong brown (10 YR 5/8 moist); sediment deformation common.
- UNIT 6: SILT, SILT WITH SAND LAMINAE, MEDIUM, AND COARSE SAND**
 Unit fines upwards. Strong brown (7.5 YR 5/8 moist), yellowish brown (10 YR 5/8 moist), light olive brown (2.5 Y 5/4 moist). Sediment deformation in uppermost silts. Basal pea-sized gravel.
- UNIT 5: SILT, SILT AND SAND, FINE AND MEDIUM SAND**
 Unit fines upwards. Light olive-brown (2.5 Y 5/4 moist), and grayish brown (2.5 Y 5/2 moist). Basal pea-sized gravel or sand interfingers with underlying silt.
- UNIT 4: SILTY, PEATY SILTY SAND, SILTY SAND WITH SOME PEBBLES, GRAVEL**
 Unit fines upwards. Dark yellowish brown (10 YR 4/6 moist), yellowish red (5 YR 4/6 moist), light olive-brown (2.5 Y 5/4 moist), and grayish brown (2.5 Y 5/2 moist); abundant organic material at base of silt and within peat layer. Gravel is subangular, poorly sorted and poorly graded; coarse sand size to 30 cm; 46 percent chert, 37 percent quartz-rich metavolcanic and metasedimentary rocks, 13 percent quartz, 4 percent graywacke sandstone, 2 percent clay balls, rare sand lenses.
- UNIT 3: SAND**
 Olive-brown (2.5 Y 4/4 moist); medium-grained; subrounded to subangular; contains discontinuous thin (2 mm to 4 cm) silt lenses.
- UNIT 2: SAND WITH SILT INTERBEDS**
 Yellowish brown (10 YR 5/6 moist) and light brownish gray (2.5 Y 6/2 moist); fine- to medium-grained; laminated, some sediment deformation and cross-bedding.
- UNIT 1: INTERBEDDED SAND AND GRAVEL**
Gravel: 1 mm to 15 cm; poorly sorted and poorly graded; thinly bedded; 53 percent chert, 23 percent metavolcanic and metasedimentary rocks, 11 percent quartz, 11 percent graywacke sandstone, 2 percent clay balls.
Sand: strong brown (7.5 YR 4/6 moist); massive; medium-grained; subangular.
- UNIT F: SILTY CLAY**
 Very dark gray (10 YR 3/1 moist); slightly sticky and slightly plastic; rare shattered sea shells. Grades to interbedded and intermixed silt and sand, sand. Unit fines upwards. Interbedded and intermixed silt and sand is dark brown (7.5 YR 3/4 moist) and dark grayish brown (10 YR 4/2 moist). Sand is olive-brown (2.5 Y 4/4 moist); medium-grained; subrounded to subangular; contains some discontinuous, thin (2 mm to 4 cm) silt lenses.

Composite stratigraphic section and description of lithologic units exposed in Site trenches 11-T6a, 11-T6b, and 11-T6c (Modified from: Woodward-Clyde Consultants, 1980, Appendix C).

Figure 4A-11



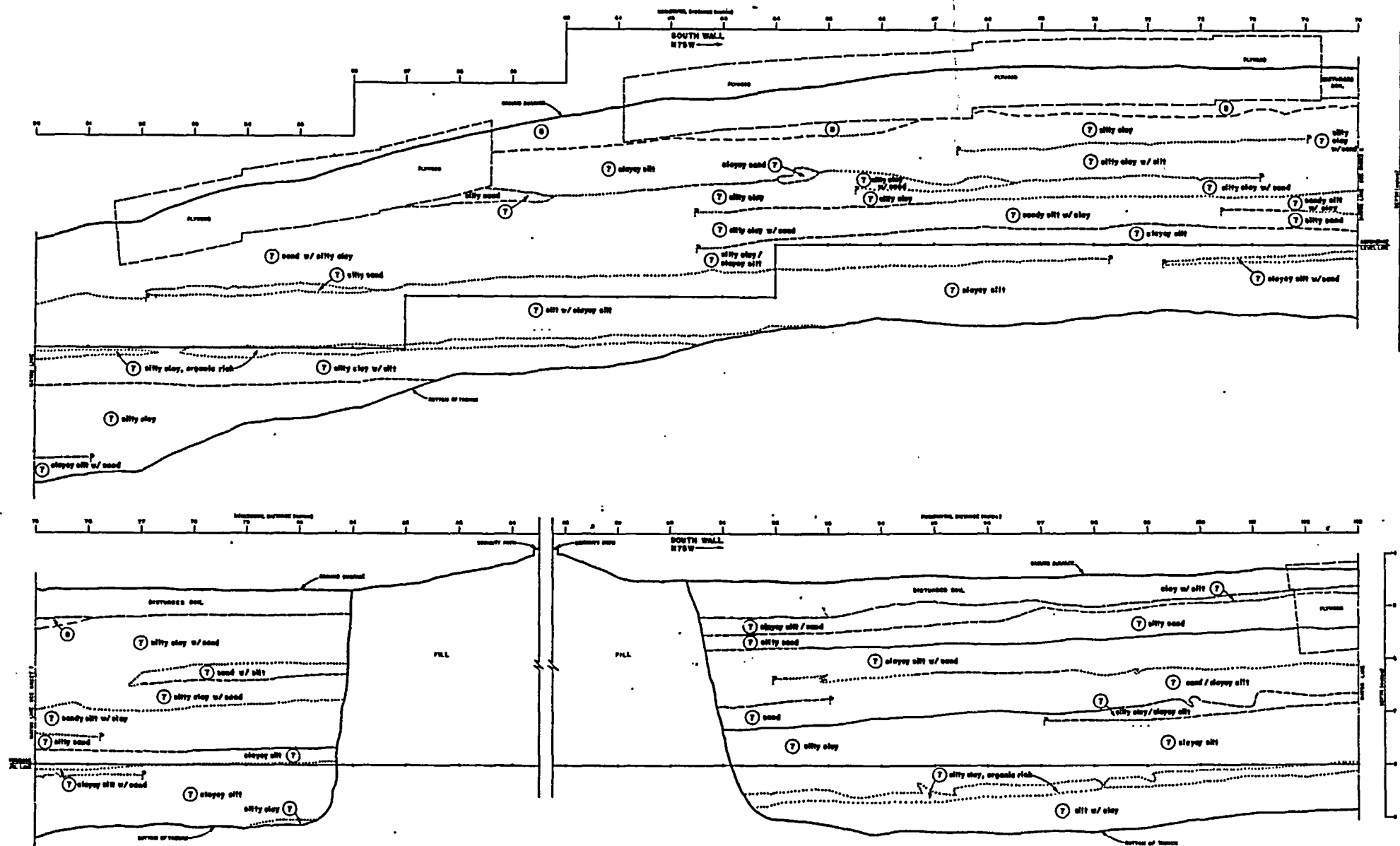
- EXPLANATION**
- Lithologic Contact; solid line where resolution is less than 2 cm, dashed line where 2-5 cm, dotted line where 5-15 cm.
 - Soil Contact
 - Disturbed Soil Contact
 - Fault; solid line where resolution is less than 2 cm, dashed line where 2-5 cm, dotted line where 5-15 cm; strike and dip of fault plane indicated; arrows indicate sense of relative movement.
 - N75W 80M
N70W 55M
Shears

Log of trench 11-T6a (From Woodward-Clyde Consultants, 1980, Figure C-29). See Figure 4-2 for location of trench. Station numbers are in meters.

Figure 4A-12 - Sheet 1 of 4

S:\51005\5117\...009\ask_1302_0916_s4a\lg_4A-12-01 (87).ai

S:\51005\51. .117.009\task_1302_0916_s4a_fig_4A-12-02(68).ai

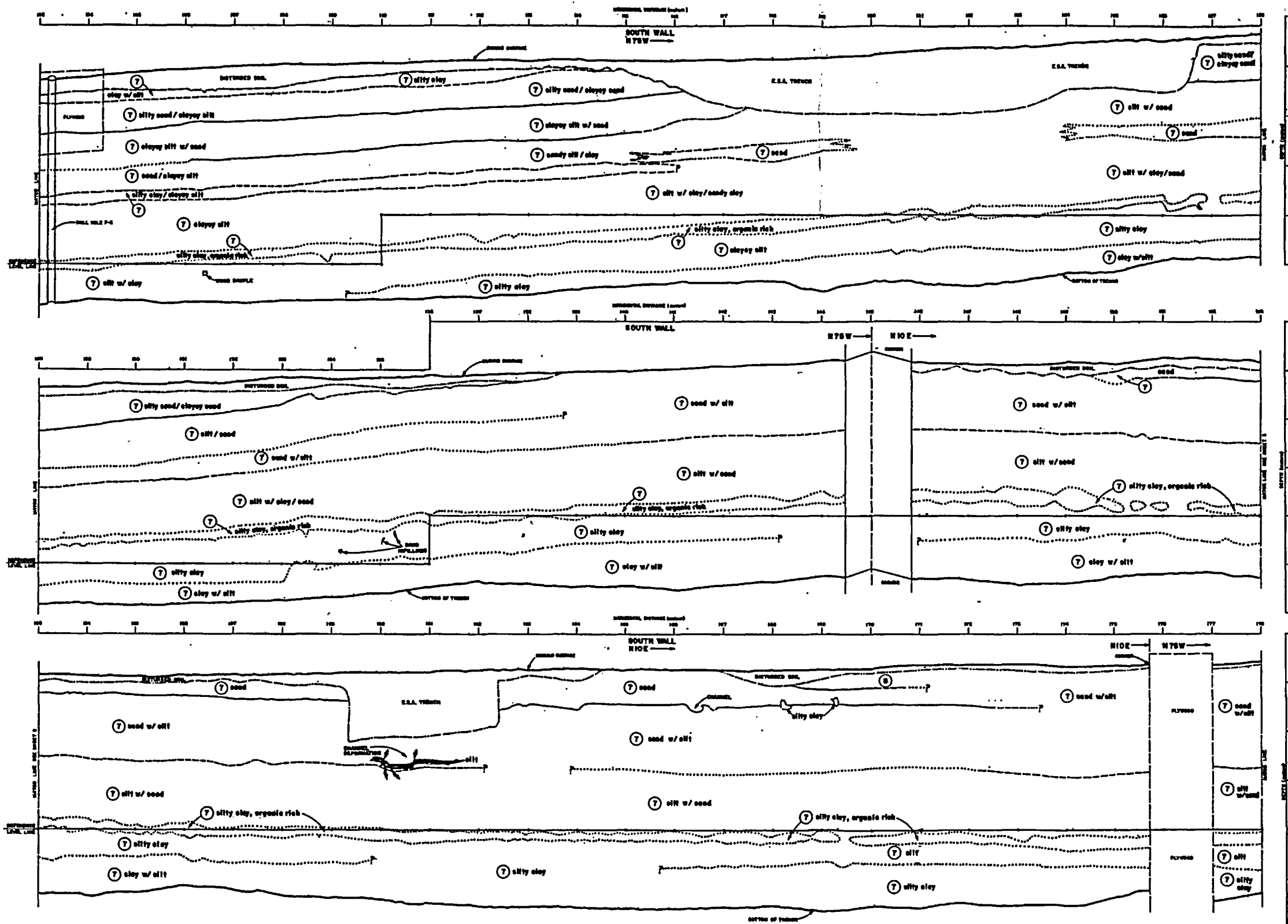


EXPLANATION

- Lithologic Contact; solid line where resolution is less than 2 cm, dashed line where 2-5 cm, dotted line where 5-15 cm.
- Soil Contact
- Disturbed Soil Contact
- Fault; solid line where resolution is less than 2 cm, dashed line where 2-5 cm, dotted line where 5-15 cm; strike and dip of fault plane indicated; arrows indicate sense of relative movement.
- N75W 60N
- N70W 55N
- Strike and Dip of Jointing
- Shears

Log of trench 11-T6a (From Woodward-Clyde Consultants, 1980, Figure C-29). See Figure 4-2 for location of trench. Station numbers are in meters.

Figure 4A-12 - Sheet 2 of 4



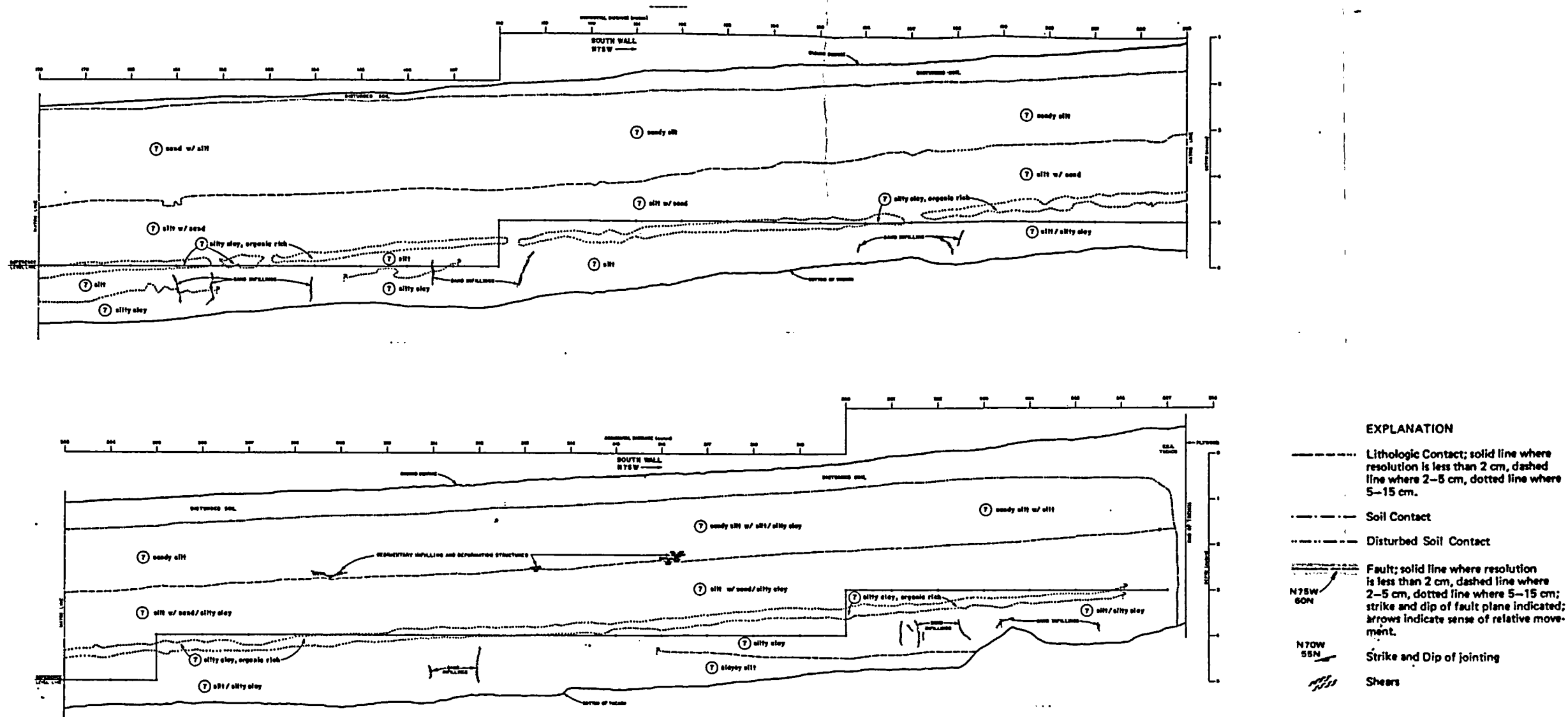
- EXPLANATION**
- Lithologic Contact; solid line where resolution is less than 2 cm, dashed line where 2-5 cm, dotted line where 5-15 cm.
 - - - Soil Contact
 - - - Disturbed Soil Contact
 - █ Fault; solid line where resolution is less than 2 cm, dashed line where 2-5 cm, dotted line where 5-15 cm; strike and dip of fault plane indicated; arrows indicate sense of relative movement.
 - N75W 60N Strike and Dip of Jointing
 - N70W 55N Strike and Dip of Jointing
 - Shears

Log of trench 11-T6a (From Woodward-Clyde Consultants, 1980, Figure C-29).
See Figure 4-2 for location of trench. Station numbers are in meters.

Figure 4A-12 - Sheet 3 of 4

S:\15100s151\17.009\mask_13102_0916_s4a_fig_4A-12-03(66).ai

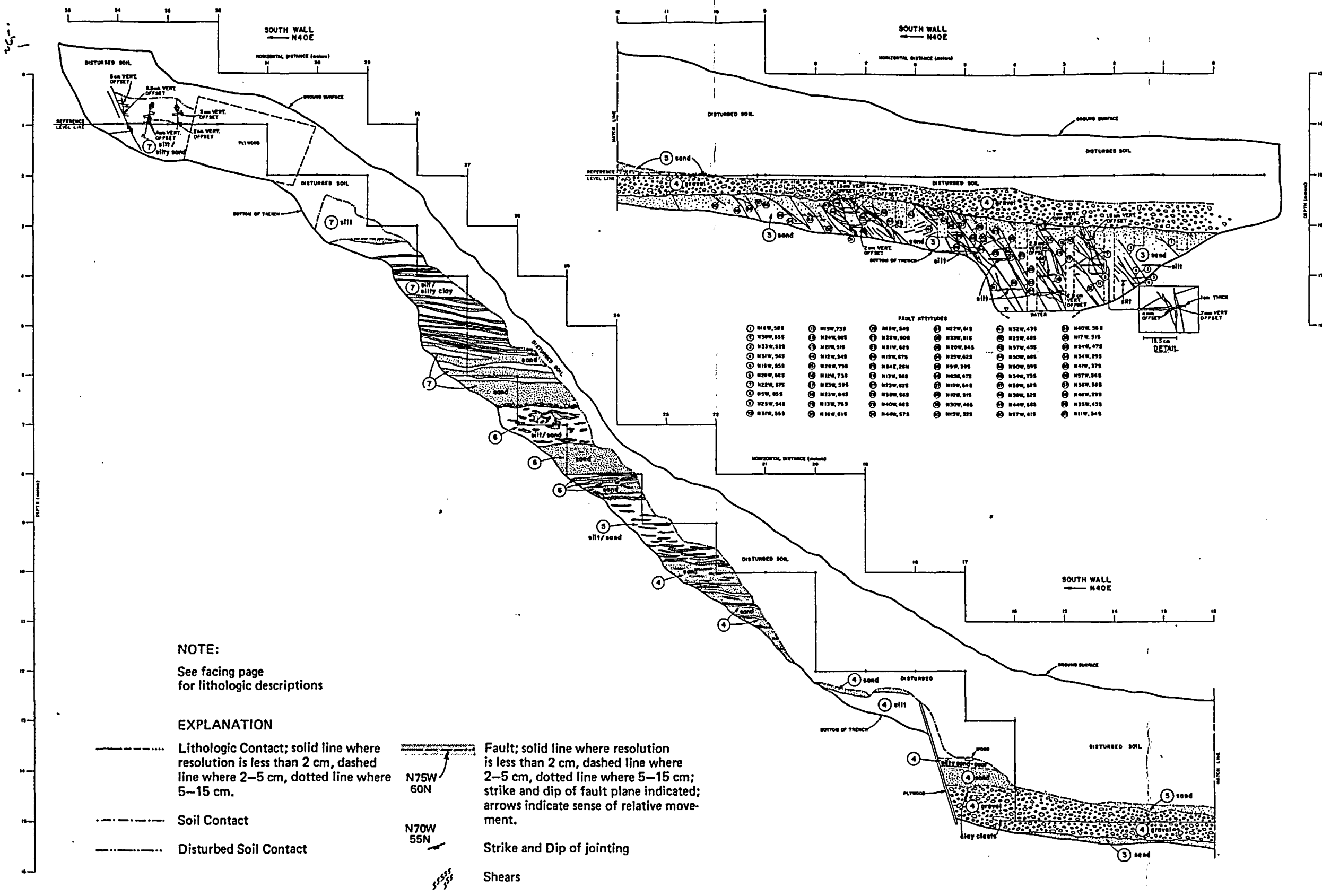
S:\5100s\51. .17.009\task_13102_0916_s4a\fig_4A-12-04(69).ai



Log of trench 11-T6a (From Woodward-Clyde Consultants, 1980, Figure C-29).
See Figure 4-2 for location of trench. Station numbers are in meters.

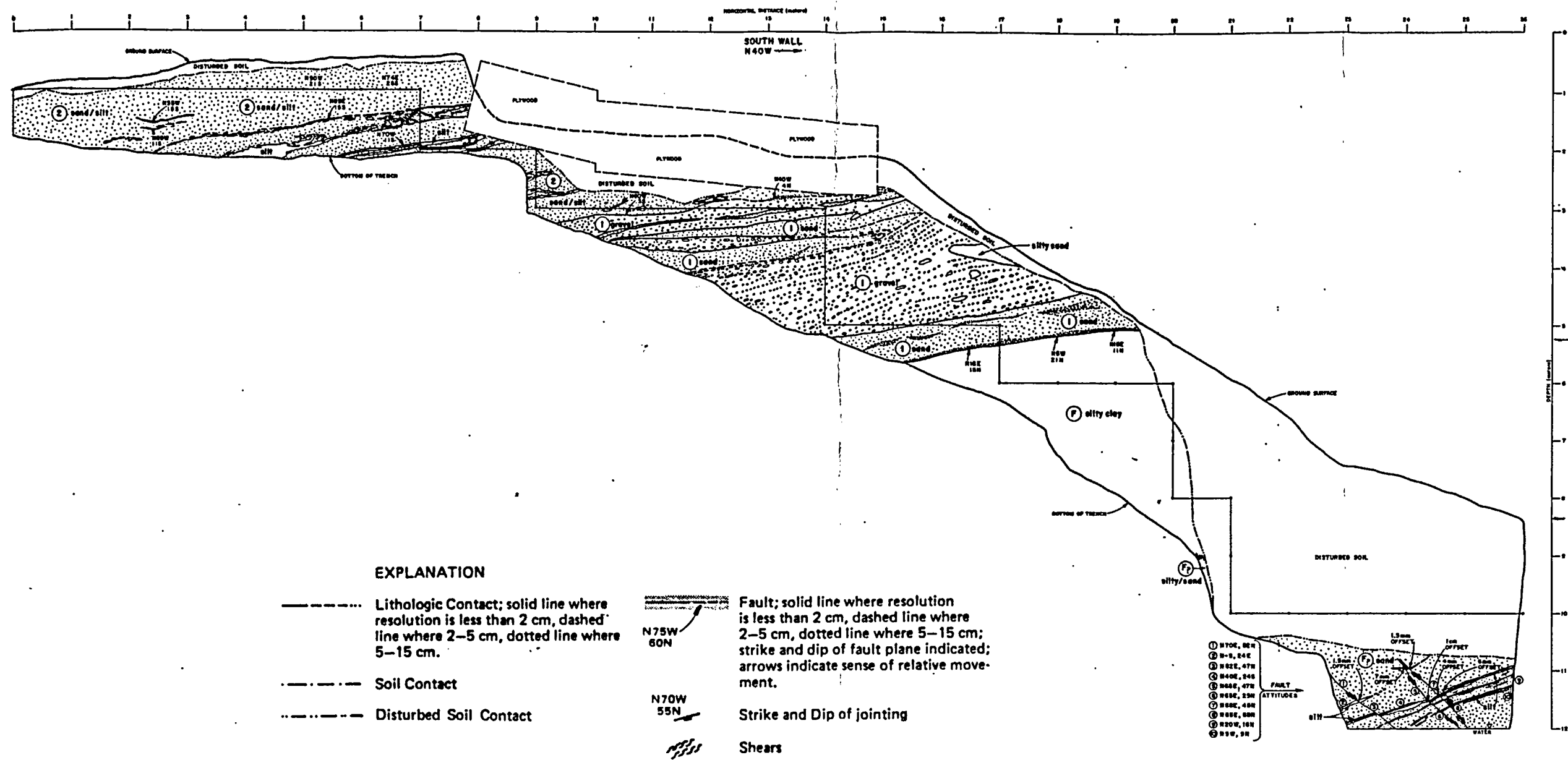
Figure 4A-12 - Sheet 4 of 4

S:\5100s\51. 17.009\mask_13\02_0916_s4a_fig_4A-16(73).ai



Log of trench 11-T6b (From Woodward-Clyde Consultants, 1980, Figure C-33). See Figure 4-2 for location of trench. Station numbers are in meters.

Figure 4A-16



Log of trench 11-T6c (From Woodward-Clyde Consultants, 1980, Figure C-35). See Figure 4-2 for location of trench. Station numbers are in meters.

Figure 4A-17

S:\51005151..._17.009\task_13102_0916_s4a_fig_4A-17(74).ai

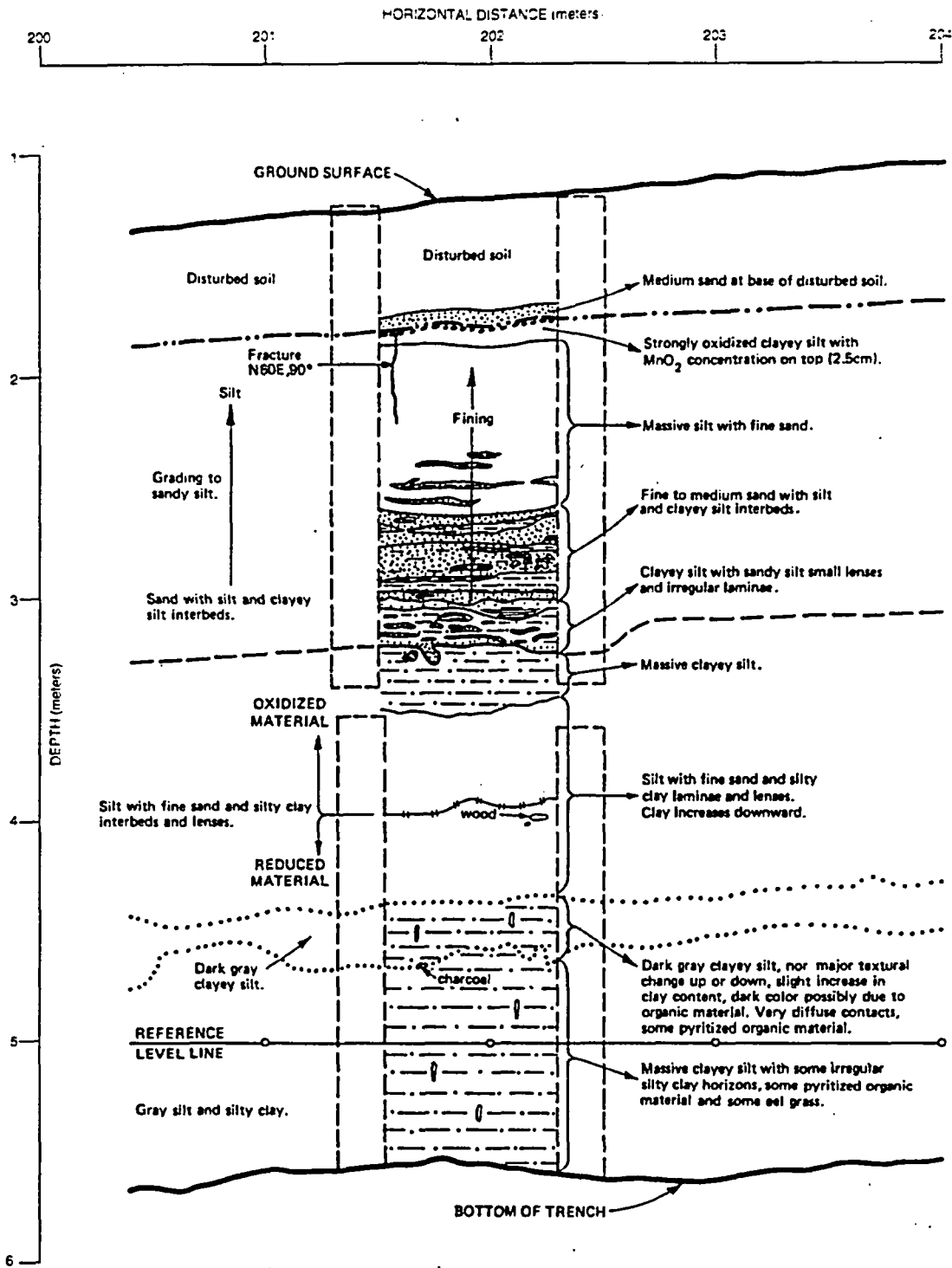


Figure 4A-13 Detail of stratigraphy in trench 11-T6a at station 75.5 meters
 (From Woodward-Clyde Consultants, 1980, Figure C-30c).

117.009task_1302_0916_s4a_fig_4A-13(70).ai

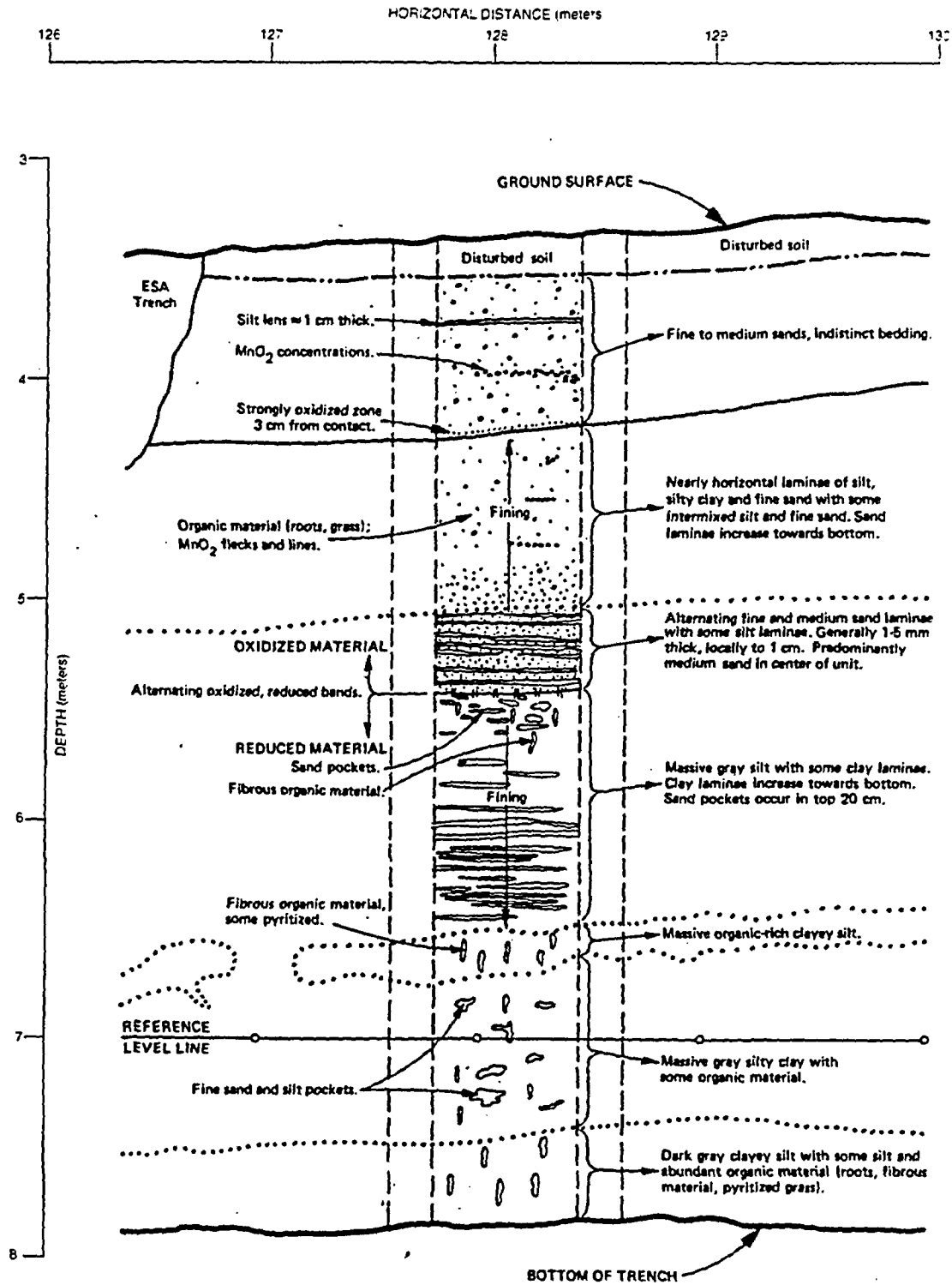


Figure 4A-14 Detail of stratigraphy in trench 11-T6a at station 128 meters
(From Woodward-Clyde Consultants, 1980, Figure C-30b).

117.000task_1302_0016_sdat_fig_4A-14(71).ai

S:\51005\...



Humboldt Bay ISFSI Project
Technical Report
TR-HBIP-2002-01

Appendix 4A
Logs of
Site Trenches
Rev. 0, September 16, 2002

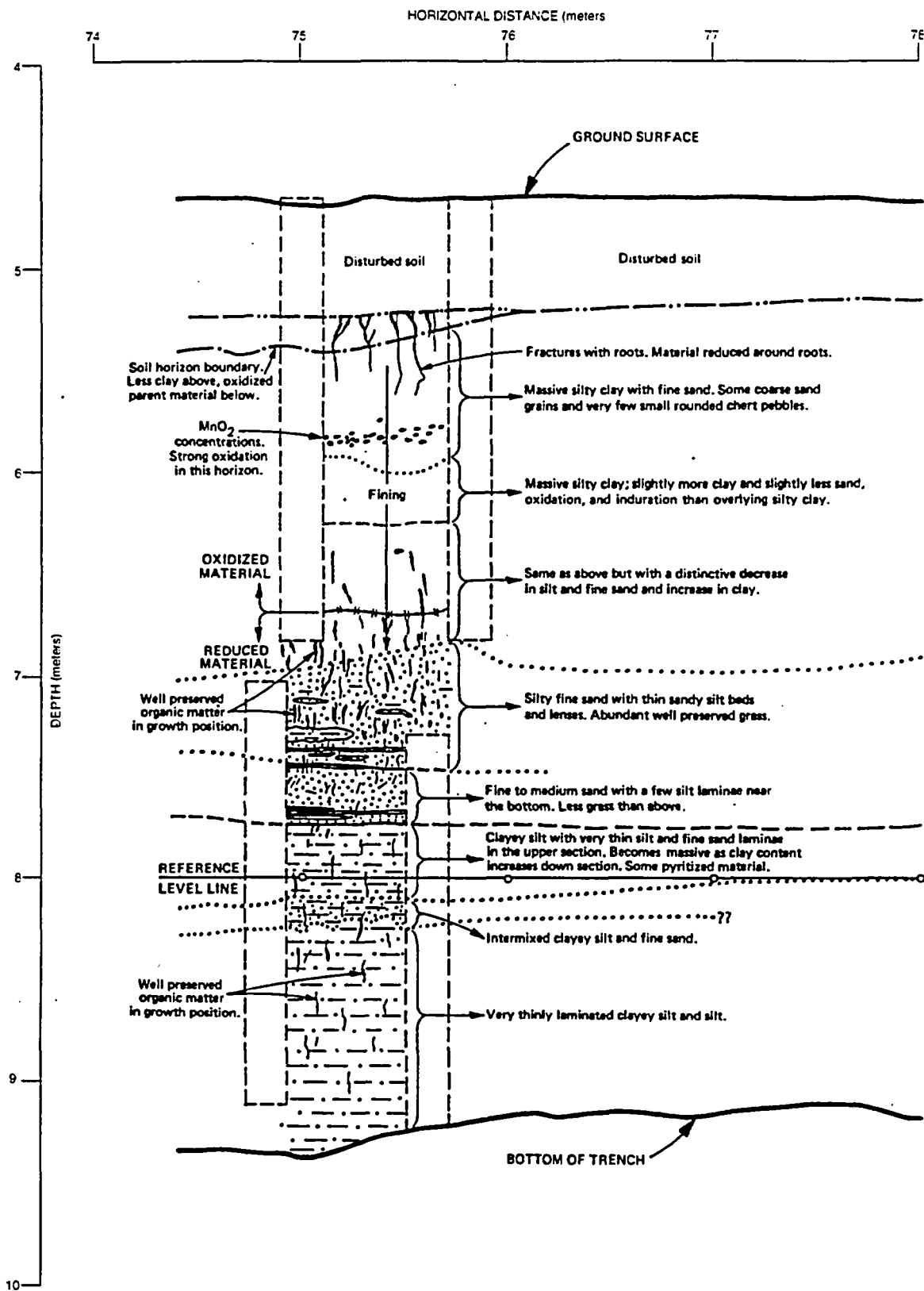


Figure 4A-15 Detail of stratigraphy in trench 11-T6a at station 200 meters
(From Woodward-Clyde Consultants, 1980, Figure C-30a).

117.009task_1302_0916_s4a_fig_4A-15(72).ai

Seismic Source Characterization of Cascadia Subduction Zone

INTRODUCTION

Interpretations of the tectonic framework of the Mendocino triple junction region have evolved rapidly during the past few decades as new geologic, seismologic, and crustal structure information has become available. In particular, the characterization of the Cascadia subduction zone has changed dramatically. Prior to the mid 1980s, the Cascadia subduction zone was judged not to be seismically active by the majority of seismologists and geologists, and was interpreted not to have the capability of producing significant earthquakes. As new geologic evidence was identified during the mid and late 1980s, the perception of the capability of the subduction zone changed, and by the mid 1990s, a new scientific consensus that the subduction zone is capable of generating great earthquakes had evolved (Atwater and others, 1995).

Because the scientific community increasingly accepted the Cascadia subduction zone as a potential source for earthquakes, the California Seismic Safety Commission, along with the California Department of Transportation (Caltrans) and the Oregon Department of Transportation, sponsored studies to define the characteristics and assess the consequences of a Cascadia subduction earthquake. In California, the California Division of Mines and Geology (CDMG) prepared a Cascadia earthquake scenario analysis (Topozada and others, 1995). The CDMG scenario earthquake was defined as a "Gorda segment" rupture, involving slip on the southern 240 kilometers of the Cascadia interface and generating a magnitude 8.4 earthquake¹. Additionally, the CDMG scenario event included slip on the Little Salmon fault zone that was triggered by slip on the subduction interface. The Little Salmon fault zone was interpreted to be a crustal thrust fault above the Cascadia interface. The scenario earthquake was also considered to be a source for generating a local tsunami.

¹ Earthquake magnitudes are moment magnitudes, *M*, unless otherwise stated.



Since publication of the CDMG Cascadia earthquake scenario (Topozada and others, 1995), additional evidence pertaining to the tectonics and seismic source characteristics of the Cascadia subduction zone and the Mendocino triple junction has been discovered, and is either published or in the process of being published. The most significant characteristics that are departures from the previous source characterization models are the following:

- The Cascadia subduction zone appears to have ruptured repeatedly from Humboldt Bay north to at least northern Washington (about 1,100 km), producing earthquakes of magnitude 9 (Figure 2-1). Several similar great earthquakes have occurred during the past several thousand years, with the most recent one occurring in January 1700 AD.
- The Little Salmon fault zone appears to be structurally and kinematically associated with other thrust faults offshore of northern California and southern Oregon (Figure 2-3). This fault system, which is referred to as the Little Salmon fault system in this report, is interpreted to accommodate much of the up-dip slip of the subduction zone, and thus slips simultaneously with subduction zone slip during a great Cascadia earthquake.
- The Little Salmon thrust system produces surface deformation consistent with a fault dip of about 45 degrees at depth, and thus can cause large amounts of vertical seafloor displacement capable of generating large, local tsunamis.
- Additional sources of large subduction zone earthquakes are interpreted to include the Eel River and Petrolia subduction zone segments south of Humboldt Bay (Figure 2-3, 2-5 and 2-6). The 1992 Petrolia earthquake apparently was independent of the larger and more northerly Cascadia events.

MAIN CASCADIA INTERFACE

As described in Section 2.0, there is a consensus among the scientific community that the interface between the Gorda and North American plates (i.e., the Cascadia interface) is seismically active and is capable of generating great subduction zone earthquakes. The



occurrence of the 1992 Petrolia earthquake at the southern end of the interface may represent the first observation of a Cascadia interface earthquake (Oppenheimer and others, 1993).

The southern end of Cascadia interface is segmented forming the main Cascadia interface plus two smaller subplates, the Eel River subplate and the Petrolia subplate. The Table Bluff fault is not considered to be an independent source, but rather it is interpreted to be an imbricate thrust in the Little Salmon fault zone at the southern edge of the main Cascadia plate onshore. The Little Salmon fault system is considered to be part of the main Cascadia interface.

Source Geometry

The total length of the Cascadia subduction zone from the Mendocino triple junction to the Explorer plate is about 1,100 kilometers (Figure 2-1). The main Cascadia interface ends about 50 kilometers north of the triple junction (Figure 2-6).

In the southern part of Cascadia, the main Cascadia interface has an average dip of about 7 degrees. The Cascadia interface becomes the Table Bluff fault, which forms a thrust wedge in the upper several kilometers where it has a southwest dip of about 35 degrees. At greater depth it is northeast dipping. (Figure 3-4).

The discussion of the tectonic framework in Section 2.0 presents evidence that suggests that earthquakes on the main Cascadia zone have had very long ruptures that extend from northern California to at least central Washington or possibly farther north. Currently, there is no data on the timing of past Cascadia earthquakes north of Central Washington. Two rupture segment lengths are considered: a rupture from the Table Bluff fault to Central Washington (700 km), and a rupture from the Table Bluff fault to the Explorer plate (1,050 km). Because there is no evidence to favor one rupture length over the other, these two rupture lengths are assigned equal weight.



Earthquake Recurrence Intervals

The main Cascadia interface has been seismically quiescent during the historical period, thereby precluding the use of seismicity data to constrain the recurrence rate. Consequently, we relied on paleoseismic evidence for earthquake recurrence intervals to estimate recurrence rates on the plate interface.

In previous studies, the recurrence rate has been estimated by balancing the moment rate on the subduction zone, as is typically done for crustal faults; however, the locking factor, "a", needs to be specified. The only data available from which a can be constrained are the paleoseismic data. This approach does not add any new information that is not already considered from the paleoseismic data directly; therefore, it was not used in this study.

Geologic studies of the timing of coastal subsidence and tsunami deposition are discussed in Sections 2.0, 3.0, and 9.0. These studies provide information on the timing and recurrence intervals between earthquakes. Table 5A-1 gives the dates of the last eight events along the southern part of the Cascadia subduction zone. The mean recurrence interval is 500 years \pm 100 years. However, the events appear to occur in triplets, with each triplet defining one megacycle. The total time interval for one megacycle is about 1,400 years. Each megacycle includes an initial event following a long (800 to 900 year) interval and then two events preceded by short (200 to 400 year) intervals.

PETROLIA SUBPLATE

Source Geometry

The geometry of the Petrolia subplate is defined by the rupture zone of the 1992 Petrolia earthquake, which had a length of about 18 kilometers, a down dip width of 14 kilometers, and dip of 10 degrees.

Characteristic Earthquake Magnitude

The 1992 magnitude 7.1 Petrolia earthquake provides an estimate of the characteristic magnitude for the Petrolia subplate.



Earthquake Recurrence Intervals

Tanioka and others (1995) estimate that it would require 48 years to accumulate the strain that was released during the Petrolia earthquake at their preferred strain rate of 5.6 centimeters per year.

EEL RIVER SUBPLATE

Source Geometry

The Eel River subplate has a length of about 80 kilometers. The down dip extent is limited by the Eel River syncline (Figure 2-6). The seismogenic thickness is 15 kilometers, the dip angle is 45 degrees, and the down-dip width is 21 kilometers.

Earthquake Recurrence Intervals

There is no independent evidence of the recurrence rates of earthquakes on the Eel River segment of the Cascadia interface. Therefore, the recurrence interval of the Eel River segment is assumed to be the same as the main Cascadia interface.

LITTLE SALMON FAULT ZONE AND LITTLE SALMON FAULT SYSTEM

Source Geometry

The downdip seismogenic width of the Little Salmon fault zone is defined by its average dip and the thickness of the seismogenic crust. Exploratory trenches across two traces of the Little Salmon fault indicate an average dip near the surface of about 25 degrees (Carver and Aalto, 1992). This relatively low dip persists to a depth of at least two kilometers, based on the intersection of the fault in a borehole at the Tompkins Hill gas field (Carver and Aalto, 1992). However, as described in Section 4.0, the dip of the fault at depth is interpreted to be greater than 45 degrees. The dip at depth controls the width of the fault. Therefore, the following estimates for the average dip of the Little Salmon fault zone were assigned: 40 degrees (0.2), 45 degrees (0.6), and 50 degrees (0.2).



The thickness of the seismogenic North American crust varies along the length of the fault zone. At its seaward end, the depth of the seismogenic crust is about 5 kilometers; it gradually increases to 25 kilometers at the southeastern end of the Little Salmon fault. The average seismogenic depth along the entire length of the fault, then, is about 15 kilometers.

The Little Salmon fault zone is considered to be part of an upper plate thrust system that is associated with the Cascadia subduction zone. This thrust system is called the Little Salmon fault system. Offshore, the fault system bends northward, trending parallel to the deformation front (Figure 2-5). The fault system continues north to the Thompson Ridge fault, which demarks a change from oblique crustal shortening on *en echelon* thrust faults to strike slip bounded rotational blocks. The Little Salmon fault system has a total length of 310 kilometers. The full length of the Little Salmon fault system is assumed to rupture during the maximum earthquake because it is assumed to be part of a larger Cascadia interface rupture.

The Little Salmon fault zone has several traces in the region near the ISFSI, which affect the assessment of the fault-to-site distance (Figure 2-5). The Little Salmon and Bay Entrance faults are considered to be the primary fault traces that accommodate the main slip. The Buhne Point and Discharge Canal faults are minor splay faults in the hanging wall of the Bay Entrance fault (Section 4.0). They are not considered to be main elements of the Little Salmon fault zone.

Displacement per Event

The displacement on the Little Salmon fault zone was computed using the Megathrust model assuming 100 per cent interseismic locking between the plates, and the total strain accrued by convergence of 30 to 40 mm/year was evenly divided among the three events for each megacycle. The Little Salmon fault zone is considered to accommodate half of the total slip on the subduction zone. During a 1400 year megacycle the total subduction zone slip for the three events would be 42 to 56 meters, or 14 to 18.6 meters per event. Slip per event on the Little Salmon fault zone is assigned half of these values, or 7 to 9.3 meters per event.



Rupture Synchronous with Plate Interface Events

Studies of the timing of individual displacement events on the Little Salmon fault zone and comparisons with episodes of subsidence and uplift elsewhere along the Humboldt coastal region led Clarke and Carver (1992) to postulate that the Little Salmon fault zone may undergo slip in conjunction with the plate interface.

The Little Salmon fault system is considered to be part of the Cascadia interface and always ruptures with the interface event (weight for synchronous rupture = 1).

Earthquake Recurrence Intervals

The recurrence rates developed for the plate interface are assumed to apply to the Little Salmon fault zone and the Little Salmon fault system.

MAD RIVER FAULT ZONE

Source Geometry

The Mad River fault zone is a zone up to 10 kilometers wide consisting of at least five major, northwest-trending, northeast-dipping imbricate thrust faults. Field studies focusing on displacement of marine and fluvial terraces have shown them to have a history of late Quaternary slip (for example, Carver, 1987a; 1992; Kelsey and Carver, 1988). Recent preliminary studies have identified a fault, called the Greenwood Heights fault, which intersects the northernmost tip of Humboldt Bay. This fault marks the southern boundary of the Mad River fault zone. The northwestern extent of the zone is based on seismic reflection data (Clarke, 1992), and the southeastern limit of the zone is based on the approximate location of a cluster of seismicity about latitude 40.5°N that appears to crosscut the Mad River trend. The Mad River fault zone extends for a total distance of about 80 kilometers.

The dips of individual faults in the Mad River zone are assumed to be the same as those of the Little Salmon fault zone.



Table 5A-1

RECURRENCE INTERVALS AND SLIP PER EVENT FOR THE
CASCADIA SUBDUCTION ZONE

Pacific Gas and Electric Company
Humboldt Bay ISFSI

Event	Age (ybp)	Interseismic Interval (yr)	Megacycle	Megacycle Interval (yr)	Accumulated Strain (m)		Slip/event (m)	
					At 3 cm/yr	At 4 cm/yr	At 3 cm/yr	At 4 cm/yr
			W-Future (1 event and counting)	1100+	33+	44+		
Future	?	300+			9	12	9+	12+
"Y"	300	800			24	32	24	32
			N-W (3 events)	1400	42	56	14	18
"W"	1100	200			6	8	6	8
"U"	1300	300			9	12	9	12
"S"	1600	900			27	36	27	36
			O-N (3 events)	1400	42	56	14	18
"N"	2500	400			12	16	12	16
"L"	2900	200			6	8	6	8
"P"	3100	800			24	32	24	32
			?-O	?				
"O"	3900	?						



**EMPIRICAL RELATIONSHIP BETWEEN TSUNAMI RUNUP AND EARTHQUAKE
SOURCE PARAMETERS**

by

George Plafker, Ph.D.

Plafker Geohazard Consultants
235 Highland Terrace
Woodside, CA 94062

Prepared for Pacific Gas and Electric Company

George Plafker

09/01/02



Humboldt Bay ISFSI Project
Technical Report
TR-HBIP-2002-01

9A-1

Appendix 9A
Rev. 0, August 23, 2002

CONTENTS

INTRODUCTION.....	4
Purpose	5
Terminology	5
Methods	6
NEAR-SOURCE TSUNAMI GENERATION	7
CASE HISTORIES FOR SELECTED TSUNAMIGENIC EARTHQUAKES	7
1960 Chile Earthquake.....	7
1964 Alaska Earthquake	9
1991 Costa Rica Earthquake	11
1992 Nicaragua Earthquake	12
1992 Flores Earthquake	12
1992 Hokkaido Earthquake	13
1994 Mindoro Island Earthquake	15
1998 Aitape (Papua New Guinea).....	16
1946 Aleutian Earthquake	16
1994 Java Earthquake.....	17
2001 Southern Peru Earthquake	18
RESULTS	19
Moment Magnitude vs Slip for Tsunamigenic Earthquakes	19
MOMENT MAGNITUDE VS TSUNAMI RUNUP HEIGHTS	19
Events Showing Linear Tectonic Tsunami (T _{max}) Runup/Magnitude Trend.....	20
Earthquakes Having Relatively Large Tsunami Runup Peaks (T _{peak}) of Unknown Origin	20
Tsunamis with Relatively Large Tsunami Runup Peaks (T _{peak}) of Known or Probable Landslide Origin	20
Summary.....	21



CASCADIA IMPLICATIONS..... 22
 Comparison of Model Cascadia event with Historic Tsunamigenic Earthquakes.....22
 Tsunamigenic Submarine Landslides on the Cascadia Margin?22

FIGURE CAPTIONSERROR! BOOKMARK NOT DEFINED.

TABLE CAPTIONS.....ERROR! BOOKMARK NOT DEFINED.



EMPIRICAL RELATIONSHIP BETWEEN TSUNAMI RUNUP AND EARTHQUAKE SOURCE PARAMETERS

INTRODUCTION

Background

The general association of some earthquakes with tsunamis has been known since ancient times. Tsunamis have been known in Japan since the beginning of recorded history and a catalog of 177 Japanese tsunamis between 684 and 1984 A.D. provides data on tsunami run-up heights, travel times, damage, and earthquake damage and intensity (Watanabe, 1985). In the Pacific northwest, including northern California, American native oral histories recount earthquake and tsunami events, the last of which was in 1700 (Carver and Carver, 1996), and the context of the histories makes it clear that these peoples were aware of the link between earthquakes and tsunamis long before the last event.

Recently, predicting the amount of tsunami inundation has become a concern as modern society relies more and more on coastal facilities for commerce and living. Estimating potential runups as a hazard is now done for all major coastal installations, such as nuclear power plants, liquefied natural gas loading facilities, and major harbor installations. To help address the problem scientists and engineers have gathered physical information on historical tsunamis and on prehistoric tsunamis (paleotsunamis). Recently computer models have been designed to assess the potential hazards, either regionally, such as Bernard and others, 1994, Meyers and others, 1999, or for specific coastal facilities, harbors, and communities.

In order to help assess the potential tsunami at PG&E's Humboldt Bay ISFSI site in Humboldt Bay, data for historical earthquakes worldwide was reviewed and the important events summarized. The data was then analyzed for empirical relationships and the results used to assess the potential runup heights for tsunamis generated by the Cascadia subduction zone on the northern California coast at Humboldt Bay.

The Cascadia subduction zone is a potential source of large tsunamigenic earthquakes related to slip on the megathrust and on subsidiary faults within the upper plate. Paleoseismologic data along the northern California coast have been interpreted as indicating at least 6, and possibly 7, tsunamis in approximately 3,000 years before present, with the last event about 300 years ago (Carver and others, 1998). Geologic estimates by Carver and others (1998) further suggest maximum runup heights for these tsunamis of 8–19 m in northern California and about 10 m along the coast at the ocean side of the Humboldt Bay spit.



The potential tsunami hazard to facilities at the Pacific Gas & Electric Company Humboldt Bay Power Plant site can be modeled, but the runup and current velocities obtained at coastal sites from modeling depend heavily on input parameters used for the tsunami source. In particular, the fault slip and the area affected by vertical coseismic displacements of the sea floor, together with the bathymetry, control tsunami runup at specific sites on the adjacent coasts. Because there have been no large historic tsunamigenic earthquakes on the Cascadia subduction zone, appropriate assumptions have to be made regarding earthquake mechanism, size, and expected sea floor deformation.

Purpose

This study was undertaken to help constrain input parameters for a plausible tsunami source in southern Cascadia by comparison with all large historic tsunamigenic earthquakes worldwide since 1943. Included in this group are those events for which the faulting mechanism is understood, the moment magnitude and fault slip have been calculated, and for which observational data are adequate to characterize the tsunamis such as local tsunami runup, arrival times, and coseismic shoreline displacement.

For most of the tsunamigenic earthquakes, the associated tsunamis are primarily generated by large-scale coseismic vertical tectonic displacement of the sea floor. However, in some events, such as the 1946 Aleutian, 1964 Alaska and 1991 Flores island earthquakes, by far the highest runup was from local waves associated with earthquake-triggered submarine landslides. Other tsunamigenic earthquakes in which there are local areas of very high runup but no known underwater landslides, most notably the 1992 Hokkaido earthquake, are clearly anomalous when compared to the majority of tsunamigenic events for which good data are available. For some earthquakes considered to be tsunamigenic most notably the 1994 Mindoro Island strike-slip earthquake, both the earthquake mechanism and the wave distribution and runup point to a landslide, rather than tectonic, origin. Analysis of the worldwide data supports the hypothesis that large submarine slides that occur as a secondary effect of earthquake shaking are probably far more common than has been generally recognized.

Terminology

The term *tsunami* does not have universal meaning, something that has resulted in a remarkable amount of confusion and imprecision in the literature because it has been applied to waves generated by a host of sources. As used here, *tsunami* refers to the general class of impulsively generated waves that are usually, but not necessarily, associated with earthquakes. *Seismic sea wave* is a term that specifically refers to long-period tsunami caused by large-scale earthquake-related displacement of the sea floor and characteristically propagate for hundreds to thousands of kilometers. The term *landslide-generated wave* is used to describe more local tsunami generated by submarine or subaerial landslides.

A *tsunamigenic earthquake* is any earthquake that generates a tsunami. Tsunamigenic earthquakes are most commonly caused by slip on thrust faults in arc subduction zones and in



back arc tectonic settings. The terms “*slow*” or “*tsunami*” *earthquake* are used to describe earthquakes for which the moment magnitude is significantly greater than the shear wave magnitude due to slow rupture velocity. These have been attributed to generating tsunamis that have disproportionately higher runup than “normal” earthquakes of comparable shear wave magnitude (Kanamori, 1972). However, this relationship can only be confirmed for two events in my analysis.

Terms used for wave height are also ambiguous. Rigorously defined, *wave height* is the distance from crest to trough of the wave before it runs up on the land. *Runup height* or elevation is the highest altitude above tide level or some other datum (such as mean sea level or extreme high tide level) that the water reaches as it runs up on the land. Comparison of runup heights requires information on the tide stage at which the wave arrived and the vertical coseismic displacement of the shoreline at that site, information that is seldom available. *Tsunami maps* show graphical or numerical plots of measured wave runup for tsunamigenic earthquakes at near-source coastal sites.

Methods

For this study, I have compiled near-field tsunami runup data, coseismic vertical displacement data, and seismologic data for selected better-described large tsunamigenic earthquakes.

Included are:

- Compilation of unpublished tsunami runup maps, and relevant data on coseismic vertical shoreline displacements, and wave arrival times for the 1960 Chile, 1964 Alaska, and 1991 Costa Rica earthquakes (Tables 1-3; Figures 1-3) and a new tsunami runup map for the 1946 Aleutian earthquake (Fig. 9).
- Analysis of tsunami histories and tsunami runup maps for the 1946 Aleutian, 1960 Chile, 1964 Alaska, 1991 Costa Rica, 1992 Nicaragua, 1992 Flores Island, 1994 Hokkaido, 1993 Mindoro Island, 1998 Papua New Guinea, 1946 Aleutian, 1994 Java, and 2001 Peru earthquakes (Figs. 1-11). These events were chosen for analysis because they include some of the largest and best-studied earthquakes, or because they illustrate the effects of complexities on tsunami generation and runup, such as landslides, “slow” earthquakes, differential slip at the earthquake source, intraplate faults, and topography.
- Summary of critical earthquake source parameters, particularly calculation of seismic moment and seismically determined slip for 35 of the largest tsunamigenic earthquakes since 1943 (Table 4; Figure 12)

Synthesis of relevant data on tsunami runup for 35 tsunamigenic earthquakes (Table 5) and derivation of an empirical relationship between maximum tsunami runup versus earthquake magnitude (Fig. 13).

The data used focus on tsunamis generated by tectonic displacement and on submarine landslides. Data for tsunamis generated by other sources such as subaerial landslides,



meteorites, underwater explosions, and volcanic explosions are not included because they do not apply to the potential for tsunamis generated by earthquakes on the Cascadia subduction zone.

NEAR-SOURCE TSUNAMI GENERATION

The rate and amount of vertical displacement of the seafloor, whether by tectonic displacement or gravitational sliding, are the critical factors in generation of earthquake-related tsunamis. Unfortunately, the vertical component of displacement in offshore subduction zones and back arc settings have rarely been well defined by fieldwork, geodetic data, or seismologic data. Recent advances in the capabilities of the WWSN and GPS networks, have resulted in greatly improved capabilities for determining fault parameters in most parts of the world.

Among the earthquake source parameters evaluated by Geist (1998), the magnitude of slip and the spatial variations of slip have the dominant effect on excitation of near-source tectonically-generated tsunamis. Our data indicate that both average fault slip and maximum regional tsunami runup correlate generally with earthquake size as measured by seismic moment or earthquake magnitude—but only after removal of those tsunamis caused by large earthquake-triggered submarine landslides.

CASE HISTORIES FOR SELECTED TSUNAMIGENIC EARTHQUAKES

In this section we briefly review data for selected tsunamigenic earthquakes that provide insights regarding mechanism of tsunami generation and, in particular, problems involved in distinguishing between tectonic *versus* landslide or other origins for the near-source waves. Tsunamigenic events discussed are the 1960 Chile, 1964 Alaska, 1991 Costa Rica, 1992 Nicaragua, 1992 Flores Island, 1994 Hokkaido, 1993 Mindoro Island, 1998 Papua New Guinea, 1946 Aleutian 1994 Java, and 2001 Peru (Figures. 1-11).

1960 Chile Earthquake

The 1960 Chile M_w 9.5 earthquake was the greatest instrumentally recorded earthquake in the world. It occurred near the southern end of the Peru-Chile continental margin arc where it ruptured a segment of the megathrust between 900 and 1200 km long and 150 to 300 km wide down dip (Figure 1). The earthquake produced the largest and most destructive trans-Pacific tsunami modern times and a near-source tsunami with runups of 10 to 15 m along some 550 km of the Chilean (Sievers and others, 1963; Plafker and Savage, 1970). Within Chile, the earthquake and tsunami took more than 2,000 lives and caused an estimated \$550 million in property damage. The transoceanic seismic sea waves killed an additional 230 people and caused an estimated \$125 million in Japan, Hawaii and the Philippine Islands.

The 1960 main shock was the culmination of a complex seismic sequence that lasted 33 hours. Details on the 1960 earthquake mechanism and, in particular, the dip angle, down dip extent, and



slip on the causative fault and seismic moment are poorly determined (Table 4). Kanamori and Cipar (1974) estimated the seismic moment to be 2.7×10^{23} Nm with an average dislocation of 24 m; the main shock moment was later revised by Kanamori (1977) to 2.0×10^{23} Nm. In summary, the geodetic data suggest average slip between 8 and 20 m and a seismic moment close to 1.0×10^{23} Nm whereas More recent seismologic investigations indicate average slip in the range of 19 to 32 m and moment of 1.0 to 3.2×10^{23} Nm depending upon assumptions regarding dip and width of the fault surface (Cifuentes, 1989; Linde and Silver, 1989).

A best-fit uniform slip dislocation model of the horizontal and vertical tectonic displacements suggests average slip of about 20 m on a fault plane 850 x 130 km, dip $\sim 20^\circ$ and moment 0.6 to 1.2×10^{22} Nm (Plafker and Savage, 1970). Using a variable slip dislocation model for a fault 900 km long and 150 km wide, Barrientos and Ward (1990) obtained average slip of 8 m, local concentrations of slip to 41 m, average dip of 15° to 25° , and total moment release of 9.5×10^{22} Nm; a uniform dislocation model for these same data yields 17 m average slip and a moment of 9.4×10^{22} Nm. In summary, the geodetic data suggest average slip between 8 and 20 m whereas the seismologic data indicate average slip in the range of 19 to 32 m and maximum slip is 40+ m.

The earthquake was accompanied by regional coseismic uplift of at least 5.7 m, subsidence of as much as 2.3 m, and large transverse horizontal displacements in a seaward direction (Figure 1). The tsunami was generated by tectonic uplift of roughly 10,000 km² of the continental shelf and slope. In the near field, measured tsunami runup heights of 4 to 15 m were measured along some 850 km of the outer coast, on offshore islands, and in the southern archipelago (Fig. 1, Table 1). Wave runup was 3 m or less in inland waters of the Golfo de los Chonos adjacent to the southern part of the earthquake source region (Nos. 1-3, 5, 6).

The 15 m maximum tsunami runup height is within the range of geodetically calculated average slip on the megathrust (8-20 m) and it is considerably less than the range of seismologically determined slip (19-32 m). The vertical component of slip, assuming it is all on the megathrust and average near-surface dip is 20° , about 3 to 11 m. Dislocation modeling of the coseismic vertical displacement data suggests that a subsidiary reverse fault, with an average dip of approximately 40° splays off the southern part of the megathrust and breaks through the upper plate to the surface near the edge of the continental shelf in the southern part of the tsunami source region (Plafker and Savage, 1970). For a subsidiary fault that accommodates most 75% of the dip slip (as occurred in 1964 Alaska earthquake), the vertical component of uplift near the shelf edge could be 5.5 to 19 m and for maximum slip and (or) steeper dips it could be twice as much. Uplift at the tsunami source in the upper part of this range is capable of producing the runup observed.

Hatori (1966) used the tsunami energy calculated from circum-Pacific tide gages to derive an average vertical displacement at the tsunami source of 5.7 to 10 m over a source area of 138,000 km² (based on the offshore focal region). These results are significant because they indicate that large submarine uplifts of the type postulated for the southern part of the source region must have occurred over most of the region to generate the tsunami that was recorded throughout the Pacific Ocean basin.

Surprisingly for the size of this event, no landslide-enhanced tsunamis are evident in the data. In part this may be because sediment supply to the continental shelf and slope is low and deep



water near shore is unusual. Any slide-generated waves that originated off the shelf were likely to be obscured by the ubiquitous tsunami that was generated there by tectonic uplift. Submarine slides that have gone unreported may have well have occurred in the sparsely inhabited southern archipelago area where very few measurements of wave runup were made.

Although many puzzling aspects of the 1960 Chile earthquake remain to be resolved, it is clear that the tsunami generated by the largest earthquake in recorded history was tectonic in origin and that the 15 m measured maximum runup heights are reasonably compatible with known and inferred tectonic uplift on the continental shelf.

1964 Alaska Earthquake

The great 1964 Alaska M_w 9.2 earthquake, the second largest instrumentally recorded earthquake in the world, was located at the eastern end of the Aleutian arc where the arc extends obliquely onto the North America continental margin (Figure 2; Table 2).

The earthquake and waves took 129 lives and caused more than \$300 million damage. In Alaska, nine deaths were attributable to structural failures and subaerial landslides. The other deaths and property damage in Alaska were from slide-generated waves (85) and seismic sea waves (20). In coastal areas from British Columbia to northern California the seismic sea waves took 15 lives and caused extreme damage locally.

The earthquake was generated by rupture of a segment of the Aleutian megathrust that is about 650 km long and 175 to 290 km wide down dip. Displacement occurred along the megathrust at least two subsidiary splay thrust faults that broke through the upper plate at Montague Island and the adjacent continental shelf to the southwest. Dip of the megathrust averages 9° and average dip slip has been estimated from seismological data as 8.6 and 12.1, with maximum slip of 18 m (Table 2). Two splay faults exposed on Montague Island dip 50 to 85° and have maximum measured dip-slip of 7.9 and 6.0 m. At least one additional active splay fault is inferred near the edge of the continental shelf based on 3.5 m coseismic uplift and landward tilting of Middleton Island. The measured horizontal and vertical coseismic displacements, together with faulting, suggest that maximum slip is more than 20 m, and possibly as much as 30 m in the northern part of the displacement field (Plafker, 1972).

Seismic Sea Waves

Coseismic uplift over some 120,000 km² of the continental shelf and slope generated a major seismic sea wave train (tsunami) having a period of about 50 minutes (Plafker, 1969). The first wave arrivals at inhabited sites along the Gulf of Alaska coast were recorded by residents some 19–20 minutes after start of the earthquake. Arrival times indicate that the wave source corresponds with a well-defined zone of intraplate splay faults and maximum uplift that extends SW from Montague Island offshore at least 450 km to the southern Kodiak Islands .

Near field measured runup heights, corrected for vertical tectonic displacements that accompanied the earthquake, range from 3 to 12.7 m, and runup of 10 to 12.7 m occurred at



widely separated sites along some 500 km of this sparsely inhabited coast (Fig. 2, Table 2). Maximum runup height of 12.7 m is close to the probable average slip on the megathrust. This is also close to the measured vertical component of coseismic uplift at the tsunami source (11.3 m) and its inferred offshore extension. Along Shelikof Strait on the inland side of the Kodiak Islands group, recorded runup was 2.8 m or less indicating significant damping of the wave amplitudes in the more enclosed water bodies. Compared to the 1960 Chile earthquake, runup was more variable, possibly reflecting the considerably more irregular bathymetry and configuration of the glaciated outer coast of the Kenai Peninsula and Kodiak Islands.

Submarine Slide-Generated Waves

The 1964 Alaska earthquake triggered numerous submarine and subaerial landslides and associated short-period local waves ("tsunami") along the walls of the steep-sided fiords that indent the shores of Prince William Sound and the coastal mountains to the southwest of the sound (Kachadoorian, 1965; Coulter and Migliacci, 1966; Lemke, 1967; Plafker and others, 1969). Comparable underwater slides and waves also occurred in some of the large glacial lakes, most notably in Kenai lake (McCulloch, 1966). The slides were concentrated mainly in unstable, poorly consolidated delta and glacial deposits, but undoubtedly involved bedrock at some localities.

The resulting waves, which were the main cause of earthquake-related damage and loss of life from the earthquake, were generated during or immediately after the earthquake. These landslide-generated waves had completed their destruction long before arrival of the seismic sea waves generated by coseismic uplift of the continental shelf. Run up was extremely variable with heights at scores of localities above 10 m, tens of sites above 30 m, and the highest measured run up was close to 52 m in Valdez Arm. This slide-generated runup is as much as 4 times higher than the highest runup (12.7 m) attributable to the tectonically generated tectonic tsunami (#2, Fig. 2) and it is the highest runup documented for a submarine slide wave.

Lessons learned from the Alaska earthquake include:

- Splay faults are an efficient mechanism for generating regional tectonic tsunamis and that the steeper the fault dip the higher the tsunami for a given amount of slip;
- Maximum wave runup along irregular open coasts approximates measured maximum tectonic uplift and the calculated average slip on the fault source from seismologic data;
- Earthquake-triggered landslides near shore are ubiquitous in poorly consolidated deposits and areas of steep underwater slopes such as are present in fiords and rugged mountainous coasts;
- Waves generated by submarine slides can be violently destructive within a few kilometers distance of their origin and they attenuate rapidly away from the source;
- Submarine slide generated waves can be almost any height up to a maximum of 4 times the highest runup of a tectonic tsunami; and

- Both the submarine slide failures and the waves they generate are inherently extremely dangerous to coastal residents and property because they commonly occur in unstable fiord deltas which are the preferred areas for locating coastal communities and port facilities;
- Because landslide-generated waves can strike so quickly after start of an earthquake, the opportunity for residents to escape to higher ground is drastically reduced relative to the tectonic tsunamis—in Alaska, they accounted for 85 of the 105 deaths attributable to waves.

1991 Costa Rica Earthquake

The 1991 Costa Rica M_w 7.5 earthquake occurred by rupture of a back arc thrust fault 80 km long and 40 km wide that dips about 30° landward on the Caribbean Sea side of the Middle America arc (Figure 3; Table 3). The earthquake and tsunami caused 75 deaths, 563 injuries, and left nearly 10,000 people homeless along the Caribbean coast of Costa Rica and northern Panama. This earthquake is of interest here because the generally smooth and gently sloping sea floor together with a dominantly linear low-lying coast precludes the possibility of large earthquake-triggered landslide waves and large wave amplification effects of topography. In addition, coseismic vertical displacements have been measured along the coast so that corrections for tectonic displacement could be made for the measured runup heights (Fig. 3, Table 3) and tidal fluctuations are so small that they need not be considered.

The earthquake occurred on a shallow back arc thrust fault that dips southwest beneath the coast of Costa Rica and the Middle America arc (Plafker and Ward, 1992). Combined geodetic and seismologic data suggest that the main rupture is 40 km 80 km long by 40 km wide and that it dips landward at 30 - 38° . Measured vertical uplift along the coast increases gradually from 30-40 cm in the south to 1.6 m near the northern end near where the fault trace intersects the coast at a structural and topographic high. The dislocation models suggest 2.2 m average slip on the causative fault, and the average vertical component of slip averages 1.1 to 1.4 m.

Measured tsunami runup heights range along 80 km of coast near the earthquake source for all measurements except one range from 0.65 to 1.55 m—equal to, or less than, the maximum measured shoreline uplift of 1.6 m. At one locality, runup reaches 2 meters, 1.25 maximum measured uplift or 1.4–1.8 times the calculated average coseismic uplift (Table 3).

In summary, the 1992 event is of interest because it provides data for the relationship of maximum runup to the vertical component of fault displacement for a tectonic tsunami that is not unduly complicated by landslides, unusual bathymetry, or irregular configurations of the coast. Like the great 1960 Chile and 1964 Alaska earthquakes at the opposite end of the magnitude



scale for tsunamigenic earthquakes, runup heights are less than average fault slip and they are close to maximum measured uplift.

1992 Nicaragua Earthquake

The 1992 M_w 7.7 earthquake, which was generated by slip on the Middle America arc megathrust off the coast of Nicaragua, is shown as an example of a "slow" earthquake for which excellent source and runup data are available (Fig. 4). Seismologic data indicate average fault slip ranging from 0.5 to 1.3 m, maximum slip of 10 m, and a fault dip of 10° (Table 4). Average near-source tsunami runup averages about 6 m with two broad peaks of runup to about 8 and 10 m (Table 5).

For this event, maximum vertical displacement is 1.8 m, based on the maximum value for slip and the fault dip. Thus, runup is 4 to 6 times larger than the vertical component of displacement at the tsunami source, assuming that the slip is entirely on the megathrust. This large difference between vertical component of slip and runup height contrasts markedly with those deduced for the 1960 Chile, 1964 Alaska, and 1991 Costa Rica events described above for which the runup height of the tectonic tsunamis is close to vertical tectonic displacement.

One proposed explanation for this discrepancy is non-uniform slip distribution along strike so that areas of highest moment release along the fault would match the somewhat bimodal distribution of the highest tsunami runup (Geist, 1998) much more than the 10 m maximum displacement on the megathrust. Alternative explanations for the runup heights and distributions are that two or more very large earthquake-triggered submarine landslides occurred on the continental slope or that partitioning of slip onto steeply dipping splay faults in the upper plate occurred in the areas of high moment release. Existing data do not allow for a choice between the various alternatives.

1992 Flores Earthquake

The 1992 Flores Island M_w 7.5 tsunamigenic earthquake accompanied rupture of a segment of the Flores fault in the backarc region of the Indonesia island arc (Fig. 5). The shaking and tsunami resulted in 1,974 deaths, 2,126 injuries, and \$80 to \$100 million property damage; about half of the death toll and damage is attributed to the shaking and half to the tsunami.

The earthquake involved rupture of a segment of the Flores thrust fault about 100 km long by 40 km wide that dips southward beneath the Indonesian arc. Coseismic vertical shoreline displacements of as much as 1.05 m help to constrain the earthquake mechanism, and the tsunami runup heights have been well determined from field studies (Fig. 5). Dip of the causative fault is about 40° and average slip is about 3.2 m. The calculated maximum vertical component of slip is about 2.4 m assuming uniform slip on the Flores thrust (Plafker, 1997).

The tsunami exhibits both a regional component (tectonic) of observed runup heights (<5 m) roughly compatible with computed runup heights, as well as local areas of higher runup (to 26 m) that are significantly larger than computed heights (Fig. 5). The lower runup occurs in the western part of the source region where topography both onshore and offshore is relatively



subdued and at most offshore islands. Much more variable and higher runup occurs in areas of rugged submarine and subaerial topography that characterize much of the coast of Flores Island and Babi island in the eastern half of the affected area.

Most of the anomalously high runup areas in the extreme eastern part of Flores island are known to result from submarine landslides or combination submarine and subaerial landslides (Yeh and others, 1993; Plafker, 1997) and many other slides for which nearshore evidence is lacking undoubtedly occurred elsewhere. Along these coasts, fringing coral reefs up to a few hundred meters wide drop precipitously into water depths of 200 meters or more and there was abundant evidence for earthquake-related rock falls, extensional cracks, and landslides along the reef fronts (Plafker, 1977). Maximum runup in the western region is about twice as large as average vertical fault displacement (2.4 m), whereas for known landslide-generated waves it is nearly 11 times higher (Fig. 5).

Evidence for a landslide origin of the highest runup on Flores and adjacent islands typically includes one or more of the following features in the immediate vicinity:

- Visible landslides and rock falls occurred along shorelines having steep subaerial and submarine slopes;
- Local segments of fringing coral reefs were visibly cracked or destroyed by landslides;
- Shoreline vegetation and facilities showed directional damage, indicating that waves radiated away from point sources at or near the shoreline;
- Eyewitness's reports of movement of large waves parallel to the shoreline during or immediately after the earthquake;
- High and destructive waves arrived at coastal communities during or immediately after the earthquake. SCUBA divers mapped areas of extensive damage to the generally sheer reef walls of Besar, Babi, and nearby small islands north of Flores Island that they attribute to underwater rock falls and landslides at the time of the earthquake.

For this event, the data suggest that the local high (to 26 m) and variable tsunami runup throughout the eastern half of the source region was caused by numerous submarine and combination subaerial and submarine slides that were triggered by earthquake shaking. These slide-generated waves were subsequently followed by a tectonically generated wave train that had runup less than ~5 m throughout the region.

1992 Hokkaido Earthquake

The 1992 Hokkaido M_w 7.7 to 7.9 tsunamigenic earthquake ruptured a complex of at least 3 thrust fault segments that total 100 to 120 km long by 30 to 60 km wide in the backarc region of the northern Japan island arc (Satake and Tanioka, 1995; Somerville, 1995). The earthquake and



tsunami caused 231 fatalities on Okishiri Island of which 208 deaths were attributed to the tsunami. Property losses on Okishiri and Hokkaido Islands have been estimated at \$1 billion primarily due to tsunami and fire damage (Bernard, Gonzales, and Sigrist, 1995).

Based on seismological data, the fault zone trends north-south and has variable dip directions and angles; the northern segment dips east at a low angle and has 2 m of average slip whereas two longer southern segments dip west and have average slip of 2–6 m (Satake and Tanioka, 1995). Dip of the causative fault, as interpreted by several investigators from seismological data, range from 25 to 45°. Assuming maximum values for slip and dip, the average vertical component of sea floor displacement at the tsunami source can be no more than 4 m.

Detailed studies indicate that tsunami runup along the coast of Hokkaido and all but a small segment of Okushiri Island and western Hokkaido Island had wave runup of 12 m or less. This is up to 3 times larger than the maximum vertical component of slip at the tsunami source (Fig. 6). By contrast, a 20 km long portion of the south end of Okushiri Island was swept by waves that had runup of 15 to 32 m, or 8 times the vertical slip component.

The exceptionally high runup has been attributed to the close proximity of the wave source to the south end of Okushiri Island and to near-shore wave amplification by submarine and subaerial topography (Matsuyama and Tanaka, 2001; Satake and Tanioka, 1995; Titov and Synolakis, 1997). The wave directions from the northeast and east at the southeast tip of the island were attributed by investigators to refraction of waves as they propagated around the south end of the island from a source region west of the island (Hokkaido-Nanseki-Oki Earthquake Reconnaissance Team, 1995).

Experimental flume modeling of the pocket beach where maximum runup occurred (Matsuyama and Tanaka, 2001) and numerical analysis of the entire region using a shallow water wave approximation model (Titov and Synolakis, 1997) appear to adequately reproduce the regional tsunami runup for a source wave of about 4 m. If the assumed source uplift and the modeling are valid, this is the only tsunamigenic earthquake for which runup height is as much as 4 times maximum coseismic vertical displacement at the source.

Despite the intensive investigations into this event, some of the data suggest to me that submarine slide-generated waves probably caused some or all of the exceptionally high runup on southern Okishiri Island. A possible landslide origin is indicated by the following:

- The highest runup areas coincided with unusually steep coastal and offshore topography;
- Large onshore landslides were triggered by the earthquake in the same general area;



- Shorelines in areas of highest runup were inundated within minutes after the earthquake suggesting a nearby source; and
- Reports by investigators that the early waves that struck the southeast tip of Okishiri Island came from the NE, on the opposite side of the island from the tsunami source and with the opposite sense of predicted movement for tectonically-generated waves.

1994 Mindoro Island Earthquake

The 1994 Mindoro island M_w 7.1 earthquake occurred within the Philippines island arc by rupture of at least 35 km of the Aglubang dextral strike-slip fault on northern Mindoro Island and offshore beneath Verde Island Passage (Fig. 7). The earthquake generated a tsunami that devastated several small villages on northern Mindoro Island and on several offshore islands with loss of at least 58 lives (PHIVOLCS, 1994; Wells and Porazzo, 1994).

Measured onshore fault slip was 3.45 m horizontal with a local vertical component of as much as 1.2 m near the southern end of the rupture. Shortly after the earthquake, a tsunami struck parts of the coast of northern Mindoro Island, local areas of southern Luzon Island, and small islands in the intervening Verde Island Passage. Data on runup heights, which reach 7.3 m on Baco Island, and inferred direction of wave travel are shown on Figure 7. There are no reports of coseismic vertical tectonic displacements of shorelines, and none are to be expected for this small dominantly strike-slip event.

The data indicate to me that the tsunami that followed the earthquake were caused by multiple submarine landslides, the largest of which was located near the epicenter in South Pass off the Aglubang River delta. Other possible submarine landslide sources could account for the tsunami runup on Luzon Island near Lobo and possibly in Batangas Bay.

A landslide interpretation is supported by:

- Topography characterized by steep and irregular volcanic shorelines along which large subaerial landslides were triggered by the earthquake;
- Reports by fishermen of upwelling water and bubbles after the earthquake offshore from Baco suggesting that one or more submarine slides from river deltas in the area released methane entrapped in the sediments;
- The generally radiating pattern of wave movement directions from an offshore area southwest of Baco Island, that suggests one or more point sources as would be expected for submarine landslides on the Aglubang River delta; and
- (4) Arrival of the waves within 2–5 minutes of the earthquake indicating near-shore wave sources.

There are no data to support the interpretation that the tsunami was somehow directly related to tectonic displacement on the Aglubang fault as suggested by Imamura and others (1995).



1998 Aitape (Papua New Guinea)

The 1998 Mw 7.1 Aitape earthquake (also referred to as Papua New Guinea earthquake) occurred south of the New Guinea Trench that marks the plate boundary between the Australian plate on the south and the obliquely underthrusting ocean crust of the North Bismark Sea plate to the north. The seismologic data indicate that this was a “slow” earthquake on a 40-km long reverse fault with steep south dip and average slip of 2.15 m (Geist, 1998).

The earthquake was followed within 11 to 19 minutes by the arrival of three successive waves along a 40-km segment of the northern coast of New Guinea (Fig. 8). Maximum runup of 10 to 15 m in a 14-km segment of coastline was centered on the villages of Arop, Warapu, and Nimas along the margins of Sissano Lagoon (Fig. 8). The tsunami obliterated all three villages, resulted in about 2,200 deaths, 1,000 serious injuries, and left some 10,000 people homeless; there were no casualties reported due to earthquake shaking.

Tsunami runup for this event is unusually large for the magnitude. Despite intensive research into all aspects of this event, the source of the tsunami remains controversial. It has been attributed to either a steep offshore fault (Geist, 1998; Hurukawa and others, Satake and Tanioka, 1999; etc.) or a massive sediment slump (Tappin and others, 2001; Synolakis and others, 2002; etc.). Results of extensive marine surveys reveal a recently active submarine landslide with an area of ~25 km² offshore from Sissano Lagoon that can account for the tsunami arrival time and runup distribution along the adjacent coast. In contrast, the surveys in the possible tsunami source area have not found any evidence of faulting adequate to generate the observed tsunami runup heights and in a location consistent with the wave arrival time.

1946 Aleutian Earthquake

The 1946 Aleutian earthquake (Mw 8.6) was situated ~150 km offshore from Unimak Island along the inner wall of the Aleutian Trench (Fig. 1). This event is unique among tsunamigenic earthquakes in that it generated both very high near-field runup (to 43 m) and a very large and destructive trans-Pacific tsunami that caused extensive damage and casualties in the Hawaiian Islands (to 16 m) and other South Pacific islands (Shepard and others, 1946). With an Mw of 8.2 and Ms of only 7.4, it is a classic “slow” or “tsunamigenic” earthquake (Kanamori, 1972).

Aftershock data indicate that the earthquake was generated by rupture of a segment of the Aleutian megathrust about 90 km long by 115–160 km wide down dip (Johnson and Satake, 1997). The earthquake mechanism is poorly known but most likely involves slip that averages about 7.6 m on a gently-dipping (6°) segment of the Aleutian megathrust (Johnson and Satake, 1997).

An alternative interpretation is that a gigantic landslide on the upper continental slope caused both the local and transoceanic tsunamis and may even have been the mechanism of the earthquake (Fryer and Watts, 2001). This hypothesis is based on identification of large sea floor topographic features interpreted as one or more landslide scars and a possible mound that is



inferred to be a landslide deposit. The near-field tsunami obliterated a reinforced concrete lighthouse and its crew of five Coast Guardsmen at the Scotch Cap Station on the southwestern end of Unimak Island (Fig. 9). The wave arrived 48 minutes after start of the earthquake, as reported by survivors at the station who were in a communications facility on a bench above the lighthouse. This timing places the source of the wave near the continental shelf break or uppermost slope and above the inner margin of the aftershock zone; from the Coast Guard Station the inferred source is less than half the distance to the main shock epicenter (Fig. 9, inset).

Figure 9 shows new data on tsunami runup heights and movement directions that were obtained along ocean-facing coasts between Unimak Pass on the west and Sanak Island on the east by measuring the height of driftwood deposited by the tsunami (Plafker, Synolakis, and Okal, 2001). Maximum runup is 42.7 m at the Coast Guard Station and is close to 40 m high for about 50 km east of the station. The wave attenuated rapidly east and west of this headland on Unimak Island and maximum runup on seaward-facing shores of Sanak Island was 23 m. East of Unimak and Sanak Islands runup did not reach above the high tide level along the Alaska Peninsula and offshore islands; we have no information on runup heights west of Unimak Pass. For this event, maximum near-field runup is about 5.5 times larger than the total computed average dip slip (7.6 m) at the tsunami source and it is 11 times larger than the vertical component of displacement at the fault source even for an average megathrust dip as steep as 30°.

The near-field runup data support the concept that the tsunami was generated by one or more large-scale landslides on the upper continental slope south of Unimak Island, although the exact location of the causative slide or slides has yet to be determined. Only a landslide mechanism can account for the wave arrival time at Scotch Cap, runup heights, inferred movement direction of the wave suggestive of a point source, and rapid wave attenuation away from the source. In addition, the slide mechanism is compatible with unconfirmed anecdotal reports by fishermen of local large postquake increases in water depth near the shelf edge.

Neither the near-field wave runup data nor the earthquake mechanism data are adequate to evaluate the relative contributions of tectonic displacements and submarine landslides towards generating the transpacific tsunami.

1994 Java Earthquake

The 1994 East Java earthquake (Mw7.8) occurred 250 km south of the east end of Java Island along the inner wall of the Java Trench (Fig. 10). Seismic shaking was weakly felt or not felt at all on eastern Java and Bali Islands and it did not cause any damage. The earthquake was followed about 40 minutes after the main shock by a tsunami that severely damaged several villages and killed 223 people (Tsuji and others, 1995).

Seismologic data indicate that the earthquake ruptured a segment of the Java megathrust 140 km long by 100 km wide with average slip of only about 1 m (Table 4). This apparent low slip is derived using an improbably high rigidity of 4×10^{10} Pa. Slip can be increased by a factor of about 4 if appropriate low rigidities are assumed for these very shallow near-trench events (Bilek

and Lay, 1999). With an M_w of 7.8 and M_s of only 7.2, it is another example of a classic "slow" or "tsunamigenic" earthquake (Kanamori, 1972).

Tsunami runup on the south coast of eastern Java Island ranged up to 14 m and it was up to 5 m on west Bali Island and the 40 minute travel time was consistent with a source at the earthquake focal region (Fig. 10). On Java and Bali Islands, regional maximum runup is between 3 and 6 m except in a 60 km length of the eastern Java coast where peaks of runup occur between 9 and 14 m high (Tsuji and others, 1995; Synolakis and others, 1995). Attempts to model the tsunami runup, assuming an entirely tectonic origin, have not met with great success (Synolakis and others, 1995). Even with improbably large vertical displacements (~10 m) at the earthquake source, the models obtain runup of 8.3 to 9.3 m but not the peak runup heights observed. Such large vertical displacements would require dip slip displacements of as much as 20 m even for a fault dip as steep as 30° .

Both the regional and peak runups for this earthquake have yet to be reconciled with a purely tectonic origin at the source because of the extraordinarily large slip and vertical displacement that would be required. It is of interest that the highest runup recorded occurs near the mouth of a river which suggests the possibility of a local submarine slide-generated wave. However, earthquake-triggered submarine landslides are unlikely considering the weak seismic shaking caused by the earthquake and it is incompatible with the reported wave arrival time at the coast 40 minutes after the main shock.

2001 Southern Peru Earthquake

The Peru earthquake (8.4 M_w) on 06/23/01 is of special interest because it has provided some of the most complete seismological and tsunami data for a large and relatively uncomplicated tsunamigenic event along a continental margin arc. Shaking damage killed at least 57 people and destroyed or seriously damaged more than 60,000 homes (USAID 2001) and the associated tsunami resulted in an additional 24 dead and missing people (INDEC, 2001).

The earthquake ruptured a segment of the Peru-Chile megathrust 300 km long by 125 km wide (Fig. 11, from Okal and others, in press). Most focal solutions indicate a thrust mechanism with a slight component of left-lateral strike-slip on a gently east-dipping fault plane that strikes roughly parallel to the coast. Average slip on the fault surface is ~2.6 m with a maximum of 4.5 m, centered offshore ~65 km ESE of Camaná (Kikuchi and Yamanaka, 2001). The earthquake rupture was somewhat slow, but does not exhibit the deficiency in high frequencies characteristic of a truly slow, "tsunami earthquake" (Okal and others, in press).

Distribution and maximum height of tsunami runup along the Peru coast, as reported by Okal and others (in press), is shown on Figure 11. The tsunami produced wave heights well above high tide for about 150 km from Atico to Quilca, and damaging waves along the 35 kilometers of coast straddling the Rio Camaná. The average runup height is ~5 m and maximum runup height is 7.25 m, excluding a few higher values that record eyewitness reports of heights to which water splashed against the sea cliffs. Maximum runup is approximately 1.5 times the maximum slip



inferred from source tomography (Kikuchi and Yamanaka (2001). Both the absolute amplitude of the average maximum runup height and lateral extent of the 2001 tsunami are compatible with the seismologically derived dislocation source (Okal, and others, in press). The narrow peak of runup to 7.25 m off Camaná is a few meters too high for the model and may indicate some complication of wave runup due to slumping of the Camaná River delta, submarine bathymetry, or some other unknown cause.

RESULTS

In this section data for all events in the catalog of larger tsunamigenic earthquakes (Tables 4 and 5) since 1943 are summarized and the relevance of these data for forecasting runup for a great tsunamigenic earthquake on the southern Cascadia subduction zone is considered.

Moment Magnitude vs Slip for Tsunamigenic Earthquakes

The relevant seismologic and geodetic data in this catalog suggest that as suggested by Geist (1998), average fault slip scales reasonably well with earthquake magnitude with the notable exception of the 1960 Chile for which slip estimates vary widely (Fig. 12). Furthermore tectonic slip for “slow” (or “tsunami”) earthquakes is not significantly larger than normal tsunamigenic earthquakes of comparable magnitude, assuming constant rigidity as was done for this compilation. “Slow” earthquakes tend to occur along the shallow part of the interplate megathrust near the trench. In this tectonic setting, their slow rupture velocity, relatively low shear wave magnitude, and high average slip have been attributed to a combination of rupture within relatively weak accreted sedimentary rocks and a shallow rupture that intersects the sea floor (Kanamori, 1972; Geist, 1998).

Conditions for generating “slow” earthquakes could be present in the distal part of the Cascadia margin that is underlain by an extensive accretionary prism of Cenozoic age. However, dislocation models based on the configuration of the megathrust from seismologic data, surface geodetic data, and the distribution of coseismic tectonic subsidence from paleoearthquakes, suggest that slip on the Cascadia megathrust is likely to be deeper and further landward than for a typical “slow” earthquake (Hyndman and Wang, 1993, 1995; Clague, 1997). Thus, the slip versus magnitude relationship in Figure 12 should be applicable for a great Cascadia subduction zone tsunamigenic event.

Moment Magnitude vs Tsunami Runup Heights

Moment magnitude is plotted in Figure 13 against maximum tsunami runup height for the major near-field tsunamigenic earthquakes since 1943; data and sources are given in Table 5. For purposes of discussion, the tsunamigenic events are divided into three groups shown by distinctive symbols (Fig. 13).

Events Showing Linear Tectonic Tsunami (T_{max}) Runup/Magnitude Trend

Group "A" includes 33 events for in which the regional upper limit of runup (T_{max}) shows a roughly linear relationship with magnitude (Fig. 13). Within this group are seven tsunamigenic earthquakes that occurred in continental margin arcs since 1943 including four of the largest recorded events (1960 Chile, 1964 Alaska, 2001 Peru, and 1979 Columbia). The first three of these events are discussed in more detail in the section on Case Histories.

Earthquakes Having Relatively Large Tsunami Runup Peaks (T_{peak}) of Unknown Origin

Group "B" includes seven events in which peaks of uncertain origin occur that are larger than maximum regional tsunami runup height (Fig. 13). Two of the five "slow" earthquakes in the catalog are in this group (1994 Java and 1992 Nicaragua), five are "normal" tsunamigenic events. For all of these events the attached blue symbol indicates the maximum runup height based on the general highest levels over long stretches of coast. The red symbols indicate maximum heights of anomalously high runup for the same events the case of which is uncertain. Except for Hokkaido, the heights of the peak runup is up to 2.25 times higher than the regional runup height. For the Hokkaido event, peak local runup is 4 times that of the regional tsunami maximum height (see Fig. 6 and discussion in the section on Case Histories).

The cause of the relatively high runup above regional levels for these events is uncertain. They may be attributable to peculiarities of wave amplification due to interaction of the tsunami with the sea floor and shoreline, to differential fault slip for near-shore sources, or to earthquake-triggered submarine landslides.

Tsunamis with Relatively Large Tsunami Runup Peaks (T_{peak}) of Known or Probable Landslide Origin

Group "C" includes five events for which landslide-generated waves occur that are larger than maximum regional tsunami runup height (Fig. 13). Historically, the highest waves associated with non-volcanic tsunamigenic earthquakes have been generated by earthquake-triggered submarine and subaerial landslides. Although waves generated entirely by earthquake-triggered subaerial landslides have produced by far the highest runups (524 m during the 1958 Lituya Bay, Alaska Mw 7.8 earthquake), they are not considered further in this report because they do not constitute a major hazard in coastal Cascadia.

This group includes five events (shown on Figure 13 and discussed in the section on Case Histories) in which local tsunamis were generated by multiple large near shore earthquake-triggered submarine landslides (1964 Alaska, 1992 Flores, and 1994 Mindoro) or by gigantic offshore earthquake-triggered landslides (1998 Aitape and 1946 Aleutians). Scores of submarine landslides during the great 1964 Alaska earthquake generated runups generally up to 30 m but locally up to 52 m or 4 times higher than the 12.7 m highest runup generated by tectonic displacement (Fig. 2). The Flores Island earthquake had several high local runup peaks to a maximum height of 26 m that can be directly related to earthquake-triggered slides or suspected



slides and more than 3 times estimated regional runup height (Fig. 5). The tsunami associated with the 1994 Mindoro strike-slip earthquake is inferred to be entirely generated by near shore earthquake-triggered landslides (Fig. 7). The destructive tsunami associated with the 1998 Aitape earthquake is interpreted by most workers to be mainly, if not entirely, the result of an enormous earthquake-triggered landslide some 25 km offshore (Fig. 8). New field data for the anomalous 1946 Aleutian event suggest that the near-field tsunami runup to 42 m high was generated by one or more submarine landslides located about 80 km offshore near the edge of the continental shelf (Fig. 9).

Summary

Analysis of the well-documented cases of tsunamigenic earthquakes and their associated runups from submarine causes, as shown in Figure 13, leads to some interesting results outlined below.

- Tsunamigenic earthquakes can be grouped into three types Group A, B, and C.
 - Group "A" has a roughly linear magnitude/runup relationship, the larger the earthquake the larger the runup. Tsunamis in this group are considered to be dominantly of tectonic origin.
 - Group "B" are events that have both a tectonic regional tsunami component and local peaks of runup that are larger for a given magnitude than those in Group A. The cause of these local peaks of runup is uncertain.
 - Events in Group C are local runups that result partly or entirely from submarine landslides. These can be up to 4 times as high as the background measurements of the tectonic component of runups, and the maximum runup height increases linearly from about 15 m to 52 m in the magnitude range 7.1 to 9.2, respectively.
- There is a roughly linear relationship for typical maximum runups in Group A from about one meter for magnitude 7.5 earthquakes to 15 meters for magnitude 9 earthquakes.
- The maximum tsunami runup is approximately equivalent to both average fault slip and to maximum vertical component of slip for tectonic tsunamis that are not complicated by landslides, unusual bathymetry, or irregular configurations of the coast.
- "Slow" tsunamigenic earthquakes occur in all three groups in the magnitude range of 7.5 to 8.4.
- Factors that may control the susceptibility of earthquake-triggered submarine landsliding include:
 - Submarine slope
 - Availability of thick sediment accumulation on deltas, glacial margins, and offshore basins
 - Size and frequency of large earthquakes. Large number of large events may keep the slopes "clean", so only some events cause a significant slides

- o Occurrence of subsea zones of structural weakness such as shear zones and bedding planes

CASCADIA IMPLICATIONS

A plausible tectonic model of a subduction zone earthquake for southern Cascadia subduction zone would have a maximum M_w of ~8.5–9.1. Magnitude is based on rupture of the entire Cascadia megathrust with 12 m slip, assuming ~4 cm/yr orthogonal convergence rate and 300 years since the previous great subduction zone earthquake (Clague, 1997).

This model is probably conservative because slip is likely to be no more than 8 m in the southern segment of Cascadia due to non-orthogonal convergence, possible loss of elastic strain due to permanent deformation, small earthquakes, and aseismic creep. The vertical component of slip at the sea floor is a major unknown. It would be a function of how coseismic slip is partitioned between the megathrust and splay faults within the upper plate.

Comparison of Model Cascadia event with Historic Tsunamigenic Earthquakes

The tectonic setting for Cascadia is similar to other subduction zones at continental margin arcs and very large earthquakes on it are expected to be similar to the 1960 Chile and the 1964 Alaska earthquakes (See Appendix 2A). Therefore, an event for using the Cascadia model is reasonably compatible with the empirical results for historic tsunamigenic events that are not complicated by large submarine slides (Group "A", Fig. 13). For these events, maximum near-field tsunami runup is likely to be in the range of 1 to 1.1 times of the vertical component of fault displacement. For Cascadia, this is about 4 to 6 m.)

Tsunamigenic Submarine Landslides on the Cascadia Margin?

Tsunamis generated by submarine landslides could be generated during major Cascadia earthquakes by massive slides along the lower continental slope and along the steep walls of submarine canyons that cross the continental shelf and slope. The sediment accumulation at the mouths major rivers and the steeping continental slopes from sediment being piled at the front of the subducting slab are the major sources.

Recent Sea Beam bathymetry and multichannel seismic reflection records of the Cascadia continental margin off the Oregon coast have revealed enormous landslide masses with features interpreted as indicative of catastrophic large movement of thousands of square kilometers of the lower continental slope (Goldfinger and others, 2000). Comparable geophysical data are unavailable for the southern Cascadia margin although possible gigantic submarine landslides 5 to 10 km wide and up to 30 km long have been identified at the base of the continental slope on side-scan sonar records



Data on rate of slip and age of these landslides is too sparse to determine whether they generated paleotsunami deposits or how much of a hazard they pose for future tsunamis in Cascadia. The limited data available, however, suggest that submarine slide events capable of generating tsunamis on the Cascadia continental slope are rare based on sedimentation rates on the landslide deposits and evaluation of their geomorphic appearance. These slides appear to be tens of thousands to millions of years old compared to the recurrence times for tsunamigenic earthquakes (a few hundred to a few thousand years old) in this same region (Goldfinger and others, 2000).

The steep walls of submarine canyons are commonly sites of submarine landslides at all scales and could present a potential hazard in Cascadia. An especially well documented historic case of a destructive non-seismic tsunamigenic slide in a submarine canyon occurred on 10/16/79 in the Var River submarine canyon that intersects the Mediterranean Sea coast at Nice, France. A large sediment slump in the canyon, which is estimated to consist of several hundred million cubic meters, generated a tsunami that had a maximum amplitude (from tide gages) of 3 m along approximately 12 km of the coast (Seed and others, 1988). The tsunami triggered slumps in shallow water at the Port of Nice, caused loss of several lives, and resulted in considerable property damage. No comparable slides in submarine canyons are known to have accompanied tsunamigenic earthquakes although they undoubtedly have occurred.

In southern Cascadia, the Eel River submarine canyon is probably the only canyon with sufficiently steep topography and high with a high sediment deposition rate to be a possible source of a tsunamigenic slide. High-resolution bathymetric and geophysical data are not available for assessing their probable hazard.



REFERENCES CITED

- Abe, K. (1989), Estimate of tsunami heights from magnitudes of earthquake and tsunami: *Bull. Earthquake Res. Inst. Tokyo University*, v. 64, 51–59. (Japanese with English abstract).
- Abe, Katsuyuki. 1995, Modeling of the runup heights of the Hokkaido-Nansei-Oki tsunami of 12 July 1993: *in Tsunamis: 1992–1994*, K. Satake and F. Imamura, eds, *Pure and Applied Geophysics*, v. 144, no. 3/4, p. 735–745.
- Abe, Ku., Abe, Ka., Tsuji, Y., Imamura, F., Katao, H., Iio, Y., Satake, K., Bourgeois, J., Noguera, E., and Estrada, F. (1993). Field survey of the Nicaragua earthquake and tsunami of September 2, 1992. *Bull. Earthq. Res. Inst.* 68, 23–70.
- Baptista, A. M., Priest, G. R., and Murty, T. S.: 1993, Field survey of the 1992 Nicaragua tsunami, *Marine Geodesy* 16, 169–203.
- Bernard, E., Madher, C., Curtis, G., and Satake, K., 1994, Tsunami inundation model study of Eureka and Crescent City, California: National Oceanic and Atmospheric Administration Technical Memorandum ERL PMEL-103, 80 p.
- Bilek, Susan, and Lay, Thorne, 1999, Rigidity variations with depth along interplate megathrust faults in subduction zones: *Nature*, v. 400, p. 443–446.
- Bourgeois, J., and Reinhart, M. A., 1989, Onshore erosion and deposition by the 1960 tsunami at the Rio Lingue estuary, south-central Chile (abs.): *EOS, Transactions of the American Geophysical Union*, v. 70, no. 43, p. 1331.
- Clague, John, 1997, Evidence for large earthquakes at the Cascadia Subduction Zone: *Reviews of Geophysics*, v. 35, no. 4, p. 439–460.
- Carver, G. A., Abramson, H. A., Garrison-Laney, C. E., and Leroy, T., 1998, Investigation of paleotsunami evidence along the north coast of California: Final Report for Pacific Gas and Electric Company, 164 p. plus appendices.
- Carver, D. H., and Carver, G. A., 1996, Earthquake and thunder—native oral histories of paleoseismicity along the southern Cascadia subduction zone (abs): *Geological Society of America, Cordilleran Section, Abstracts with Program, Annual Meeting*, v.28, no. 5, p. 54.
- Davies and others, 2001
- Coulter, H.W., and Migliaccio, R.R., 1966, Effects of the earthquake of March 27, 1964, at Valdez, Alaska: *U.S. Geological Survey Professional Paper* 542-C, 36 p.



Fryer, G.J., and Watts, Philip, 2001, Motion of the Uganik Slide, probable source of the tsunami of 1 April 1946: ITS 2001 Proceedings, session 6, no. 6-6, p. 683-694.

Furumoto, A. S. (1991). Source parameters of destructive tsunamis: *Science of Tsunami Hazards*, no. 9, p. 95-113.

Geist, E.L., 1998, Local tsunamis and earthquake source parameters: *Advances in Geophysics*, v. 39, p. 117-209.

Geist, E. L., 1998, Source characteristics of the July 17, 1998 Papua New Guinea tsunami: *EOS, Transactions of the American Geophysical Union*, v. 79 (supplement), p. 571.

Goldfinger, Chris, and Watts, Philip, 2001, Tsunamigenic mega-slides on the southern Oregon Cascadia margin: ITS 2001 Proceedings, session 3, no. 3-3, p. 501.

Hatori, T., 1968, Study on distant tsunamis along the coast of Japan; Pt. 2, Tsunamis of South American origin: *Tokyo University Earthquake Research Institute Bulletin*, v. 46, p. 345-359.

Herd, D.G., Youd, T.L., Hansjorgen, Meyer, Arango C., G.L., Person, W.J., and Mendoza, Carlos, 1981, The great Tumaco, Colombia earthquake of 12 December 1979: *Science*, v. 211, p. 441-445.

Hidayat, D., Barker, J.S., and Satake, K., 1995, Modeling the seismic source and tsunami generation of the December 12, 1992 Flores Island, Indonesia, earthquake: *in Tsunamis: 1992-1994*, K. Satake and F. Imamura, eds., *Pure and Applied Geophysics*, v. 144, no. 3/4, p. 537-568.

Hokkaido-Nanseki-Oki earthquake reconnaissance team, 1995, Hokkaido Earthquake Reconnaissance Report: *Earthquake Spectra*, R.M. Chung, ed., Pub. 95-01, 166 p.

Hurukawa, N., Tsuji, Y., and Waluyo, B., in press, The Papua, New Guinea earthquake and its fault plane estimated from relocated aftershocks: ITS 2001 Proceedings, session 2, no. 2-3, p. .@

Hyndman, R.D., and Wang, K., 1993, Tectonic constraints on the zone of major thrust earthquake failure: The Cascadia subduction zone: *Journal of Geophysical Research*, v. 98, p. 2039-2060.

Hyndman, R.D., and Wang, K., 1995, The rupture zone of Cascadia great earthquakes from current deformation and the thermal regime: *Journal of Geophysical Research*, v. 100, p. 22,133-22,154.

Imamura, F., Gica, E., Takahashi, To., and Shuto, N. (1995). Numerical simulation of the 1992 Flores tsunami: interpretation of tsunami phenomena in northeastern Flores Island and damage at Babi Island. *Pure and Applied Geophysics*, v. 144, p. 555-568.



Imamura, Fumihiko, Synalokis, C.E., Gica, Edison, Titov, Vasily, Listanco, Eddie, and Lee, H.J., 1995, Field survey of the 1994 Mindoro Island, Philippines tsunami: *in* Tsunamis: 1992–1994, K. Satake and F. Imamura, eds., Pure and Applied Geophysics, v. 144, no. 3/4, p. 875–890.

INDEC (2001). Resumen final de daños en distritos afectados por el sismo del 23-06-01 Y subsiguientes ocurridos en el sur del país, Instituto Nacional de Defensa Civil, Lima, Peru, <http://www.indeci.gob.pe/resumdist27nov08h.htm>

Johnson, J.M. and Satake, Kenji, 1997, Estimation of seismic moment and slip distribution of the April 1, 1946, Aleutian tsunami earthquake: *Journal of Geophysical Research*, v. 102, p. 11,765–11,774.

Kachadoorian, Reuben, 1965, Effects of the earthquake of March 27, 1964, at Whittier, Alaska: U.S. Geological Survey Professional Paper 542-B, 21 p.

Kanamori, Hiroo, and Kikuchi, Masayuki, 1972, The 1992 Nicaragua earthquake: a slow tsunami earthquake associated with subducted sediments: *Nature*, v. 361, p. 714–716.

Kikuchi, M., and Y. Yamanaka (2001). EIC Seismological note Number 105, http://www.eic.eri.u-tokyo.ac.jp/EIC/EIC_news/105E.html.

Koshimura, S., and V. Titov (2001). Preliminary model results for the 23 June 2001 Peruvian tsunami, Proceedings of the International Tsunami Symposium 2001 (ITS 2001) (on CD-ROM), Pacific Marine Environmental Laboratory, NOAA, Session 2, No. 2-2, 379.

Lemke R.W., 1966, Effects of the earthquake of March 27, 1964, at Seward, Alaska: U.S. Geological Survey Professional Paper 542-E, 43 p. Lockridge, 1985

McCulloch, D.S., 1966, Slide-induced waves, seiching, and ground fractures caused by the earthquake of March 27, 1964, at Kenai Lake, Alaska: U.S. Geological Survey Professional Paper 543-A, 41 p.

Myers, E.P., Baptista, A.M., and Priest, G.R., 1999, Finite element modeling of potential Cascadia subduction zone tsunamis: *Science of Tsunami Hazards*, 17, (1), 3-18.

Pelinovsky, Efim, Yuliadi, Dede, Prasetya, Gegar, and Hidayat, Rahman, 1997, The January 1, 1996 Sulawesi, Island tsunami: *Tsunami Hazards*, v. 15, no. 2, p. 107–120.

PHIVOLCS Quick Response Team, 1994, Philippine Institute of Volcanology and Seismology Special Report No. 2, 11 p.



Plafker, George, 1997, Catastrophic tsunami generated by submarine slides and backarc thrusting during the 1992 Flores Island, Indonesia earthquake [abs.]: Geological Society of America Abstracts with Programs, v. 29, no. 5, p.

Plafker, George, and Kachadoorian, Reuben, 1966, Geologic effects of the March 1964 earthquake and associated seismic sea waves on Kodiak and nearby islands, Alaska: U.S. Geological Survey Professional Paper 543-D, 46 p.

Plafker, George, 1969, Tectonics of the March 27, 1964, Alaska Earthquake: U.S. Geological Survey Professional Paper 543-I, 74 p.

Plafker, George, Kachadoorian, Reuben, Eckel, E.B., and Mayo, L.R., 1969, Effects of the earthquake of March 27, 1964, on various communities: U.S. Geological Survey Professional Paper 542-G, 50 p.

Plafker, George, 1972, The Alaskan earthquake of 1964 and Chilean earthquake of 1960; Implications for arc tectonics: Journal of Geophysical Research, v. 77, no. 5, p. 901-925.

Plafker, George, and Savage, J.C., 1970, Mechanism of the Chilean earthquakes of May 21-22, 1960: Geological Society of America Bulletin, v. 81, p. 1001-1030.

Plafker, George and Ward, S.N., 1992, Backarc thrust faulting and tectonic uplift along the Caribbean Sea coast during the April 22, 1991 Costa Rica earthquake: Tectonics, v. 11, no. 4, p. 709-718.

Plafker, George, 1997, Catastrophic tsunami generated by submarine slides and backarc thrusting during the 1992 Flores Island, Indonesia earthquake [abs.]: Geological Society of America Abstracts with Programs, v. 29, no. 5, p.

Richter, C.F., 1958, Elementary seismology: W.H. Freeman & Company, Inc., 768 p.

Satake, K., and Imamura, F., 1995, Introduction to Tsunamis: *in* Tsunamis: 1992-1994, K. Satake and F. Imamura, eds., Pure and Applied Geophysics, v. 144, no. 3/4, p. 373-380.

Satake, K., and Tanioka, Y., 1999, The July 1998 Papua New Guinea earthquake and tsunami: a generation model consistent with various observations [abstract]: EOS, v. 80, F750-F751.

Seed, H.B., and Rahman, M.S., 2001, Wave-induced pore pressure in relation to ocean floor stability of cohesionless soils. Marine Geotechnology, v. 3, p. 123-150.

Shepard, F.P., MacDonald, G.A., and Cox, D.C., 1950, The tsunami of April 1, 1946: Bull. Scripps Inst. Oceanography, Univ. California, no. 5, p. 1956-1962.

Sievers C., H.A., Villegas C., Guillermo, and Barros, Guillermo, 1963, The seismic sea wave of 22 May 1960 along the Chilean coast: Bulletin of the Seismological Society of America, v. 53, no. 6, p. 1125-1190.



Synolakis, C.E., J.-P. Bardet, J.C. Borrero, H.L. Davies, E.A. Okal, E.A. Silver, S. Sweet, and D.R. Tappin (2002). The slump origin of the 1998 Papua New Guinea tsunami, Proc. Roy. Soc. (London), Ser. A, 458, 763-789.

Tappin, D.R., Watts, Philip, McMurty, G.M., and Matsumoto, Takeshi, 2001, Offshore evidence on the source of the 1998 Papua New Guinea tsunami: A sediment slump: ITS 2001 Proceedings, session 2, no. 2-3, p. 381-388.

Tsuji, Y., and Matsutomi, H., 1993, Damages due to the tsunami: Report of the field survey on the Flores Island earthquake-tsunami of December 12, 1992: Rep. Grant in aid no. B-4-4, p. 70-87.

Tsuji, Y., Imamura, F., Matsutomi, H., Synolakis, C. E., Nanang, P. T., Jumadi, S., Harada, S., Han, S.S., Arai, K., and Cook, B., 1995, Field survey of the east Java earthquake and tsunami of June 3, 1994: *in* Tsunamis: 1992-1994, K. Satake and F. Imamura, eds., Pure and Applied Geophysics, v. 144, no. 3/4, p. 839-854.

USAID (2001), Peru Earthquake Fact Sheet #6 (FY 2001), U.S. Agency for International Development, ReliefWeb <http://www.reliefweb/int>.

Watanabe, H., 1985, Catalog of hazardous tsunamis in Japan: University of Tokyo Press, Tokyo, 206 p.

Wells, D.L. and Porrazzo, V.F., 1994, The 15 November 1994 M 7.1 Mindoro Island earthquake in the Philippines: unpublished report to EERI, 12/15/94).

Yamashita, T. (1976). On the dynamical process of fault motion in the presence of friction and inhomogeneous initial stress, Part I. Rupture propagation. Journal of the Physics of the Earth, v. 24, p. 417-444.

Yeh, Harry, Imamura, Fumihiko, Synalokis, Costas, Tsuji, Yoshinobu, Liu, Philip, and Shi, Shaozhong, 1993, The Flores Island tsunamis: EOS, Transactions, American Geophysical Union, v. 74, no. 33, p. 369-373.

Yeh, Harry, Titov, Vasily, Gusiakov, Viacheslav, Pelinovsky, Efim, Khramushin, Vasily, and Kaistrenko, Victor, 1995, The 1994 Shikotan earthquake and tsunami: *in* Tsunamis: 1992-1994, K. Satake and F. Imamura, eds, Pure and Applied Geophysics, v. 144, no. 3/4, p. 855-874.



Table 1. May 21, 1960 Chile earthquake ($M_w = 9.5$) near-field tsunami data and coseismic vertical displacements. [Tsunami data from Sievers and others, 1963; coseismic displacements from Plafker and Savage, 1970; Table 4]

No. (Fig. 3)	Location	Maximum runup height (m)	Coseismic displacement (m)	Comments
1	Aysen	1.0	0?	3 waves reported
2	Puerto Aguirre	3.0	0.0 to +1.0	First wave arrived 2 hours and 10 minutes after the earthquake; second wave 1 hour and 20 minutes later. Wave height estimated
3	Melinka	?	-1.1 to -1.3	Lighthouse keepers report 3 waves and wave damage, but no wave heights
4	Isla Guafo	10.0	+3.6	Sea withdrawal began about 10 minutes after earthquake and was soon followed by first wave from the west. 4 waves reported
5	Achao	2.5	-0.9	3 waves reported; highest wave reached to high tide line; no damage
6	Puerto Montt	0	0.0 to +1/2	No tsunami observed
7	Ancud	5-6	-1.3	First wave about 20 minutes after earthquake; large wave struck 50 minutes after earthquake. 4 waves reported; initial rise approximately 1 m
8	Gulf of Quetalmahue	1.5	-1.5 to -1.8	
9	Playa Chauman	15-20	-1.0 to -1.5	First wave seen offshore 18-20 minutes after earthquake about 800 m off coast; wave height estimated by lighthouse keeper (height estimate not included on Figure 1)
10	Maullin	14	-1.6 to -1.7	First wave arrival about 20 minutes after earthquake followed by withdrawal. 8 waves reported; 2d and 4th waves highest
11	Caleta Mansa	12	-1.3 to -1.6	First wave 15 minutes after earthquake. 3 waves reported; 3d wave highest. Wave height corrected for tide stage
12	Puerto de Corral	8.5-10	-2.1	First wave crest about 40 minutes after earthquake was preceded by withdrawal. At least 3 waves; 2d and 3d highest



Table 1 (Continued)

No. (Fig. 3)	Location	Maximum runup height (m)	Coseismic displacement (m)	Comments
13	Caleta Mehuin	8.5	-1.6	Rapid initial withdrawal of water followed by rapid rise beginning about 15-20 minutes after earthquake. 3 waves reported; 3d wave highest
14	Caleta Queule	4+	-2.0	Heavy damage
15	Puerto Saavedra	7-8	-1.2 to -1.6	First wave followed withdrawal beginning about 25-30 minutes after earthquake. 3 waves reported; 3d wave highest
16	Isla Mocha	15	+ 0.9 to +1.8	3 waves reported; 1st wave highest and preceded by withdrawal beginning about 10 minutes after earthquake
17	Lebu	3-4	+0.9 to +1.0	3 waves reported
18	Lota	1.5	0.0	First wave at about 50 minutes after earthquake followed withdrawal. 5 waves reported



Table 2. March 27, 1964 Alaska earthquake (Mw = 9.2) near-field tsunami data and coseismic vertical displacements. [After Lemke, 1967; Plafker, 1969; Plafker and Kachadoorian, 1966, fig. 18; Plafker, and others, 1969]

No.	Location	#Maximum runup height (m)	Coseismic displacement (m)	Comments
KODIAK ISLANDS REGION				
1	Sitkinak Island	0	+0.3	
2	Kaguyak	5.2+	-0.6	1st wave arrived 38±5 minutes after start of earthquake
3	Sitkalidak Island	7.5	+0.2	
4	Port Hobron	4.3+	-0.9	
5	Old Harbor	3.7	-0.8	1st wave arrived 48 minutes after start of earthquake. 3d wave between 8:30 and 9:30 P.M. highest and most destructive.
6	Shearwater Bay	4.4	-0.9	
7	Ugak Bay (Pasagshak Bay)	6.1±0.6	-0.9	1st wave arrived at Saltery Cove, Ugak Bay, about 30 minutes after start of earthquake
8	Sacramento River	12.7	-0.6	Assumes measured runup was for 1st wave
9	Myrtle Creek	5.7	-1.5	6 waves recorded on streamflow gage about 1,600 m above stream mouth. 1st wave arrived 70 minutes after start of earthquake
10	Cape Chiniak	12.2	-1.2	1st wave arrived 38 minutes after start of earthquake. Height assumes measured runup was for 1st wave
11	Womens Bay	3.9	-1.6	10 waves reported. 1st wave crest at 6:35 P.M. 63 minutes after start of earthquake; 2d wave at about 7:40 P.M. was highest and most destructive



Table 2, continued

No.	Location	#Maximum runup height (m)	Coseismic displacement (m)	Comments
KODIAK ISLANDS REGION				
12	Afognak	3.3	-1.4	3d wave between 8:30 and 9:30 P.M. highest and most destructive
13	Kitoi Bay	2.7+	-1.7	
14	Cape Current	3.7+	-1.3	
15	Port William	1.5+	-1.2	
16	Terror River	2.8	-1.2	5 waves reported on streamflow gage 1,127 m above stream mouth. Probably includes seiche waves
17	Uganik River	1.9	-1.0	3 waves recorded on streamflow gage 800 m above stream mouth
18	Uyak Bay	1.3	-0.6	
19	Karluk	0.5	-0.3	
KENAI PENINSULA				
20	Rocky Bay	2.7	-1.5	1st wave arrived approximately 30 minutes after start of earthquake (runup about 2.7 m). Highest and most damaging wave at midnight near high tide (runup about 1.5 m above tide level)
21	Seward	9-12	-1.1	1st wave arrived about 28-29 minutes after start of earthquake. 3d wave probably highest
22	Whidbey Bay	12.2	+0.45 to 0.6	1st wave arrived 19½ minutes after start of earthquake (runup about 10.7 m). 2d wave at about 30-32 minutes after start of earthquake was highest
23	Puget Bay	8.5	+1.5	1st wave arrived about 20 minutes after start of earthquake (runup about 5.5 m). 3d wave at about 2½ hours after start of earthquake was highest and most destructive



Table 2 (Continued)

No.	Location	Maximum runup height (m)	Coseismic displacement (m)	Comments
PRINCE WILLIAM SOUND				
24	Phipps Point	8.5	+1.8	
25	Hook Point	10.7	+1.8	
26	Cordova	4.8	+1.9	Highest and most damaging wave, which almost coincided with high tide at 12:30 A.M. on 3/28/94, was 4.8 m above tide level
ISLANDS & MAINLAND COAST EAST OF PRINCE WILLIAM SOUND				
27	Cape St. Elias		+2.4	1st wave arrived from southeast about 39 minutes after start of earthquake. Immediately followed by 2d wave which was the highest wave
28	Cape Yakataga	3.0	0.0	8 waves reported

Corrected for stage of tide where known; "+" sign after numeral indicates uncorrected value



Table 3. April 22, 1991 Limon, Costa Rica earthquake ($M_s = 7.5$) tsunami data and coseismic vertical displacements [From Plafker and Ward, 1992].

No.	Location (Lat./Long).	Maximum runup height (m)	Coseismic displacement (m)	Comments
1	10°02'18"N./83°07'54"W.	1.35	0	
2	10°00'16"N./83°05'55"W	0.65 to 0.71	+1.27	1st wave arrival 5 minutes after start of earthquake
3	09°56'59"N./83°00'57"W	1.30+	+0.74	
4	09°54'06"N./82°58'42"W	0.65 to 1.70	+0.52	
5	09°43'15"N./82°49'00"W	1.16	0.73	
6	09°39'29"N./82°45'31"W	1.55	+0.38	1st wave arrival 3 to 5 minutes after start of earthquake
7	09°38'42"N./82°41'12"W	2.00+	+0.40 to +0.45	1st wave arrival 10 minutes after start of earthquake
8	09°38'06"N./82°39'33"W	1.30	+0.30	1st wave arrival 5 minutes after start of earthquake
9	09°38'15"N./82°39'15"W	0.83	+0.40	
10	09°35'55"N./82°36'24"W	1.25+	+0.30 to +0.40	

Table 4. Selected source parameters for post-1943 tsunamigenic earthquakes for which runup ≥ 2 m. Tsunami runup data associated with these events are given on Table 5.

No.	Date	Region (*slow eq.)	Mo (10^{20} Nm)	Mw	^a Average Slip (m)	Maximum Slip (m)	Length (km)	Width (km)	References
1	05/22/60	Chile (Fig. 1)	2000.	9.5	24				Kanamori and Cipar (1974); Kanamori (1977)
					20.3	54	920	300	Linde and Silver (1989)
					8 ^b	41 ^b	900	150	Barrientos and Ward (1990)
2	03/28/64	Alaska (Fig. 2)	630	9.2	8.6	18	500	300	Johnson and others (1996)
			630.		~12.1	20±5 ^b	650	200	Plafker (1969);
3	02/04/65	Rat Islands	140.	8.7	~9.7	12.0	600	60	Beck and Christensen (1991)
4	03/09/57	Aleutian	88.	8.6	~1.3	7.0	1100	150	Johnson and Satake (1993)
5	06/23/2001	*S. Peru (Fig. 11)	47.	8.4	~2.6	4.5	300	125	Okal and others (in prep.); Mw and Mo from Harvard CMT
6	10/04/94	Shikotan	30.	8.3	~4.3		~220	~80	Yeh and others (1995). Mw and Mo from Harvard CMT
7	12/12/79	Colombia	29.	8.3	~3.2	5.8	230	100	Beck and Ruff (1984)
8	12/20/46	Nankaido	39.	8.2	~1.5	2.4	360	180	Satake (1993)
9	05/16/68	Tokachi-Oki	28.	8.2	~4.7		150	100	Kanamori (1971); Mw from Abe (1995)
10	02/17/96	Irian Jaya	24.	8.2	~3.4		~180	~80	Imamura and others (1997); Mw and Mo from Harvard CMT



Table 4 (Continued)

No.	Date	Region (*slow eq.)	Mo (1020Nm)	Mw	^a Average Slip (m)	Maximum Slip (m)	Length (km)	Width (km)	References
11	04/01/46	*Aleutian (Fig. 9)	23.	8.2	~7.6		95	80	Johnson and Satake (1997)
12	08/01/69	Kurile	22.	8.2	~3.6		180	85	Abe (1973)
13	12/07/44	Tonankai	20.	8.2	~0.8	1.6	270	180	Satake (1993)
14	08/16/76	Mindanao	19.	8.1	~3.7		160	80	Stewart and Cohn (1979)
15	03/04/52	Tokachi-Oki	17.	8.1	~9.4		90	50	Hatori (1966); Mw and Mo from Kanamori (1972)
16	07/30/95	Chile	14.2	8.1	~2	3.5	195	90	Delouis and others (1997)
17	03/03/85	Chile	15.	8.0	~1.6	2.9	200	120	Mendoza and others (1994)
18	10/09/95	Mexico	14.2	8.0	~2.1	3.5	185	90	Zobin (1997)
19	01/01/96	Sulawesi	7.8	7.9	~7.5		65	40	Pelinovsky and others (1997); Mw and Mo from Harvard CMT
20	06/17/73	Nemuro-Oki	6.7	7.8	~2.8		100	60	Shimazaki (1974)
21	10/13/63	*Kurile	6.	7.8	~3		110	45	Beck and Ruff (1987); Mw from Pelayo and Wiens (1992)
22	06/02/94	*Java (Fig. 10)	5.34	7.8	~1		140	100	Tsuji and others (1995); Mw and Mo from Harvard CMT
23	12/12/92	1992 Flores I. (Fig. 5)	5.1	7.7	~3.2		100	40	Back arc thrust. Yeh and others (1993); Mw and Mo from Harvard CMT



Table 4 (Continued)

No.	Date	Region (*slow eq.)	Mo (10 ²⁰ Nm)	Mw	^a Average Slip (m)	Maximum Slip (m)	Length (km)	Width (km)	References
24	07/12/93	Hokkaido (Fig. 6)	4.6	7.7	~2.6	6.0	150	30	Back arc thrust. Hokkaido-Nanseki-Oki earthquake Reconnaissance Team (1995); Mw and Mo from Harvard CMT
25	05/26/83	Akita-Oki	4.55	7.7	~3.2	7.6	120	30	Fukuyama and Irikura (1986); Mw and Mo from Harvard CMT
26	06/16/64	Niigata		7.6	^b ~6	10	~90	~40	Nakamura and others (1964); Hatori (1965);
27	09/02/92	*Nicaragua (Fig.4)	3.4	7.6	~1.1		160	50	Kikuchi and Kanamori (1995); 1998); Mw and Mo from Harvard CMT
28	04/22/91	Costa Rica (Fig. 3)	3.3	7.6	~2.2		75	50	Back arc thrust. Plafker and Ward (1992); Mw and Mo from Harvard CMT
29	09/21/85	Mexico	2.5	7.5	~1.3	2.00	70	70	Mendoza (1995); Mw and Mo from Harvard CMT
30	02/21/96	N. Peru	2.2	7.5	~1.3		110	40	Ihmle and others (1996); Mw and Mo from Harvard CMT
31	06/10/75	*Kurile	2.	7.5	~0.8		100	60	Pelayo and Wiens (1992)
32	04/01/68	Miyazaki-Oki	1.8	7.4	~2.5		56	32	Shono and others (1976)
33	02/01/74	Solomon Is.	1.4	7.4	~1.2		40	75	Lay and Kanamori (1980)

Table 4 (Continued)

No.	Date	Region (*slow eq)	Mo (10 ²⁰ Nm)	Mw	^a Average Slip (m)	Maximum Slip (m)	Length (km)	Width (km)	References
34	01/01/94	Mindoro I. (Fig. 7)		7.1		^b 3.4	~30		PHIVOLCS (1994). Mechanism is dominantly dextral strike-slip on a steeply-dipping N-S fault.
35	07/17/98	Aitape (PNG) (Fig. 8)		7.0	1-2		~40	~15	Geist (200); NOAA website. Mechanism probably dip-slip on a steeply dipping offshore E-W trending fault. Earthquake triggered a large submarine landslide

^a Calculated assuming $\mu = 4 \times 10^{10}$ Pa

^b From onshore surface deformation



Table 5. Large tsunamigenic earthquakes and near-source tsunami runup, 1943-2001. **T_{max}** is the *regional* upper limit of runup caused by tectonic deformation or very large landslides. **T_{peak}** refers to *local peaks* of runup $0.75 \geq$ times **T_{max}** that may be generated by landslides or by amplification of the tectonic tsunami due to bathymetry, shoreline configuration, or wave reinforcement. Earthquake source data for these events are given on Table 1.

No.	Date	Region (*slow eq.)	M _w	T _{max} (m)	T _{peak} (m)	Tsunami Data Sources	Comments
1	05/22/60	Chile (Fig. 1)	9.5	15.0		Sievers and others (1963)	First tsunami waves reached outer coast 15-59 minutes after start of earthquake with measured regional runup of 10 to 15 m along 600 km of the coast.
2	03/28/64	Alaska (Fig. 2)	9.2	5-12.7	52	Lemke, 1967; Plafker (1969); Plafker and Kachadoorian (1966); Plafker and others (1969); McCulloch (1966)	Tectonic tsunami struck 19½±½ minutes after start of earthquake; T _{max} 7.5 to 12.7 m along 550 km of coast. Scores of highly destructive landslide-generated waves in fiords and lakes with T _{peak} 20--52 m
3	02/04/65	Rat Island	8.7	10.7		Stover and Coffman (1993)	10.7 m on Shemya I; flooding at Amchitka I. No other local runup data available
4	03/09/57	Aleutian	8.6	15		Stover and Coffman (1993)	15 m runup at Scotch Cap, Unimak I.; 8 m at Sand Bay, Great Sitkin I. No other local runup data available
5	06/23/2001	*S. Peru (Fig. 11)	8.4	5	7	Okal and others (2001)	Inundation along ~300 km of coast
6	10/04/94	Shikotan	8.3	5-7	10.0	Yeh and others (1995)	
7	12/12/79	Colombia	8.3	3.8		Herd and others (1981)	First wave arrival 10-15 minutes after start of earthquake. 1.5 m coseismic subsidence at site of highest runup
8	12/20/46	Nankaido	8.2	~4	4.8	Abe, (K.), (1989)	
9	05/16/68	Tokachi-Oki	8.2	3.5		Abe, (K.), (1989)	

Table 5 (Continued)

No.	Date	Region (*slow eq.)	Mw	Tmax (m)	Tpeak (m)	Tsunami Data Sources	Comments
10	02/17/96	Irian Jaya	8.2	4.5	7.7	Imamura and others (1997)	Peak runup, located on opposite side of Biak Island from the tectonic tsunami source inferred to be generated by a near-shore submarine landslide
11	04/01/46	*Aleutian (Fig. 9)	8.2	~42		Shepard and others (1950); Fryer and Watts (2001); Plafker and others (2001), Okal and others (in prep)	First and highest tsunami, with 42 m runup at Scotch Cap, was probably landslide-generated. A major transoceanic tsunami of uncertain origin caused damage and deaths in Hawaii and elsewhere in the south Pacific Ocean
12	08/01/69	Kurile	8.2	4.5	5.9	Lockridge and Smith (1984)	
13	12/07/44	Tonankai	8.2	5.0		Abe, (K.), (1989)	
14	08/16/76	Mindanao.	8.0	5.0		ITIC Newsletter	
15	03/04/52	Tokachi-Oki	8.1	4.0		Abe, (K.), (1989)	
16	07/30/95	Chile	8.1		2.8	Ramirez and others (1997)	
17	03/03/85	Chile	8.0	2.4	3.5	Lockridge (1985)	
18	10/09/95	Mexico	8.0	3.5	5	ITIC Newsletter	
19	01/01/96	Sulawesi	7.9	3.4		Pelinovsky and others (1997)	
20	06/17/73	Nemuro-Oki	7.8	4.5		Abe, (K.), (1989)	
21	10/13/63	*Kurile	7.8	4.2	4.4	Iida and others (1967)	



Table 5 (Continued)

No.	Date	Region (*slow eq.)	Mw	Tmax (m)	Tpeak (m)	Tsunami Data Sources	Comments
22	06/02/94	*Java (Fig. 10)	7.8	3-6	13.9	Tsuji and others (1995)	First wave arrival 40 minutes after start of earthquake. Regional inundation of ~300 km of coast 3 to 6 m with local peaks of 9 to 13.9 m.
23	12/12/92	1992 Flores I (Fig. 5)	7.7	~5	26	Yeh and others (1993); Tsuji and Matsutomi (1993); Tsuji and others (1995); Hidayat, Barker, and Satake (1995); Imamura and others (1995); Plafker (1997)	Tmax ~ 5 m in western part of source region. Numerous subaerial and submarine landslides. Probable and known landslide-generated waves in the Babi Island area and eastern Flores Island had peaks of 11-26 m. First Tpeak waves struck coast in less than 3 minutes from start of earthquake
24	07/12/93	Hokkaido (Fig. 6)	7.7	8	32	Hokkaido-Nanseki-Oki Earthquake Reconnaissance Team (1995); Abe, (K.), (1989)	First waves arrived 3-5 minutes after start of earthquake at Okushiri Island with Tmax of 5-15 m. Three local peaks of 20-32 m near the southern tip of the island. Tmax on Hokkaido Island ~5 m with local peaks up to ~9.5 m.
25	05/26/83	Akita-Oki	7.7	4.0	7.5	Abe, (K.), (1989)	
26	06/16/64	Niigata	7.6	6.4		Abe, (K.), (1989)	
27	09/02/92	*Nicaragua (Fig.4)	7.6	6	10.0	Abe, (Ku) and others (1993); Baptista and others (1993)	



Table 5 (Continued)

No.	Date	Region (*slow eq.)	Mw	Tmax (m)	Tpeak (m)	Tsunami Data Sources	Comments
28	04/22/91	Costa Rica (Fig. 3)	7.6	2.0		Plafker and Ward (1992)	Back arc thrust fault source. First wave arrivals 3-10 minutes after start of earthquake.
29	09/21/85	Mexico	7.5	1.9	2.5	Farreras and Sanchez (1991)	
30	02/21/96	*N. Peru	7.5	5		Bourgeois and others (1999)	Runup 2-5 m from 8° to 10° S.
31	06/10/75	*Kurile	7.5	4.0	5.9	Pelayo and Wiens (1992)	
32	04/01/68	Miyazaki-Oki	7.4	4.5	6.8	Abe, (K.), (1989)	
33	02/01/74	Solomon Is.	7.4	3.4	4.5	Geist (1998)	
34	01/01/94	Mindoro I. (Fig. 7)	7.1		7.3	Imamura, and others (1995)	Numerous subaerial landslides. Waves struck coast 2-5 minutes after the earthquake in areas of large deltas and steep topography. Data suggest probable multiple slide sources for the tsunami
35	07/17/98	*Aitape (PNG) (Fig. 8)	7.1		15	Int. Tsunami Survey Team (1998); Tappin and others (2001); Davies and others (2001)	Waves arrived 10-25 minutes after the earthquake. Most likely main tsunami source is a gigantic submarine slide ~5 x 5 km in area that has been identified on the continental slope by marine geophysical surveys



9A-42

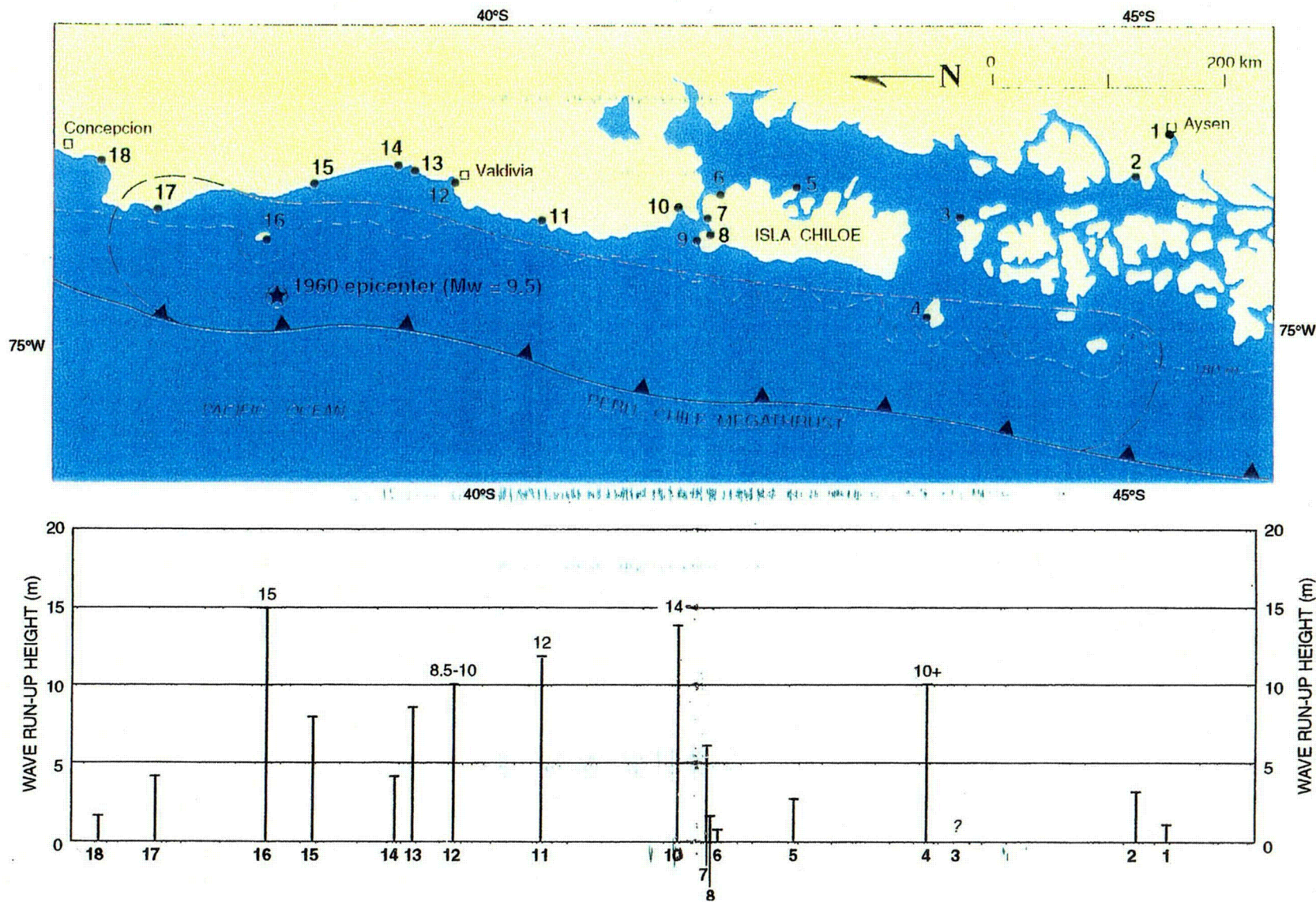


Figure 1. Map showing 1960 Chile M_w 9.5 earthquake tsunami runup heights (bar graph) zone of coseismic uplift (outlined by dashed line and megathrust) and main shock epicenter (star). [Tsunami and coseismic displacement data in Table 1].

9A-43

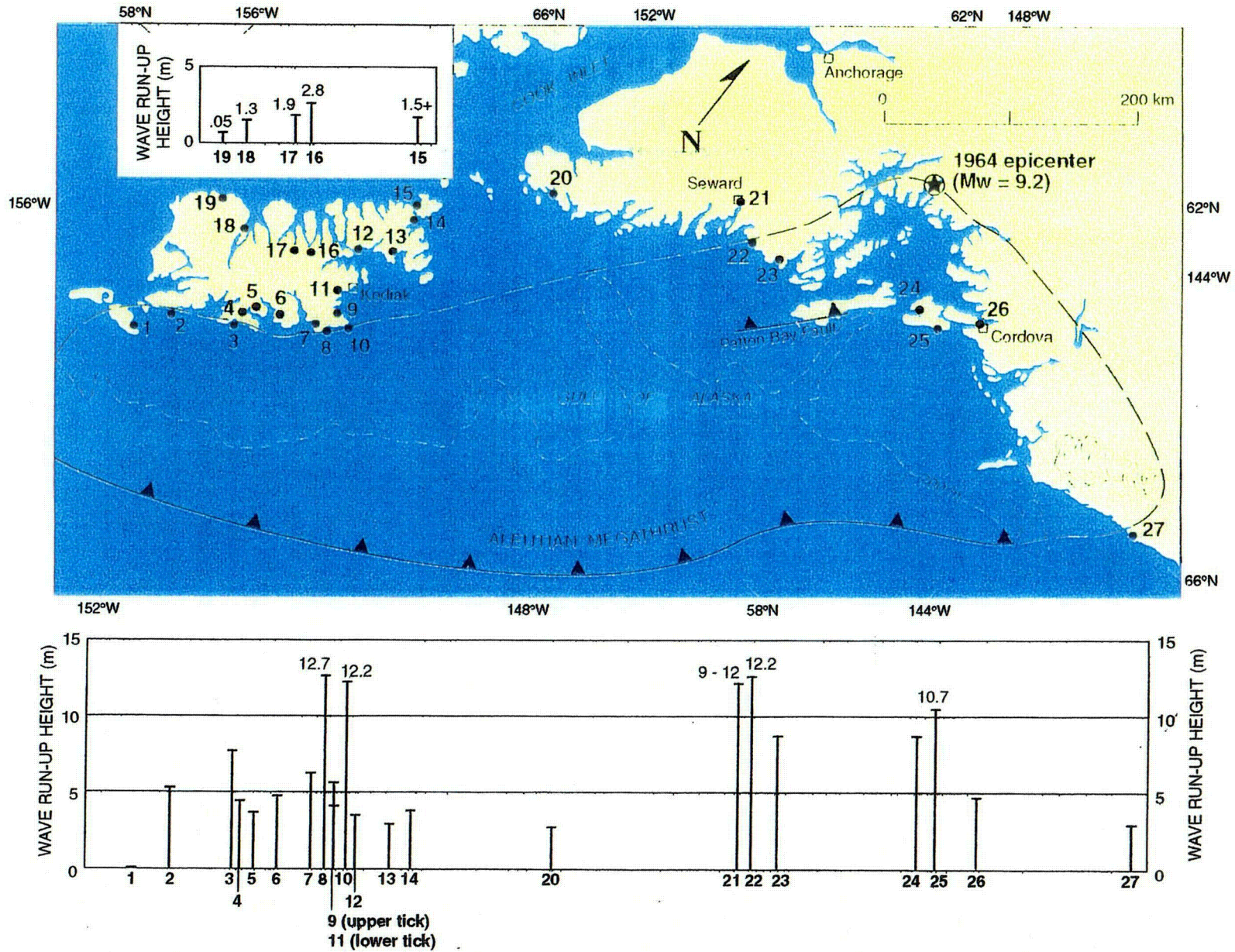


Figure 2. Map showing 1964 Alaska M_w 9.2 earthquake tsunami runup heights (bar graph), zone of coseismic uplift (outlined by dashed line and megathrust) and main shock epicenter (star). [Tsunami and coseismic displacement data in Table 2].

9A-44

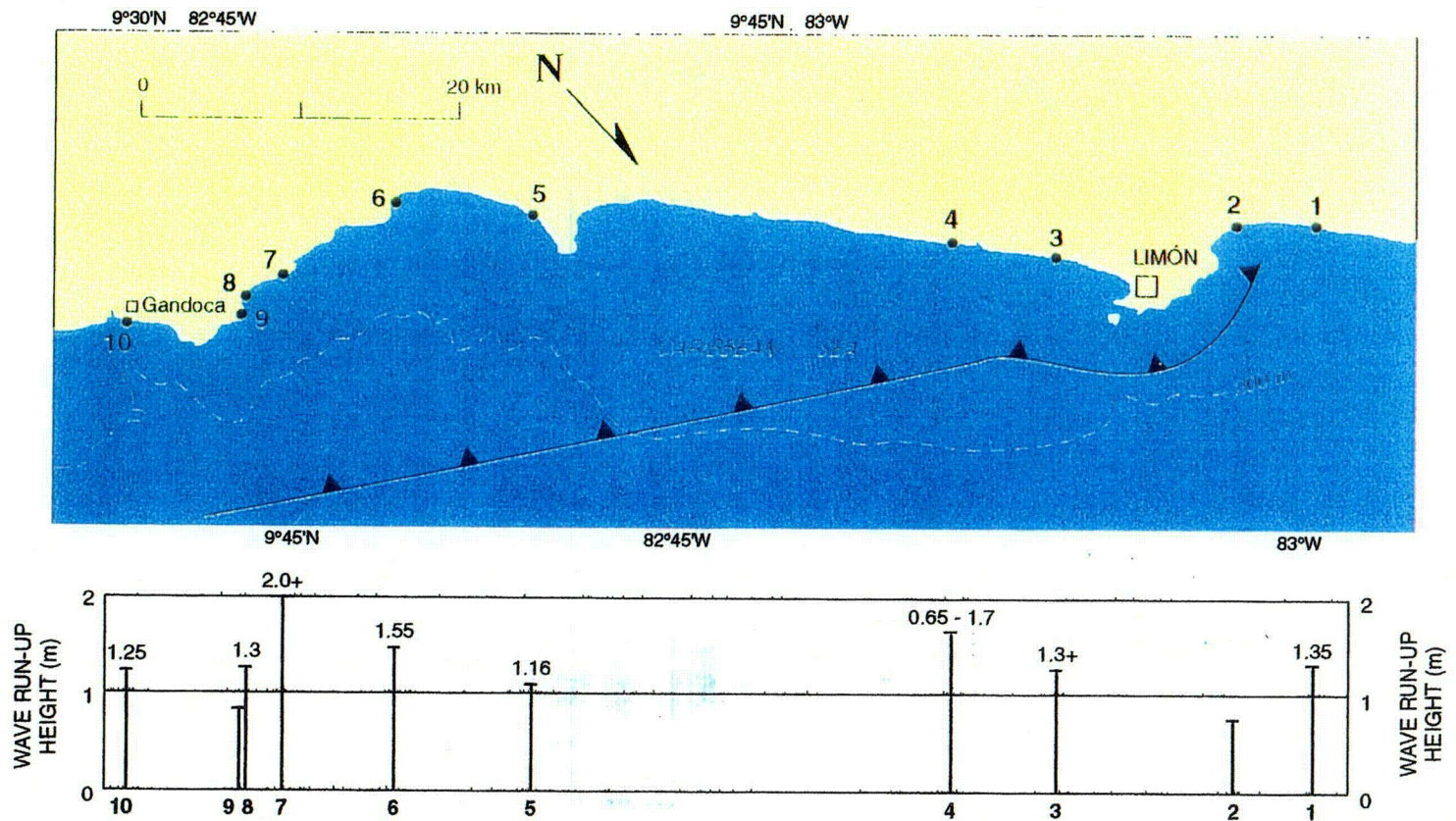


Figure 3. Map showing 1991 Costa Rica M_s 7.5 earthquake tsunami runup heights (bar graph) relative to the back-arc thrust on which the earthquake occurred. Coseismic uplift affected all of the area between the thrust fault and coast. The main shock epicenter is off the map (33 km south of Limón). [Tsunami and coseismic displacement data in Table 3].

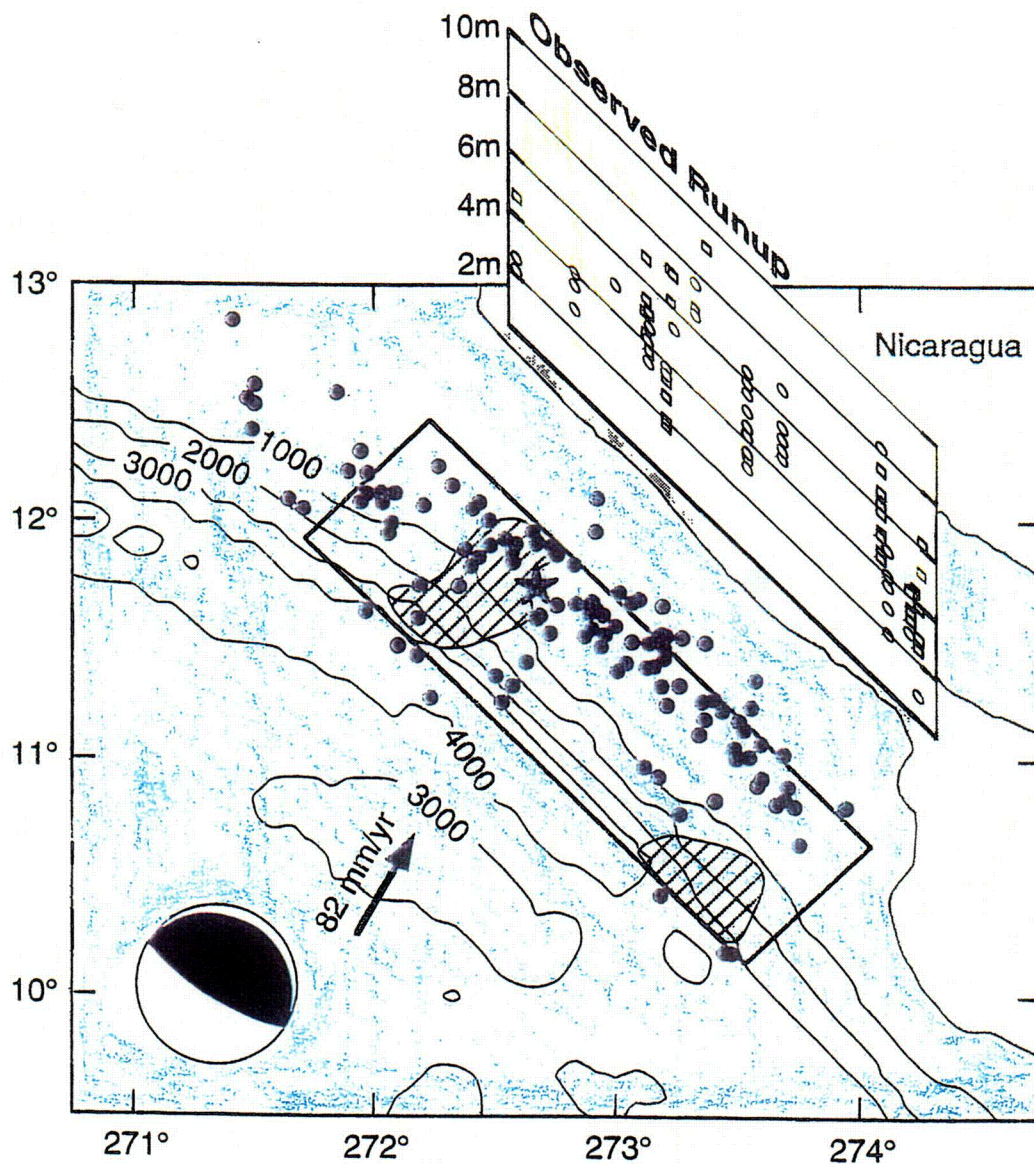


Figure 4. 1992 M_w 7.7 Nicaragua earthquake and tsunami runup. Source area is indicated by the rectangle; solid dots are aftershocks and shaded areas represent regions of high moment release. Mechanism of earthquake in lower left corner. Arrow indicates Cocos-Caribbean relative plate motion. The highest tsunami runup shows a general correlation with offshore areas of highest moment release. [From Geist (1998)].

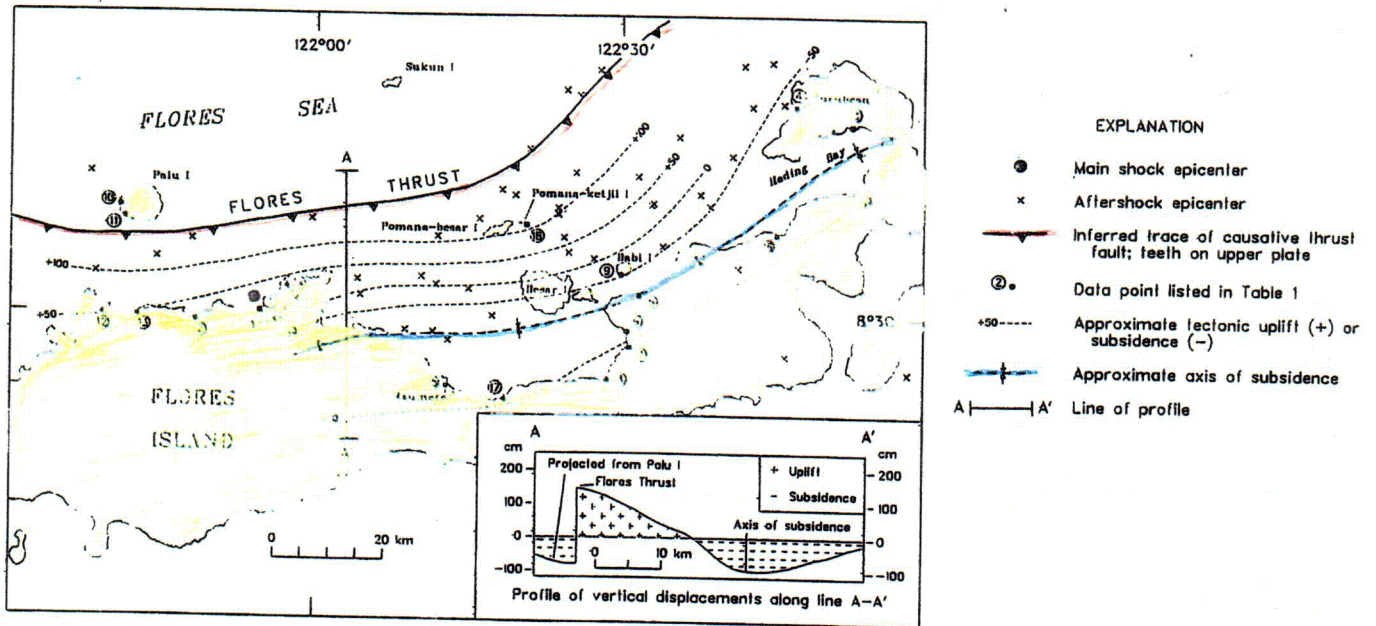
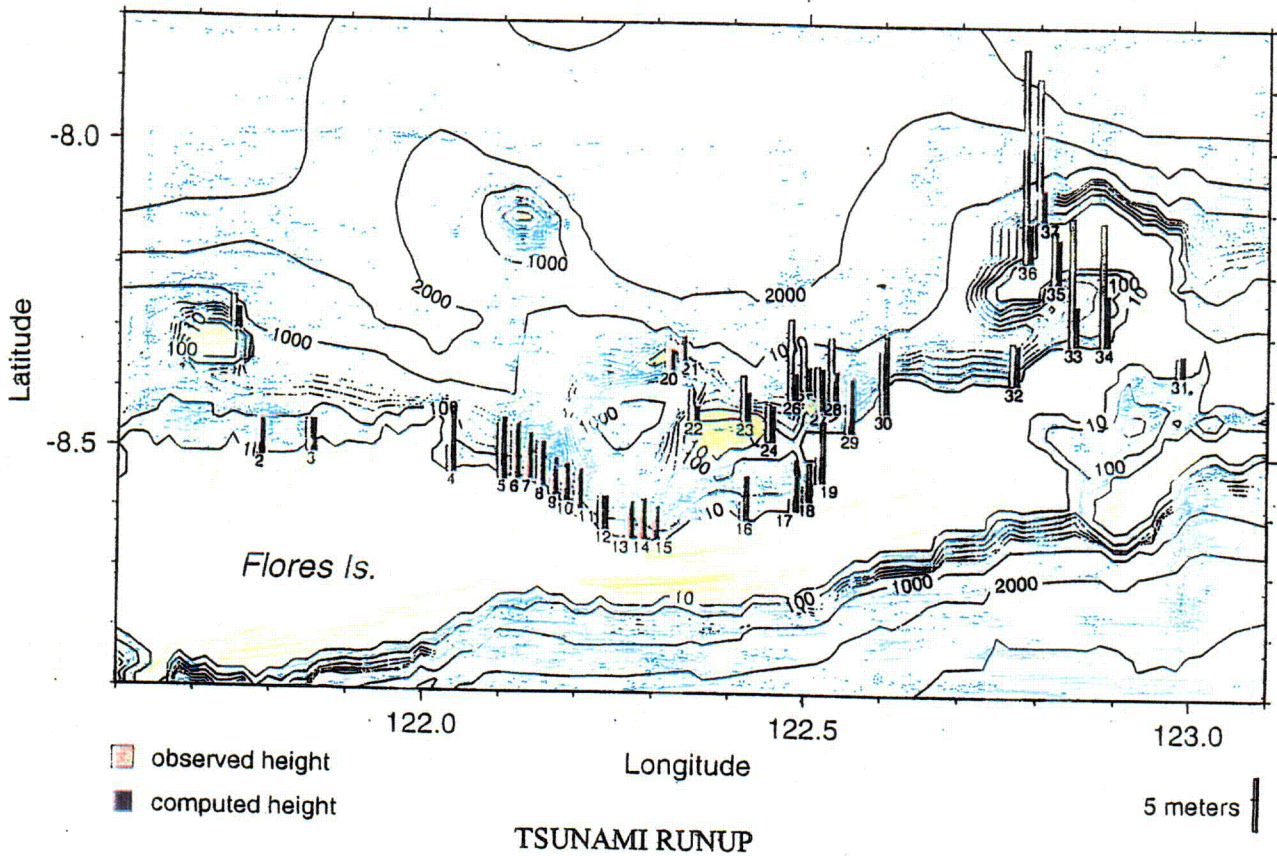
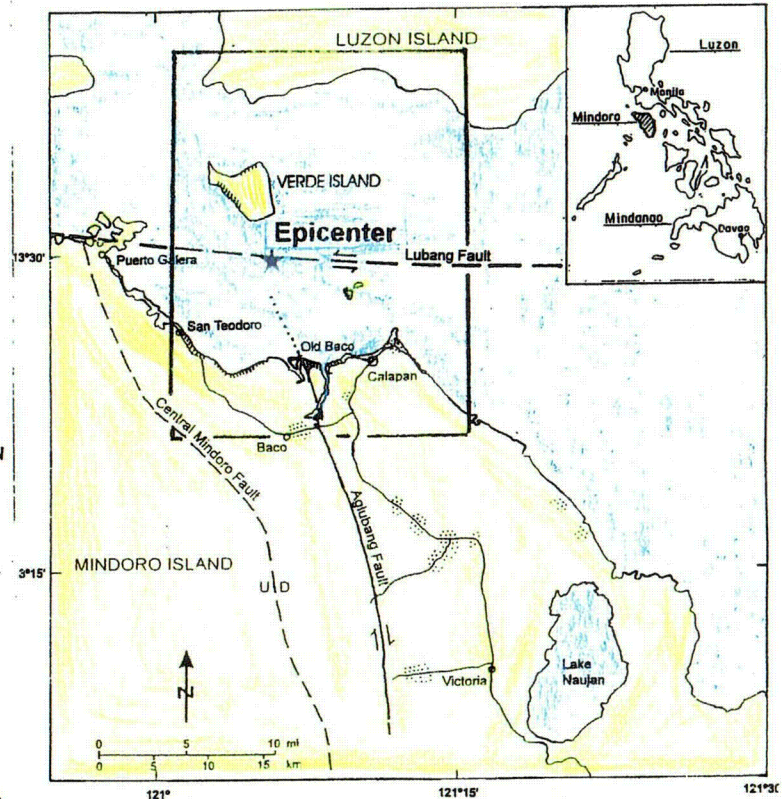
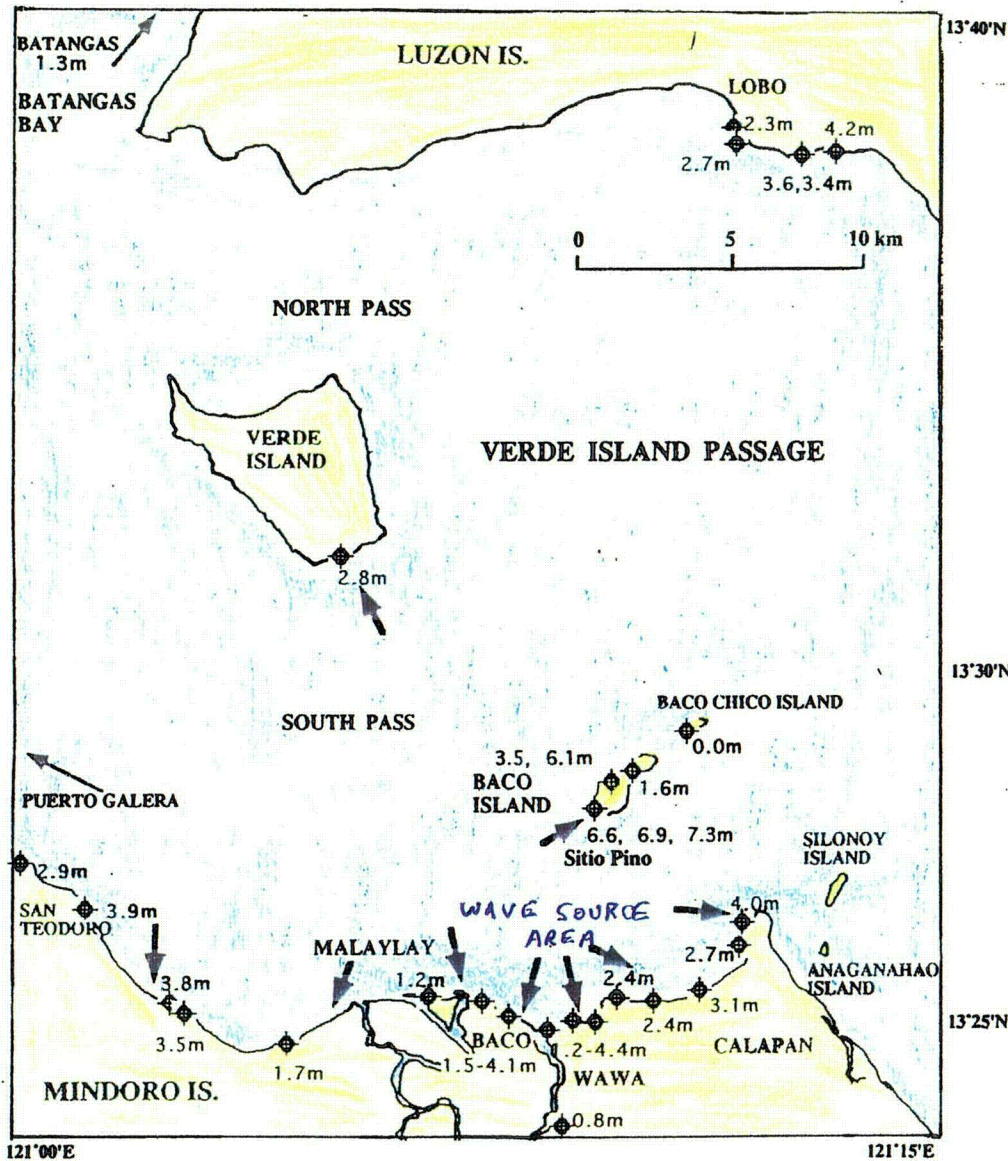


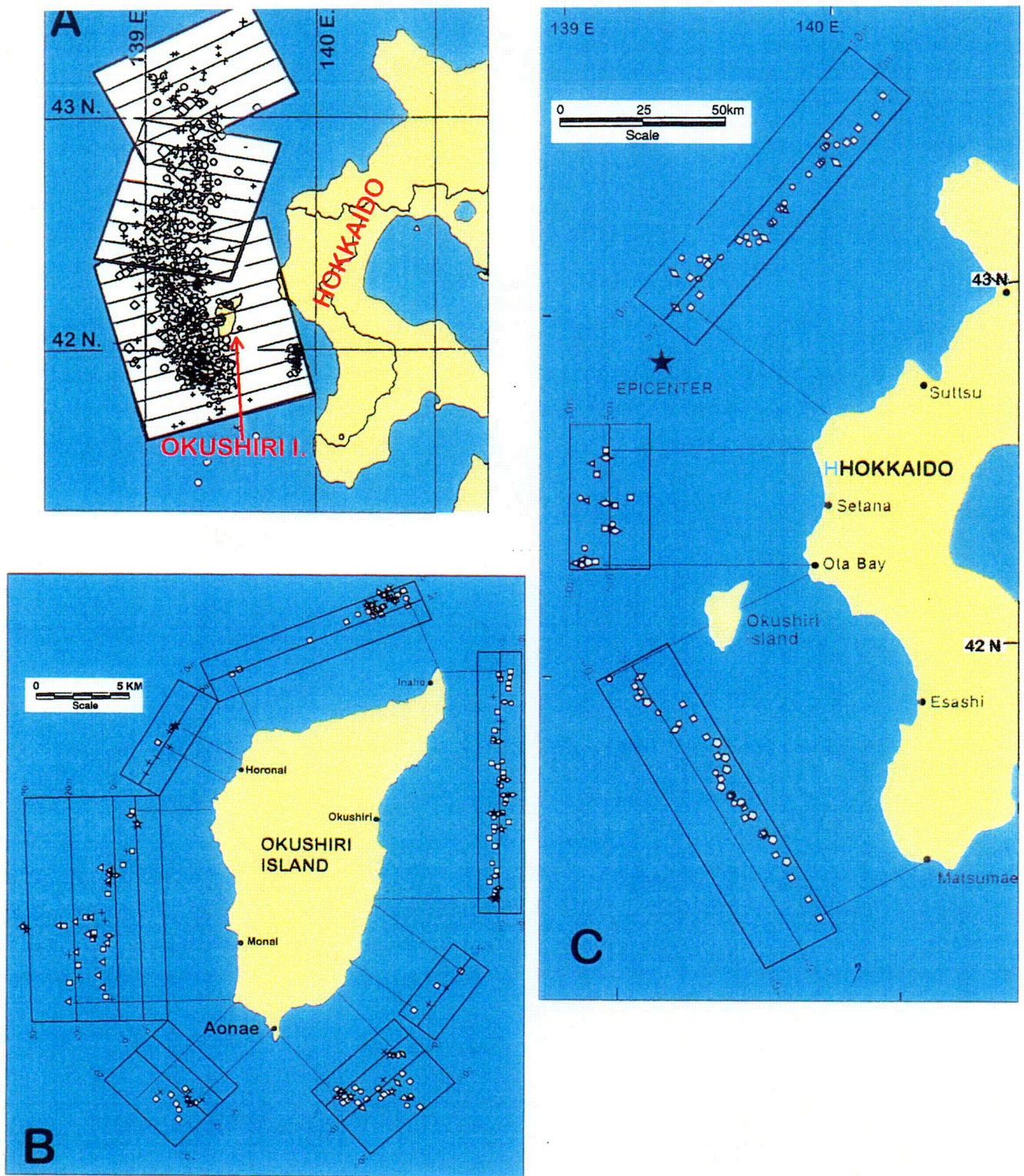
Figure 5. Observed (shaded) and computed (solid) runup heights of the tsunami that accompanied the 1992 M_w 7.5 Flores, Indonesia earthquake. Anomalously large local runups (to 26 m) at the topographically rugged eastern end of Flores Island and at Babi Island are at least in part caused by submarine landslides based on marine studies and arrival of initial waves at some localities during or immediately after the earthquake. [Tsunami data from Hidayat and others, 1995; Tectonic setting from Plafker (1997, and unpublished data)].

9A-47



TECTONIC SETTING AND LOCATION OF DETAILED MAP

Figure 7. Observed run up heights and inferred movement directions of tsunami that accompanied the 1994 M_w 7.1 Mindoro Island earthquake in the Philippines. The earthquake source is the dominantly dextral strike-slip Aglubang fault. A submarine landslide origin is probable for most or all of these waves based on their local distribution, arrival at shorelines within a few minutes after the earthquake, and a roughly radial pattern of movement. [Wave data from Imamura and others, 1995; tectonic setting from Philippine Institute of Volcanology and Seismology Special Report No. 2.11 p.].



6
 Figure 6. A. The 1993 M_w 7.7 Hokkaido earthquake source (lined rectangles) and aftershocks. B and C. Measured runup heights of the accompanying tsunami on Okushiri Island and Hokkaido. Possible submarine slide origins for the highest waves (~12–32 m) in southern Okushiri Island is suggested by localized runup peaks, by wave arrival immediately after the earthquake, and by local steep offshore topography. [Data from Hokkaido Tsunami Survey Team (http://www.pmel.noaa.gov/tsunami/okushiri_devastation.html)].

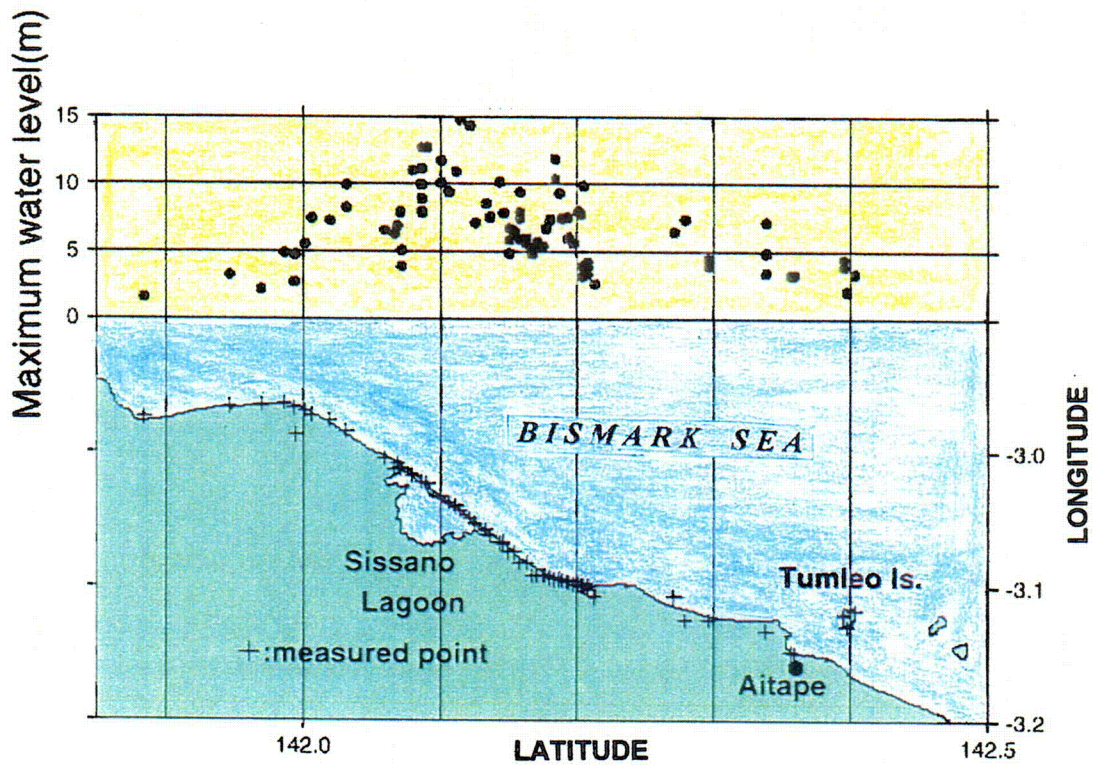


Figure 8. Observed tsunami runup heights associated with the M_w 7.1 1998 Papua, New Guinea earthquake. Note the distinctive bell-shaped distribution of runup heights. [From International Tsunami Survey Team (http://www.tsunami.civil.ohoku.ac.jp/hokusai2/news/PNG-measured_tsunami2.html)].

9A-49

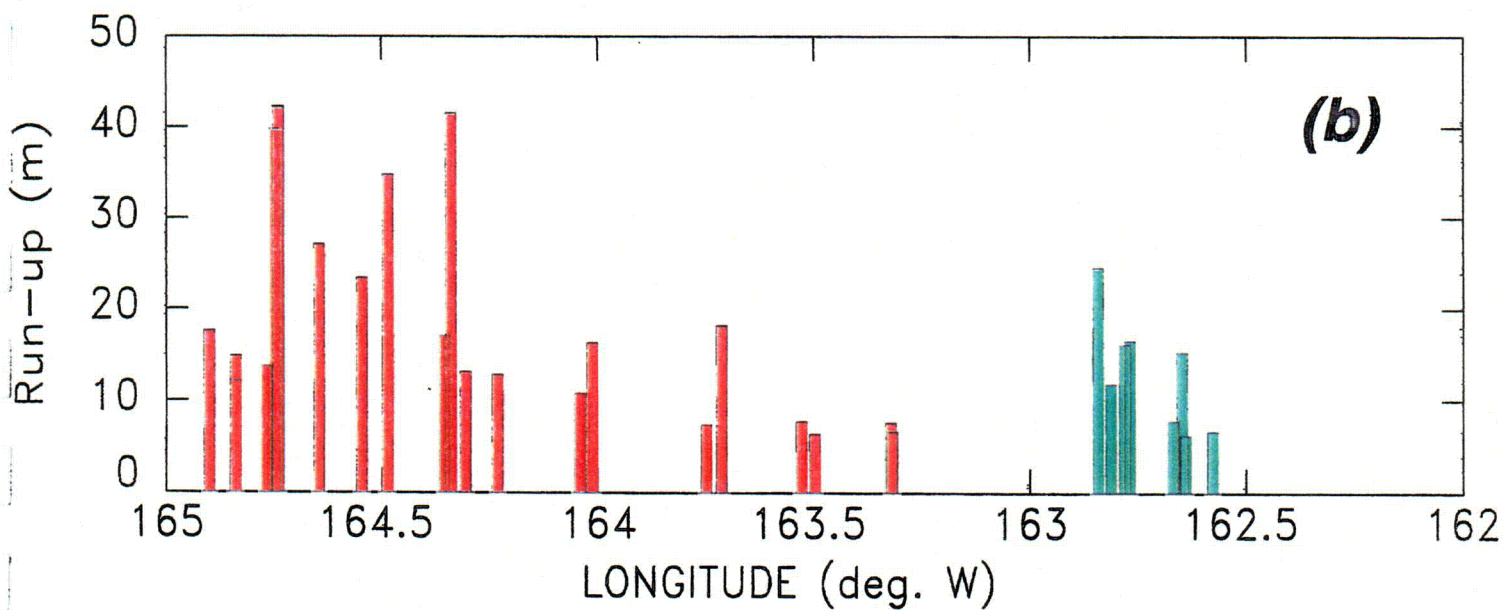
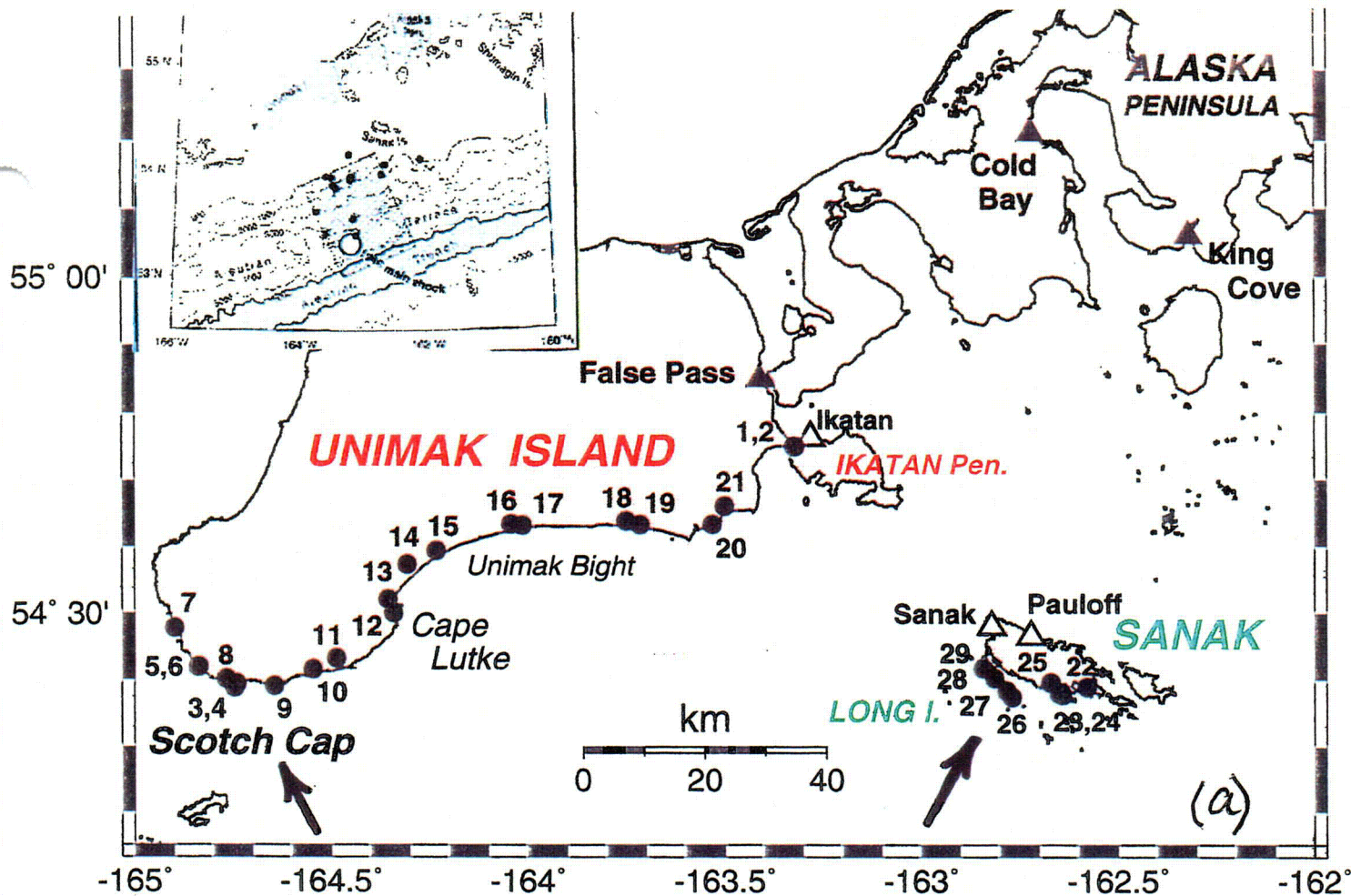


Figure 9. Near-field tsunami associated with the Mw 8.2 April 1, 1946 Aleutian earthquake (from Plafker, Synolakis, and Okal, 2001). Wave heights, movement directions, arrival time at Scotch Cap light station, and attenuation strongly suggest a landslide source close to the continental shelf edge. Inset shows probable earthquake source area on the Aleutian megathrust and major aftershocks (after Johnson and Satake, 1997).

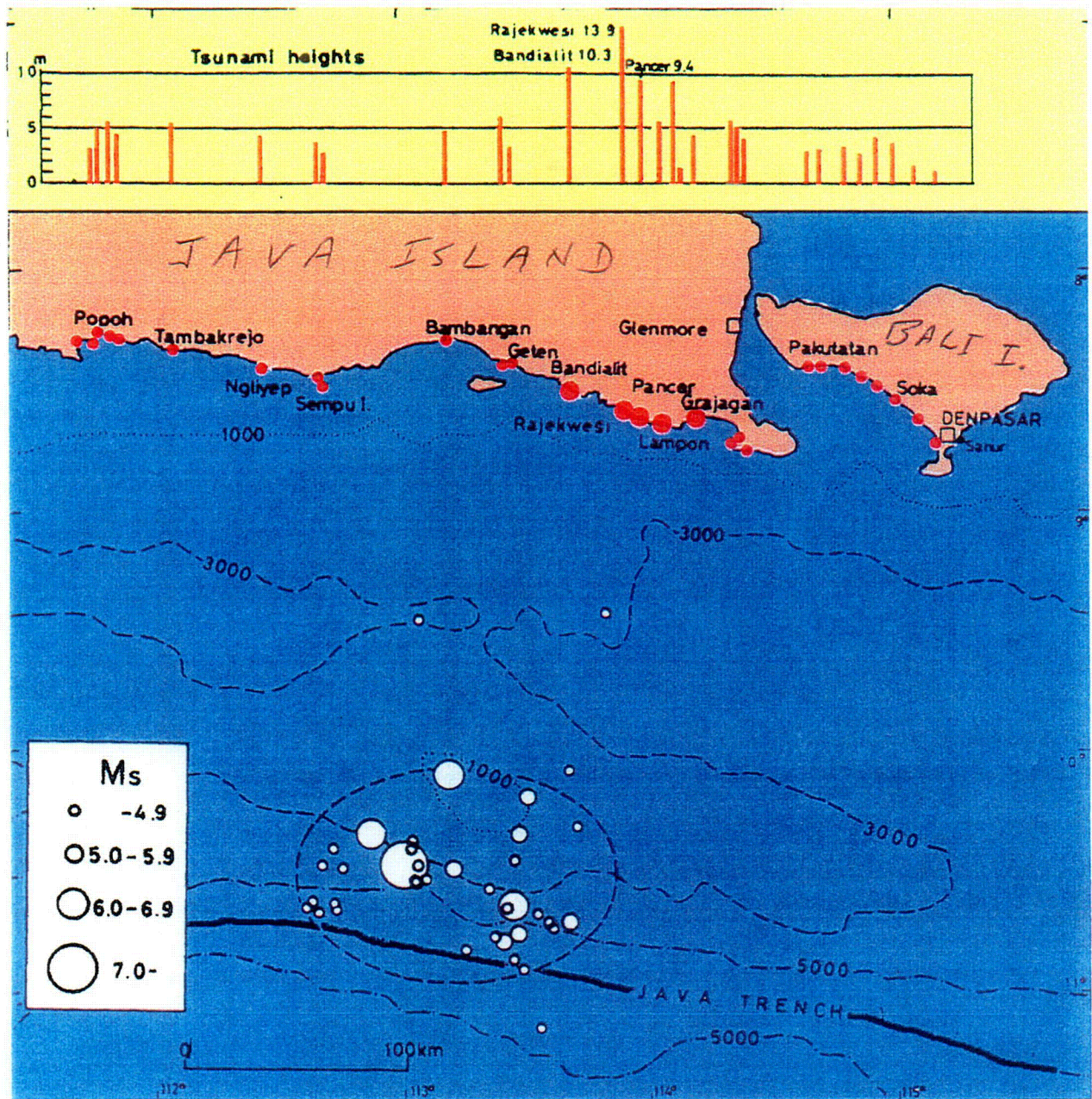


Figure 10. Observed tsunami runup heights (vertical bars) and focal region (dashed line) for the 1994 East Java earthquake (M_w 7.8). Aftershocks shown occurred within 10 days of the earthquake. Onshore red dots show tsunami measurement locality; larger dots indicate areas of severe damage (From Tsuji and others, 1995).

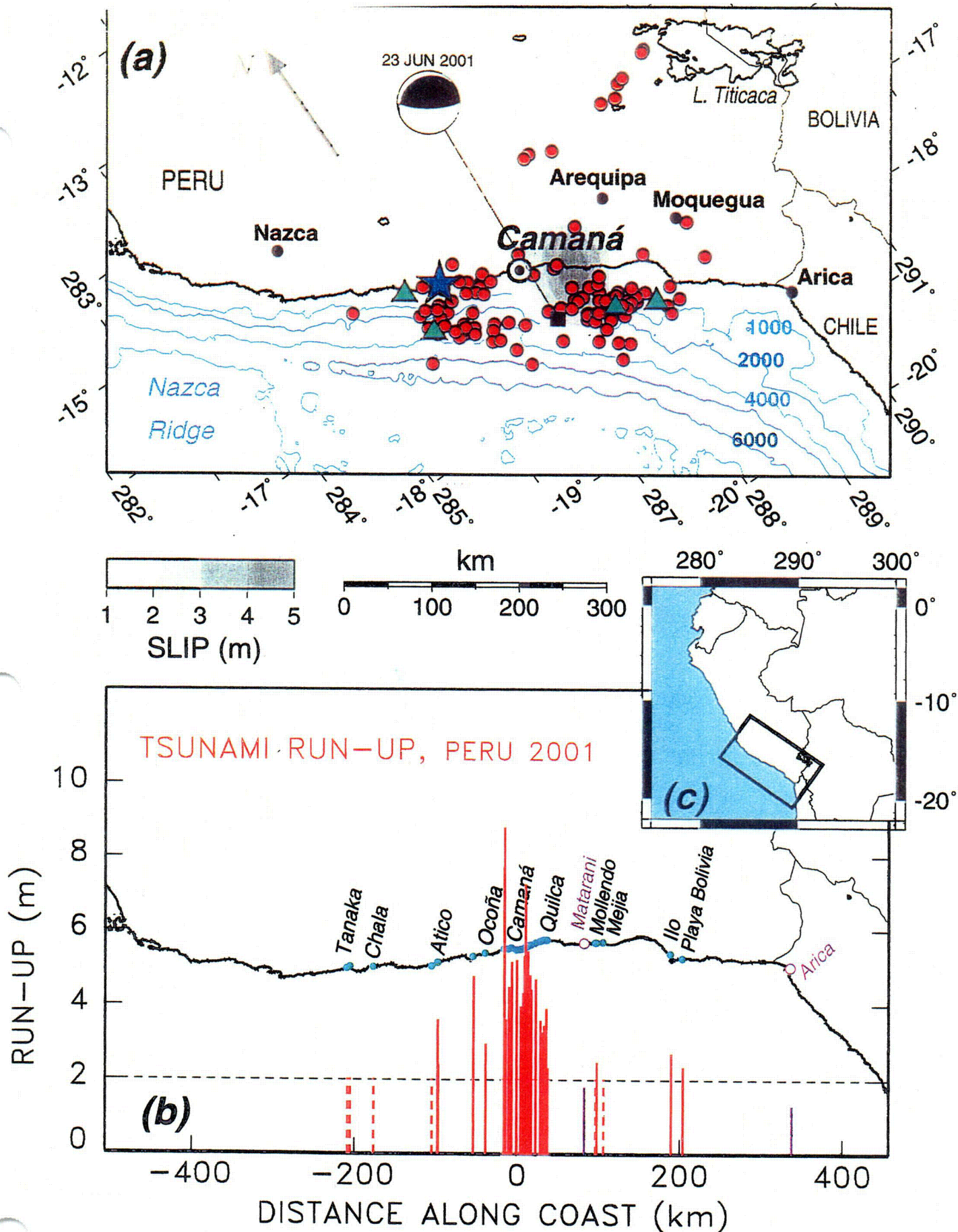


Figure 11. (a): Map of the Southern coast of Peru showing the epicenter of the mainshock (star), and of the one-month aftershocks (red dots); the larger events ($M > 5.8$) are shown as green triangles. The areas shaded in gray show the results of Kikuchi and Yamanaka's (2001) tomographic investigation of the source slip (maximum 4.5 m). Also shown is the final Harvard CMT solution. Bathymetric contours in meters. (b): Map shows tsunami runup measurement locations (green dots) and red bars show measured runup (c): Location map

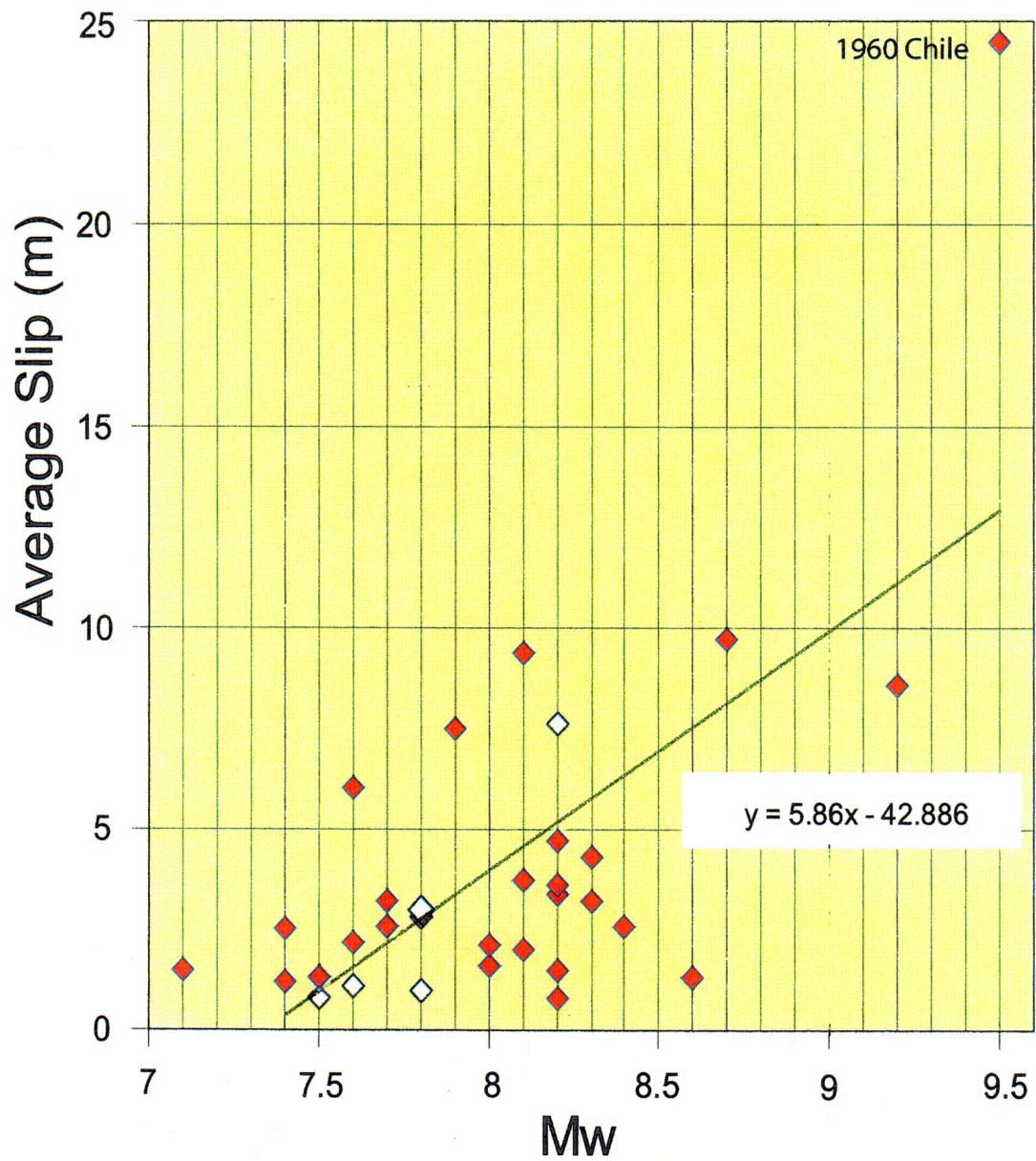


Figure 12. Moment magnitude (M_w) versus average slip for earthquakes that have generated tsunamis. Open points are "slow" earthquakes. [Data and references in Table 4].

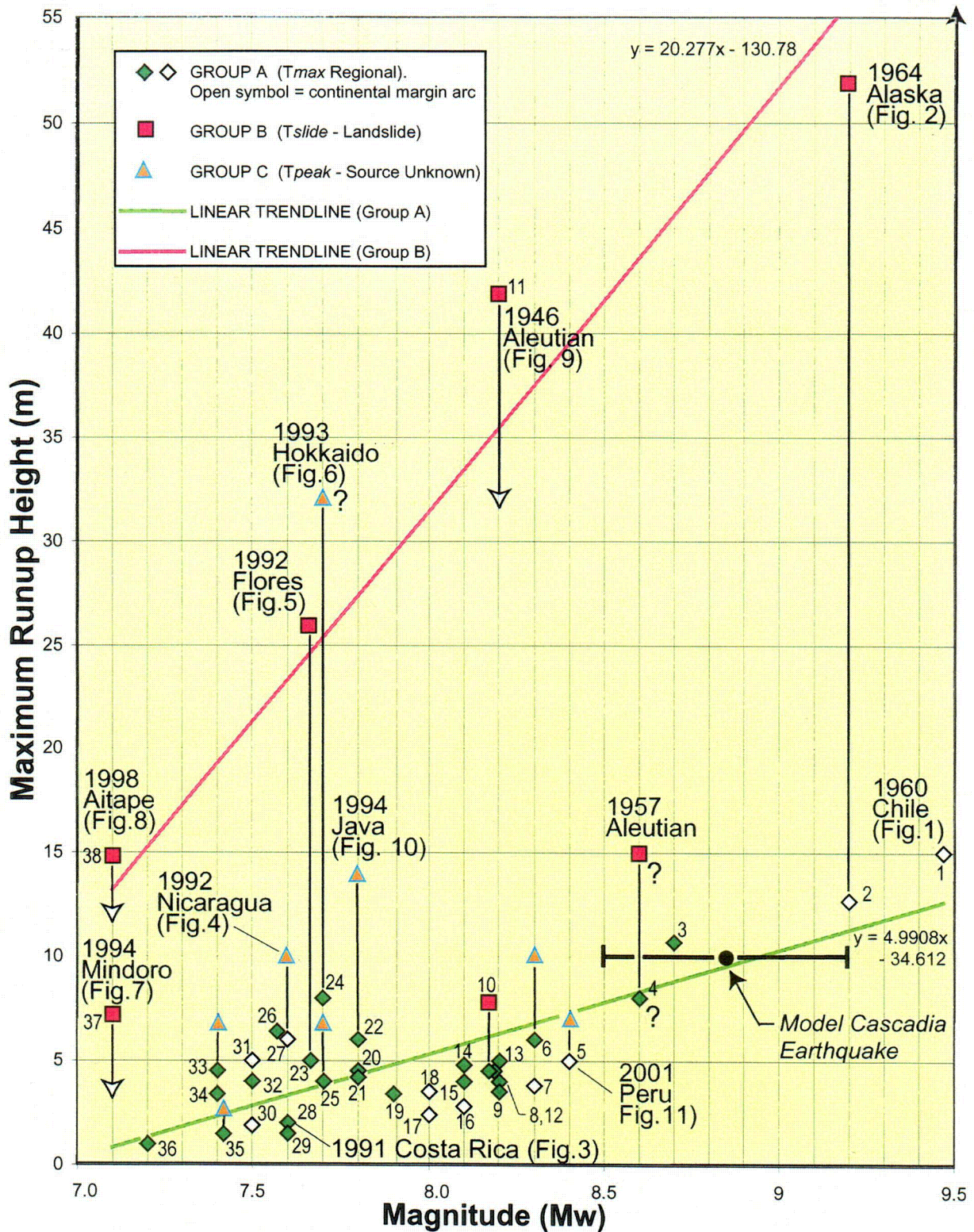


Figure 13. Near source tsunami runup for post-1943 tsunamigenic earthquakes. Group A (Tmax) shows regional maximum tsunami runup. Group B (Tslide) is the maximum runup height of local waves caused by known or inferred submarine landslides. Downward pointing arrows indicate that the corresponding Tmax is obscured by Tslide. Group C (Tpeak) indicates local runup height of uncertain origin for events in which Tpeak is at least 1.5 times Tmax. Least mean square trendlines are shown for Tmax and the upper limit for Tslide. See Tables 1 and 2 for data sources.